GLASS WOOL LAYER FORMATION AND FIBRE DENSITY DISTRIBUTION IN THE COLLECTING CHAMBER

Boris Kraševec

Doctoral Dissertation
Jožef Stefan International Postgraduate School
Ljubljana, Slovenia

Supervisor: Prof. Dr. Branko Širok, Faculty of Mechanical Engineering, Ljubljana, Slovenia

Evaluation Board:
Prof. Dr. Aleksander Zidanšek, Chair, Jožef Stefan Institute, Ljubljana, Slovenia
Prof. Dr. Marko Hočevar, Member, Faculty of Mechanical Engineering, University of Ljubljana, Slovenia
Prof. Dr. Matjaž Hriberšek, Member, Faculty of Mechanical Engineering, University of Maribor, Slovenia

MEDNARODNA PODIPLOMSKA ŠOLA JOŽEFA STEFANA
JOŽEF STEFAN INTERNATIONAL POSTGRADUATE SCHOOL



Boris Kraševec

GLASS WOOL LAYER FORMATION AND FIBRE DENSITY DISTRIBUTION IN THE COLLECTING CHAMBER

Doctoral Dissertation

FORMIRANJE PLASTI STEKLENE VOLNE IN PORAZDELITEV GOSTOTE VLAKEN V USEDALNI KOMORI

Doktorska disertacija

Supervisor: Prof. Dr. Branko Širok

Ljubljana, Slovenia, December 2016

To my life traveller Katja, son David and daughter Eva.

Acknowledgments

First and foremost I would like to thank my life traveller Katja for supporting me during my doctoral study. Your advice, optimism and power of positive thinking showed me the way to success. Special thanks to my son David and daughter Eva for your laugh and high spirits. You have been my big motivation to finish my PhD work.

I would like to express my sincere thanks to my supervisor Prof. Branko Širok and his department at the Faculty of Mechanical Engineering for the cooperation on my doctoral work. Thanks to Assoc. Prof. Dr. Marko Hočevar and As. Dr. Benjamin Bizjan for cooperation on experiments at the Ursa plant and at the Faculty of Mechanical Engineering, and for comments regarding my scientific articles and dissertation. Thanks also to Mr. Aleš Malneršič for his support with experimental drawings. I worked with great people and I am sure that we will find new challenges to connect the industry and science.

Thanks a lot to Prof. Milena Horvat at the Jožef Stefan International Postgraduate School, who gave me the opportunity to study. I have become acquainted with personnel of several different research departments at the Jožef Stefan Institute whose continuous innovations present potential support to our production.

I would also like to thank the company Ursa Slovenia, d.o.o. for supporting my doctoral study. Special thanks to the human resources manager Mr. Aleš Križman and plant manager Mr. Andrej Novak. I am confident that my future work at our plant will benefit from the knowledge and experience I have gained during my studies.

Abstract

Glass wool is one of the most widely used insulation materials and is specially known for its excellent thermal insulation properties. The main benefit of the glass wool production process is the use of a waste glass as a base material to produce a high quality insulation material. Glass wool is commonly used for thermal and sound insulation in buildings, resulting in economic, health and environmental benefits for the society. The glass wool production process is highly complex, consisting of several different production phases. Adequate understanding and control of each phase is required in order to optimize the properties (e.g. thermal conductivity, homogeneity and mechanical properties) and production costs of end products. Glass fibre distribution in the end product must be as homogeneous as possible to obtain optimal thermal conductivity properties. With optimal glass fibre distribution, the consumption of raw materials and energy is minimized, while also minimizing the thermal conductivity of end products. Due to the fact that the glass wool production process is affected by many different parameters, the correlation between process variables of fiberization machines and collecting chamber and the end product quality is highly complex.
The proposed PhD thesis is in agreement with requirements of the industrial production process of glass wool. New knowledge will enable improved understanding of the process of glass wool layer formation and fibre density distribution in the collecting chamber. The modelling procedure may be applied in the production process where the main expected benefit is an improvement of the end product properties and a reduction of waste and second-class products quantity. Experimental and numerical models for fibre properties and quality of final product are also provided.
The process of fibre layer formation and fibre distribution in the forming chamber can be optimized and controlled by measurement and control of several selected process parameters.

We have formed the following two hypotheses:
- Based on measurements of the volume flow rate of air, volume flow rate of gas, spinner rotational speed, mass flow rate of melt, air pressure and melt temperature, a model for prediction of the glass wool fibre thickness can be formed.
- Reliable prediction of the transversal fibre density distribution in the forming chamber and in the end product can be achieved using parametric model based on the same set of input variables, allowing for an improved process control.

In Chapter 2 a model which allows glass wool fibre thickness prediction is presented and the first hypothesis is addressed. Fibre thickness is an important parameter of glass wool quality as it influences the local thermal insulation properties (thermal conductivity) and significantly affects the fibre density distribution in the collecting chamber.
In the experiment with a model spinning machine, we analysed the normalized standard deviation of the optical intensity (σ_{Gn}) of acquired visualization images, local fibre accumulation rates (ψ), and dimensionless distance between the fibre layer centre of gravity and centre of accumulation grid (δ). Multiple regression models for δ and σ_{Gn} have shown an important effect of the suction flow, coaxial and tangential blow-away flows as well as fibre deposition time on the fibre layer properties. Also, these models are in a good agreement with measured values of δ and σ_{Gn} and also with the estimated fibre accumulation rate. Regression models and qualitative analysis results improve the understanding of the fibre transport and the fibre layer formation process, leading to new possibilities for process monitoring and automation. The topic is presented in Chapter 3 and is addressed in the second hypothesis.
In Chapter 4 a model is presented with correlation between air suction flow velocity on the bottom of the collecting chamber and glass wool transversal fibre density distribution on the

final product. An assumption was made that the glass wool quality can be improved by increasing the uniformity of the air flow velocity distribution, and has been confirmed by analysis of acquired experimental data. The results of velocity measurements in the collecting chamber will also allow for a more precise process control.

Based on the key parameters that influence the transversal fibre density distribution in a layer of glass wool and with the aid of density measurements performed by the X-Ray device we have formed the main regression model. It can be used by the glass wool line operator as a guide for setting the operating parameters instead of relying solely on past experience. The topic is presented in Chapter 4 and is addressed in the second hypothesis.

Povzetek

Steklena volna je eden najbolj razširjenih izolacijskih materialov, ki se odlikuje z zelo dobro toplotno izolativnostjo. Glavna dodana vrednost v procesu proizvodnje steklene volne je proizvodnja visoko kvalitetnega izolacijskega materiala z možnostjo uporabe odpadnega stekla kot vhodne surovine. Steklena volna največkrat služi za toplotno in zvočno izolacijo zgradb, kar ima na ravni družbe pozitivne ekonomske, bivanjske in okoljske učinke. Proizvodni proces steklene volne je zelo kompleksen in se sestoji iz več zaporednih proizvodnih faz. Za izboljšanje lastnosti končnih izdelkov (toplotna prevodnost, homogenost in mehanske lastnosti) in hkratno znižanje proizvodnih stroškov le teh je potrebno zadostno razumevanje in nadzor vsake posamezne faze. Porazdelitev steklenih vlaken v končnem izdelku mora biti čim bolj homogena, da dobimo optimalne toplotno izolacijske lastnosti. Z optimalno porazdelitvijo steklenih vlaken se zniža poraba vhodnih surovin in energije v proizvodnem procesu, hkrati pa je dosežena najnižja toplotna prevodnost materiala. Zaradi velikega števila procesnih spremenljivk in nastavitev parametrov strojev za razvlaknjenje (centrifug) ter usedalne komore so relacije med temi parametri in lastnostmi končnih izdelkov zelo kompleksne.
Predlagana doktorska disertacija je v skladu z zahtevami industrijskega proizvodnega procesa steklene volne. Z novim znanjem bo omogočeno boljše razumevanje procesa nastajanja plasti steklene volne in porazdelitve gostote vlaken v usedalni komori. Postopek modeliranja se lahko uporablja v proizvodnem procesu, kjer je glavna dodana vrednost izboljšanje lastnosti končnih proizvodov, zmanjšanje izgub in količine izdelkov slabše kvalitete. Doktorska disertacija vsebuje eksperimentalne in numerične modele za opis lastnosti vlaken in kakovosti končnega izdelka.
Proces nastanka plasti steklene volne in porazdelitev vlaken v usedalni komori je mogoče izboljšati z merjenjem in nadzorom več izbranih procesnih parametrov.

Oblikovali smo sledeči hipotezi:
• Na osnovi meritev volumskega pretoka zraka, volumskega pretoka plina, hitrosti vrtenja rotorja, zračnega tlaka, masnega pretoka in temperature taline lahko oblikujemo model, ki omogoča napoved premera vlaken steklene volne.
• Zanesljivo napoved prečne porazdelitve gostote vlaken v usedalni komori in v končnem izdelku je mogoče doseči z uporabo parametričnega modela, ki temelji na naboru vhodnih spremenljivk in omogoča izboljšano kontrolo procesa.

V poglavju 2 je predstavljen model, ki omogoča napovedovanje debeline vlaken steklene volne in se nanaša na prvo hipotezo. Debelina vlaken je pomemben parameter za presojanje kakovosti steklene volne, saj vpliva na lokalne toplotno izolacijske lastnosti (toplotna prevodnost) in ima velik vpliv na porazdelitev gostote vlaken v usedalni komori.
Na modelu centrifuge je bil analiziran normaliziran standardni odklon optične intenzivnosti (σ_{Gn}), pridobljene iz vizualizacijskih slik, lokalne stopnje akumulacije vlaken (ψ) in brezdimenzijske razdalje med središčem plasti vlaken in središčem usedalne komore (δ). Regresijski modeli za δ in σ_{Gn} so pokazali pomemben učinek odsesa vlaken, koaksialnega in obodnega odpiha vlaken, kot tudi časa nalaganja vlaken na lastnosti vlaken v plasti. Poleg tega se modeli dobro ujemajo z izmerjenimi vrednostmi δ in σ_{Gn}, pa tudi z oceno stopnje akumulacije vlaken. Regresijski modeli in kvalitativni rezultati analize prispevajo k boljšemu razumevanju transporta vlaken in oblikovanja primarne plasti ter vodijo do novih možnosti za nadzor in avtomatizacijo procesov. Tematika je predstavljena v poglavju 3 in je naslovljena na drugo hipotezo.
V poglavju 4 je predstavljen model z odvisnostjo med hitrostjo pretoka zraka na dnu usedalne komore in prečno porazdelitvijo gostote vlaken steklene volne v končnem izdelku. Ocenili smo, da se kakovost steklene volne lahko izboljša s povečanjem enakomernosti porazdelitve hitrosti

pretoka zraka, kar smo dokazali z analizo eksperimentalnih podatkov. Meritve hitrosti v usedalni komori bodo pripomogle k natančnejšemu krmiljenju procesa.
Glavni regresijski model smo dobili na osnovi ključnih parametrov, ki vplivajo na prečno porazdelitev gostote vlaken v plasti steklene volne, ter s pomočjo merjenja gostote z X-Ray napravo. Model lahko operater linije uporabi kot vodilo pri nastavljanju obratovalnih parametrov namesto zanašanja zgolj na pretekle izkušnje. Tematika je predstavljena v poglavju 4 in se nanaša na drugo hipotezo.

Contents

List of Figures xv

List of Tables xvii

Abbreviations xix

Symbols xxi

1 Introduction 1
1.1 Glass Wool History and Environmental Aspect ... 1
1.2 Glass Wool Process ... 1
1.3 Description of the Problem ... 2
1.4 Purpose of the Dissertation ... 2
1.5 Goals of the Dissertation ... 3
1.6 Hypothesis ... 3
1.7 Methodology ... 4
1.7.1 Multiple Regression Model of Glass Wool Fibre Thickness on a Spinning Machine ... 4
1.7.2 Velocity of the Air Suction Flow in the Collection Chamber ... 4
1.7.3 Measurements of the Glass Wool Luminous Intensity (Greyness) at the Exit of the Collection Chamber ... 5
1.7.4 X-Ray Measurements ... 5
1.7.5 Model Spinning Machine with a Hollow Perforated Rotor and a Vertical Collecting Chamber ... 5
1.8 Argumentation of the Scientific Relevance ... 6

2 Multiple Regression Model of Glass Wool Fibre Thickness on a Spinning Machine 10

3 Glass Wool Layer Formation in the Collecting Chamber 23

4 Fibre Density Distribution in a Layer of Glass Wool 37

5 Summary of Results 53
5.1 Multiple Regression Model of Glass Wool Fibre Thickness on a Spinning Machine ... 53
5.2 Glass Wool Layer Formation in the Collecting Chamber ... 55
5.3 Fibre Density Distribution in a Layer of Glass Wool ... 58

6 Conclusions 61

References 63

Bibliography 69
List of publication ... 69
Journal Articles ... 69
Other Publications ... 69

Biography 71

List of Figures

Figure 1.1: Glass wool production process 2
Figure 5.1: Comparison of the experimentally measured and statistically predicted fibre diameters 56
Figure 5.2: Normalized standard deviation of optical layer intensity for different operating points (OP) 58
Figure 5.3: Average fibre accumulation rate ψ on the accumulation grid 58
Figure 5.4: Distance between centre of gravity and centre of fibres on the accumulation grid as a function of time.....59
Figure 5.5: Velocity distribution above the transporter belt in the collection chamber.....60
Figure 5.6: Fibre density distribution in a layer of glass wool [kg/m^3] 60
Figure 5.7: Correlation between air flow velocity in the collecting chamber and glass wool layer density obtained with the X-Ray device (r^2 = 0.81).....61
Figure 5.8: Comparison of experimentally measured (Range) and statistically predicted fibre density distribution (Range calculated) 62

List of Tables

Table 5.1: Characteristic and dimensionless numbers of the parametric model 55
Table 5.2: Regression model constant values according to Equation 5.1 along with the results of t-test 57
Table 5.3: Operating points for fibre layer visualization 57
Table 5.4: Regression model constant values along with the results of the t-test 62

Abbreviations

CFD	. . .	Computational fluid dynamics
CCD	. . .	Charge coupled device
DAQ	. . .	Data acquisition
VFD	. . .	Variable frequency drive
L	. . .	Left
R	. . .	Right
LM	. . .	Left middle
RM	. . .	Right middle
DF	. . .	Represents degrees of freedom
SS	. . .	Sum of squares
MS	. . .	Mean square
P	. . .	Probability

Symbols

I	. . .	Radiation intensity after passing material of thickness x
I_0	. . .	Radiation intensity before entering into the material
μ_m	. . .	Mass attenuation coefficient of the material
f	. . .	Area weight
r^2	. . .	The correlation coefficient
T	. . .	Temperature
T_0	. . .	Initial temperature
A	. . .	Constant
B	. . .	Constant
η	. . .	Dynamic viscosity
η_m	. . .	Dynamic viscosity of melt
η_A	. . .	Dynamic viscosity of air
σ	. . .	Surface tension
b_i	. . .	Constant
R	. . .	Radius of the spinner
B	. . .	Spinner height
ω	. . .	Rotational speed
T_m	. . .	Melt temperature
ρ	. . .	Melt density
$q_{m,m}$	. . .	Mass flow rate of melt
$q_{v,G}$	. . .	Volume flow rate of gas
$q_{v,A}$	. . .	Volume flow rate of air
$q_{v,m}$	. . .	Volume flow rate of melt
$q_{m,A}$	. . .	Mass flow rate of air
$q_{m,A,0}$	. . .	Reference mass flow rate of air
$q_{v,A,0}$	. . .	Reference volume flow rate of air
$q_{m,G}$	. . .	Mass flow rate of gas
d_f	. . .	Fibre diameter
p_A	. . .	Air pressure
p_0	. . .	Compressor pressure
d_i	. . .	Initial spinner hole diameter
T_A	. . .	Air temperature
CV_G	. . .	Caloric value of gas
$c_{p,m}$	. . .	Specific heat of melt
$c_{p,A}$	. . .	Specific heat of air
$A_{i,j}$	. . .	Local greyness average
std(A)	. . .	Standard deviation of greyness level
n	. . .	Number of images
nstd(A)	. . .	Normalized standard deviation of greyness
x	. . .	Material thickness

σ_{Gn} . . . Gray level normalized standard intensity
ψ . . . Fields of fibre accumulation rate
μ . . . Mean fibre layer area density
G . . . 2D scalar field of image gray level
$r_{t,A}$ . . . Layer local radial positions across the layer surface A
δ . . . Dimensionless position of its centre of gravity
Q_p . . . Blow-away airflow
Q_s . . . Suction airflow
Q_t . . . Tangential airflow
Δp . . . Pressure
U_t . . . Voltage
f_s . . . Power supply frequency
ρ . . . Raw density

Chapter 1

Introduction

1.1 Glass Wool History and Environmental Aspect

The first fibreglass insulation was introduced in 1938 by Russell Games Slayter (1896-1964), a researcher of the Owens Corning company [1]. Slayter was a prolific U.S. engineer and inventor best known for developing fibreglass, starting with a new method of glass wool manufacturing in 1933.
Glass wool is one of most used insulation materials and is specially known for its excellent thermal insulation properties. The main benefit of the glass wool production process is the use of waste glass as a base material to produce a high quality insulating material. Glass wool is commonly used for thermal and sound insulation in buildings, resulting in economic and environmental benefits for the society.
In modern glass wool production facilities, production lines are equipped with closed-loop water systems for binder preparation and recycling systems for poor quality glass wool products, which minimize the amount of environment contamination. The flue gases produced during the glass wool layer formation in the collecting chamber and binder polymerisation in curing oven are cleaned by modern wet electric filters. After that, cleaned gases are expelled into the environment as water aerosols.

1.2 Glass Wool Process

The glass wool manufacturing process begins with the preparation of raw materials. The basic component of the glass mixture is waste glass. Other components in the mixture are minerals such as borax pentahydrate (etibor), feldspar, dolomite, soda, quartz sand and calcite. The glass mixture is dosed into the furnace (Figure 1.1) (position 1), where the glass melts at about 1300°C. The molten glass mixture is first supplied into the stabilization channel (position 2) and then poured through the funnel (position 3) into the rotating spinners (position 4). Present in the area of position 4 are air and gas flows used for the combustion process, pressure arising from the air curtain, air flows from the left and right glass wool side cutting and from the recycled material. Fibres are formed by extrusion of the melt through the spinner holes and are then sprayed with the binder (position 5). The coaxial air flow with adjustable pressure orients the fibres down towards the collecting chamber (position 7). The transversal density distribution can be adjusted by air blowing nozzles (position 6). With the aid of suction fans (position 8), the fibres are collected on a conveyor belt made of perforated plates to form the raw glass wool (position 9). The layer is then transported through the polymerisation chamber (position 10), where the binder polymerisation process occurs at approximately 250 °C. The glass wool is then cooled with the aid of suction fans (position 11). With the X-Ray device the fibre density distribution is measured (position 12). The final steps in production process

include fleece cutting to required dimensions (position 13), material compression and packaging. [2]

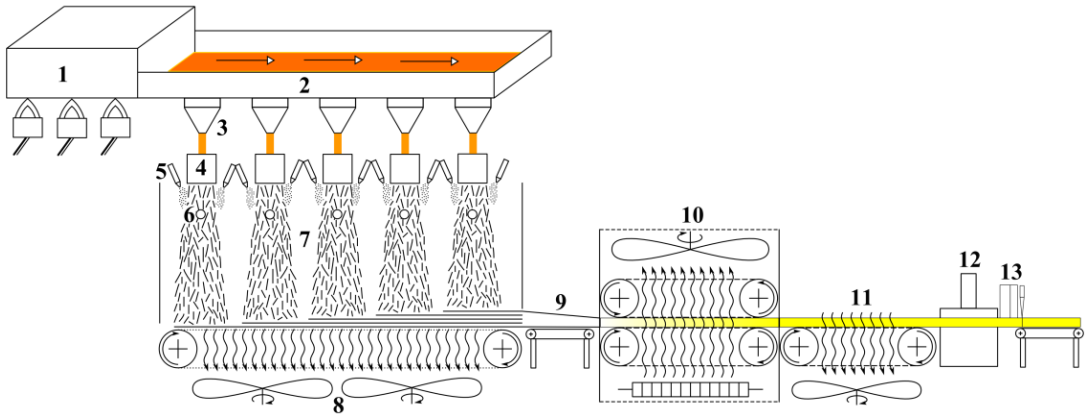


Figure 1.1. Glass wool production process

1.3 Description of the Problem

Glass wool production process is highly complex, consisting of several different production phases. Sufficient understanding and control of each phase is required in order to optimize the properties (e.g. thermal conductivity, homogeneity and mechanical properties) and production costs of end products.

Glass fibre distribution in end products must be as homogeneous as possible to obtain optimal and uniform thermal conductivity properties. With optimal glass fibre distribution, the least raw materials and energy are required for production, while the thermal conductivity is minimized. The influence of variables and parameter settings for fiberization machines and collecting chamber is complex due to the high dimensionality of the process.

With the aid of determined correlations between varied process parameters the homogeneity of fibre diameter and fibre density distribution can be improved. The fibre diameter is directly influenced by measured (input) process parameters such as the volume flow rate of air ($q_{v,A}$), volume flow rate of gas ($q_{v,G}$), spinner rotational speed (ω), mass flow rate of melt ($q_{m,m}$), air pressure (p_A), melt temperature (T_m) and chemical composition. Other important parameters include geometric constants (spinner radius (R), spinner height (B), spinner hole diameter (d_i), final spinner hole diameter (d_f) etc.), melt volume flow rate ($q_{v,m}$), melt physical properties (density (ρ), dynamic viscosity (η_m), surface tension (σ), specific heat ($c_{p,m}$)) which are a function of its temperature and chemical composition, ambient air properties (dynamic viscosity (η_A), mass flow rate ($q_{m,A}$), reference mass flow rate ($q_{m,A,0}$), reference volume flow rate ($q_{v,A,0}$), temperature (T_A), specific heat ($c_{p,A}$)), mass flow rate of gas ($q_{m,G}$), caloric value of gas (CV_G) and compressor pressure (p_0).

Uniformity of fibre density distribution can be improved by application of determined correlation between varied process parameter which presents fibre diameter (d_f), rotational speed of suction fan motors (ω_m) and positions of air blowing nozzles (α).

1.4 Purpose of the Dissertation

The purpose of the study is to analyze the glass wool formation process in the collecting chamber, which affects the fibre density distribution within the final product. During production the line operators mostly set the input parameters based on past experience. However, the purpose of this study is to improve the understanding of the fibre layer formation process, developing a more scientific method for process regulation. We would like

to influence the transversal density distribution by making proper variations of process parameters (fibre diameter, rotational speed of suction fan motors and positions of air blowing nozzles) while the X-Ray device is used to measure the fibre density distribution.
The influence of set and monitored process parameters is very complex because of the high dimensionality of the problem. Provided below are the goals of the doctoral study, supported with the scientific relevance (Chapter 1, Section 1.8) and explained methodology (Chapter 1, Section 1.7) which is the basis of obtained results. The results of the study will be useful for transfer of knowledge to other glass wool production plants which use similar production technology.

1.5 Goals of the Dissertation

The goals of the dissertation are the following:

- To set up a model which will allow prediction (and consequently control) of the glass wool fibre thickness. (Chapter 2)

Fibre thickness is an important parameter of the glass wool quality. It influences local thermal insulation properties (thermal conductivity) and has a big impact on the fibre density distribution in the collecting chamber.

- To set up a model for the transversal density distribution of glass wool fibres in final products based on measurements of air suction flow velocity on the bottom of the collecting chamber. (Chapter 4)

Velocity measurements in the collecting chamber provide valuable information required for proper selection of process variables. For instance, the ratio between the flow of gases entering the collecting chamber and the suction flow out of the chamber has an important effect on the fibre density distribution.

- To form a regression model for variables that influence the transversal fibre density distribution in a glass wool layer, based on density measurements performed with the X-Ray device. (Chapter 4)

Such model can be used by the operator as an additional guide in setting the operating parameters of the glass wool production line.

- To analyze the imaging data acquired on the model spinning machine: normalized standard deviation of the image optical intensity, local fibre accumulation rates, and dimensionless distance between the fibre layer centre of gravity and centre of accumulation grid. (Chapter 3)

Such study is difficult to perform on the industrial production process. By performing experiments on a model spinning machine instead we were able to obtain models that provide a more in-depth understanding of the primary layer formation process in the collecting chamber.

1.6 Hypothesis

The process of fibre layer formation and fibre distribution in the forming chamber can be optimized and controlled by measuring and controlling several selected process parameters. Based on the discussion above, the following two hypotheses can be formed:

1. Based on measurements of the volume flow rate of air, volume flow rate of gas, spinner rotational speed, mass flow rate of melt, air pressure and melt temperature, a model for prediction of the glass wool fibre thickness can be formed.

2. Reliable prediction of the transversal fibre density distribution in the forming chamber and in the end product can be achieved using parametric model based on the same set of input variables, allowing for an improved process control.

1.7 Methodology

The research methodology was based on experimental work at the glass wool production plant (Ursa Slovenija, d.o.o. from Novo mesto) and at the Laboratory for water turbine machines at the Faculty of Mechanical Engineering, University of Ljubljana. Measured data was used to form multiple regression models. Measurements included visualization methods by image acquisition and analysis, density measurements using the X-Ray device, airflow velocity measurements by anemometer and fibre thickness measurements.

1.7.1 Multiple Regression Model of Glass Wool Fibre Thickness on a Spinning Machine

The experiments for glass wool fibre thickness modelling were performed on a spinning machine in an industrial production process. The process parameters were set so that the product quality was adequate for packaging and sale and hence all measured variables correspond to an interval of values of real production process. Molten glass (temperature (T_m), density (ρ), surface tension (σ), dynamic viscosity (η) and mass flow rate ($q_{m,m}$)) was poured into a hollow spinner with radius R, height B and rotational speed ω (Chapter 2, Figure 2). The gas burner with volume flow rate of gas ($q_{v,G}$), volume flow rate of air ($q_{v,A}$) heated the spinner outer wall, facilitating the flow of melt through the pores in the spinner wall. An important heating parameter is the ratio between volume flow rate of air and volume flow rate of gas ($q_{v,A}/q_{v,G}$). In the fibre formation area fibres with fibre diameter (d_v) are formed. During the spinner life time, the ratio of final (d_f) to initial (d_i) spinner holes diameter is increasing due to the wear of the material. With the aid of air pressure p_A, the volume air flow rate orients the fibres down towards the collecting chamber.
For each experiment, samples of glass wool were taken and the thickness (diameter) of fibres was measured. The fibre diameters of mineral wool samples were determined by computer microscopy. Fibre samples were taken directly after fiberization (i.e. just before impregnation with binder). Fibres were cut in small pieces and put under the microscope. With the aid of CCD camera images of fibres were recorded.
The parametric model of glass wool fibre thickness was based on dimensionless analysis of the above mentioned variables which influence the glass wool fiberization process. We intended to assess the agreement between the measured and model predicted glass wool fibres diameters. For this purpose, the correlation coefficient between both data sets was introduced as a quantitative measure. Results of the above presented methodology are discussed in Chapter 5, while the details are presented in the article in Chapter 2.

1.7.2 Velocity of the Air Suction Flow in the Collection Chamber

At the bottom of the collecting chamber the vertical velocity of the air suction flow was measured. The air flow was produced by a combination of blow away and suction flows. Its vertical velocity component was measured using a vane anemometer. Data from the anemometer was acquired with DAQ board and measured velocity fields were analysed.
The anemometer was attached to the transporter belt of the collecting chamber so that its vane was placed approximately 20 cm above the belt. Several different transversal positions of the anemometer with respect to the collecting chamber were used (with respect to the transport direction) at equidistant separation. The anemometer was then moved together with the transporter belt across the complete length of the collecting chamber. During velocity measurements, the local air flows on all machines were set to their production values.
As a result, one dimensional profiles of the vertical air flow velocity were obtained. Assuming steady, time independent process, velocity profiles were merged into a two dimensional velocity field. The velocity field showed the local flow characteristics as a consequence of the cumulative effects of individual air flow generators and depending on the local aerodynamic characteristics of the observed flow tract. Results of the above presented methodology are discussed in Chapter 5, while the velocity measurement procedure is explained more in detail with article in Chapter 4.

1.7.3 Measurements of the Glass Wool Luminous Intensity (Greyness) at the Exit of the Collection Chamber

Measurements of the glass wool luminous intensity (greyness) at the exit of the collecting chamber were performed by a camera visualization method. The camera which captured successive glass wool layer images was installed above the conveyor belt. The structure of the layers was evaluated on the basis of the measured greyness perpendicular to the collecting chamber conveyor belt. The greyness level was assumed to be proportional to the local thickness of the glass wool deposit on the belt.
The visualization was performed using a colour camera with 1.3 megapixel resolution. The glass wool layer was illuminated from above using LEDs, arranged in groups to achieve homogenous illumination and to prevent reflections from conveyor belt. The images were stored to a computer disk for further analysis.
The experiment was performed so that spinning machines were operated individually, while the other spinners were run with equivalent parameters but without the glass melt flow. From the visualization images we were able to determine that the glass wool distribution from individual spinning machines was relatively non uniform. Visible were the areas with a thick glass wool deposit as well as the areas with little or no deposits (areas where the perforated conveyor surface is partly or fully visible). In this way it is possible to assess the quality of fibre transport and deposition process on each individual machine. Results of the above presented methodology are discussed in Chapter 5, while the luminous intensity measurement procedure is explained more in detail with article in Chapter 4.

1.7.4 X-Ray Measurements

The X-Ray measurements of glass wool density generated results with a spatial resolution of 10x10 mm. Based on the results which indicated large variations in glass wool layer density, we proceeded with experimental modelling of glass wool layer density. The glass wool layer density obtained with the X-Ray device was presented in correlation with air flow velocity in the collecting chamber. Also presented was the correlation between glass wool layer density and the fibre diameter, rotational speed of suction fan motors and positions of air blowing nozzles. The agreement between measured and calculated fibre density distribution values was examined with an F-test which evaluates the hypothesis that the regression is not significant. For this purpose, the P value (probability) is calculated. Results of the above-presented methodology are discussed in Chapter 5, while the procedure of X-Ray measurements is explained more in detail with article in Chapter 4.

1.7.5 Model Spinning Machine with a Hollow Perforated Rotor and a Vertical Collecting Chamber

The final experiments of this study were conducted on a model spinning machine with a hollow perforated rotor and a vertical collecting chamber. The spinning machine used was a modified version of a cotton candy machine and was placed inside a vertical cylindrical collecting chamber with a transparent wall. The rotor had an integrated electric heater and was supplied with crystalline sucrose prior to each fiberization experiment. During the spinner operation, sucrose was melted by the heater. Coaxial blow-away airflow (Q_p) was supplied through circular nozzles, evenly distributed around the supply ring. The rate of coaxial blow-away airflow component was regulated by a valve which controlled the overpressure (Δp) in the supply ring. Apart from the coaxial blow-away airflow, the tangential blow-away flow (Q_t) was introduced into the colleting chamber through two tangentially oriented pipes. Consequently, a swirl flow component was generated in the direction of the spinner disc rotation. The rate of the tangential blow-away flow was regulated by the control voltage (U_t) of the blowing centrifugal fan. Secondary (i.e. suction) airflow (Q_s) was generated by an axial

fan spun by a three-phase electric motor which was powered via a variable frequency drive. The fan was placed on top of the collecting chamber immediately above the horizontal accumulation grid.
In each of the operating points, the fibre layer was visualized so that it was illuminated from below and recorded with a camera from the same side. After acquisition, images were processed using a low pass filter to remove the effect of fan blade rotation and moving (airborne) fibres.
Based on the results of image analysis, a good correlation was determined between the variables of the fibre layer (σ_{Gn} and δ) and the process input parameters (Q_p, Q_s, Q_t, t,). The correlation was assessed by using power law regression models.
Results of the above presented methodology are discussed in Chapter 5, while the procedures performed on a model spinning machine are explained more in detail with article in Chapter 3.

1.8 Argumentation of the Scientific Relevance

This thesis is in agreement with requirements of the industrial glass wool production process. Improved understanding of the process of glass wool layer formation and fibre density distribution in the collecting chamber is provided. The modelling procedure may be applied in the production process where the main expected benefit is the improvement of end product properties and a reduction of waste and second-class products quantity. This work provides experimental and numerical models for fibre properties and quality of the final product.
The first goal of the study was oriented towards fibres formation. During the production process, the operator's main goal is to produce fibres of optimal and constant properties. As described by Bauchage [3] and Walzel [4], viscosity and surface tension are very important glass properties for fibre formation. Viscosity is highly dependent on the chemical composition of the melt. Therefore, for each melt composition the optimal fiberization conditions are attained at different temperatures [5]. For viscosity calculation, the Vogel-Fulcher-Tammann equation [6] was used. The surface tension of the melt is another property which depends significantly on the melt chemical composition. Based on experimental results and the literature review, Kucuk [7] set a parametric equation for estimation of surface tension of silicate melts. A similar equation for calculation of the surface tension of borosilicate glasses was developed by Goleus [8]. The experimental modelling of chemical composition, fiberization parameters and fibre diameter is presented in [9] and [10].

Until now, experimental modelling has mostly been used for other purposes such as the modelling of the strength of a glass wool composite, thermal insulation properties and distribution of fibres diameter [11, 12 and 13]. The glass wool products feature different mechanical properties, depending mostly on glass wool fibre diameters. Products with thinner fibres have better thermal conductivity properties. Some of the glass wool products require larger fibre diameters to achieve sufficiently high mechanical strength. Due to the complexity of glass fibre formation, a multiple regression model was developed for estimation of fibre thickness. The regression model was formed by a dimensional analysis as in [14] with the final goal to obtain a finite set of characteristic numbers which describe the physical process. The presented model enables online prediction of fibre thickness in a real glass wool production process.

Studies of collecting chamber operation [2] were another important goal of this thesis. First of all, velocity of the air suction flow in the collecting chamber was studied. In order to investigate the dependence of glass wool layer structure on the air flow velocity field inside the collection chamber, measurements of the glass wool layer structure distribution at selected regions on the perforated mesh were necessary [15]. Velocity of the air suction flow in the collecting chamber was already measured for the stone wool production process, where the velocities were half lower than in the case of the glass wool production [16]. Ablitzer [17] performed an analysis of the blow away velocity field in the coaxial flow of a spinner, as well as its interaction with the suction flow in the collection chamber and the influence of both flows on the formation of mineral wool primary layer on the perforated mesh in the collection chamber. Another study regarding the influence of the blow away velocity field on the primary

layer fibre structure in the mineral wool production process was performed by Širok et al. [18]. Blagojević et al. [19] studied the glass wool transversal density distribution by a computer aided visualization method. This method was used for quantitative description of the glass wool layer homogeneity and was based on acquisition of layer images after its exit from the collection chamber [20]. The density of the glass wool material produced by individual fiberization machines was measured with the X-Ray device [21] and correlated to the velocity of the air suction flow in the collecting chamber. The final part of the study presents the regression model for relation between fiberization parameters and X-Ray measurements. The model can be applied for prediction of the transversal density distribution [20].

Fibre formation phase is followed by pneumatic transport of fibres in the blow-away flow to the collecting chamber where a layer of glass wool is formed [16]. A good quality of layer is characterized by a low degree of spatial structural fluctuations of the fibre deposit, and is very important for achieving optimal insulation and mechanical properties of end products. Due to the high complexity and multiphase nature of the flow, experimental investigation of the layer formation is difficult and mostly limited to the measurement of aerodynamic characteristics and flow visualization.

The transport of fibres in an axial airflow was modelled numerically by Lin et al. [29] and experimentally by Capone et al. [30], Qi et al. [31] and Bizjan et al. [32]. In studies conducted [29-31], fibres had a relatively low aspect ratio (i.e. length to diameter ratio) and were treated as rigid bodies. The aspect ratios of actual glass wool fibres typically exceeds 10000, leading to complex 3D flows with mutual intertwining and breakage of fibres. Consequently, the spatial structure of the fibre layer deposited on the accumulation grid may show significant inhomogeneities. To model the fibre transport more accurately, Bizjan et al. [32] performed an experiment on a model spinning machine with sucrose as a working medium, which basically resembled the industrial glass wool spinners. The bulk and surface density of the fibre layer were measured, and were determined to depend significantly on the spinner rotational rate and the flow rate of the blow-away and suction flow.

To overcome the limitations of the industrial glass wool production environment (i.e. harsh operating conditions and the limited range in which the operating parameters can be varied), a model spinning machine similar to the glass wool spinners was developed. The fibre layer was analysed by a visualization method and its quality was characterized by multiple regression models. Fibres detached from the spinning machine enter the coaxial blow-away airflow to form complex multiphase flow structures. The blow-away flow with fibres enters the collecting chamber while its velocity is reduced from an initial magnitude in excess of 100 m/s to below 10 m/s. Apart from the blow-away flow, the suction flow is also present in the collecting chamber to allow the fibres to settle on the accumulation grid and thus form the glass wool layer. The glass wool layer quality on industrial production lines is usually controlled with an X-Ray scanning device [20-21]. The method is based on radiation absorption and allows for the measurement of local layer densities. Usually, the X-Ray device is located far away from the collecting chamber, resulting in a relatively slow and difficult control of the glass wool layer quality. This results in formation of significant quantities of lower quality glass wool layer with highly inhomogeneous fibre density distribution.

Another possible measurement method is the camera visualization of the glass wool layer. A good layer quality is characterized by a homogeneous structure of the fibre deposit whereas an inhomogeneous structure indicates a poor quality of the layer. Apart from the qualitative analysis, quantitative formulations based on the image gray level can be used to analyze the homogeneity and texture of visualization images. Blagojević et al. [19] and Dimovski et al. [33] used a multiple regression model to predict the layer homogeneity whereas Hočevar et al. [34] employed an approach by neural networks. The same kind of visualization setup was also used by Bajcar et al. [15] and was followed by a computational fluid dynamics (CFD) analysis of the problem, confirming a significant effect of the local aerodynamic characteristics on the layer formation.

Chapter 2

Multiple Regression Model of Glass Wool Fibre Thickness on a Spinning Machine

In this chapter, the article entitled "Multiple regression model of glass wool fibre thickness on a spinning machine" by Boris Kraševec, Branko Širok, Marko Hočevar and Benjamin Bizjan ([2]) is presented. The paper was published in an English journal Glass Technology. The author's contribution to this article is the prediction of fibre diameter which is currently measured with the computer microscopy device which is a slow method and consequently increases production costs.
This chapter addresses the first and the second hypothesis where the fibre diameter must be analysed before a study about fibre density distribution in collecting chamber can be carried out. Volume flow rate of air, volume flow rate of gas, spinner rotational speed, mass flow rate of melt, air pressure and melt temperature are the main fiberization parameters which were analysed in correlation with the fibre diameter.
Experiments were performed on a spinning machine in an industrial glass wool production and studied with the aid of dimensionless analysis and characteristic dimensionless numbers. The purpose of this article was to determine a model for prediction of the fibre diameter.

Multiple regression model of glass wool fibre thickness on a spinning machine

Boris Kraševec,[1] Branko Širok,[2] Marko Hočevar,[2] Benjamin Bizjan[3]

[1]Ursa Slovenija d.o.o., Production of glass wool, Povhova 2, 8000 Novo mesto, Slovenia
E-mail: boris.krasevec@ursa.com
[2]University of Ljubljana, Faculty of Mechanical Engineering, Aškerčeva 6, 1000 Ljubljana, Slovenia
[3]Abelium d.o.o., Research and Development, Kajuhova 90, 1000 Ljubljana, Slovenia

Keywords: Glass wool, Fibre thickness, Regression model

Manuscript received: 31 October 2013
Revision received: 9 May 2014
Manuscript accepted: 11 May 2014

Abstract

Glass wool fibre production process on a spinning machine was studied. A multiple regression model for prediction of fibre thickness was developed. Based on the key parameters that influence the glass wool fibreization and with the aid of dimensionless analysis, characteristic dimensionless numbers were selected to form the regression model. Model constants were determined from experimental results obtained on a real spinning machine. Results show a good correlation between measured and modelled fibre diameters (r^2>0.85). The multiple regression model can be applied to other spinning machines and allows for an efficient fibre thickness control as all the key process parameters in the model can be measured in real time.

1. Introduction

Glass wool is one of most commonly used insulation materials and is particularly known for its excellent thermal conductivity properties. In the manufacture of glass wool, the process begins with the preparation of raw materials. The basic component of the glass mixture is waste glass. Other components in the mixture are etibor, feldspar, dolomite, soda, quartz sand and calcite. Glass mixture is dosed into the furnace (Figure 1) (position 1), where the glass melts at about 1300°C. The molten glass mixture is stabilised into the stabilisation channel (position 2) and poured through the funnel (position 3) into the rotating spinner (position 4). A detailed sketch of the spinner is shown in Figure 2. Fibres are formed by the melt passing through the spinner holes (Figure 3) and then being sprayed with the binder (position 5). The air flow with adjustable pressure orients the fibres down to the collecting chamber (position 6). With the aid of fans (position 7), the raw glass wool is created. The collected raw glass wool (position 8) is transported with a conveyor belt through the polymerisation chamber (position 9), where the binder polymerisation process takes place. The heat from the glass wool is removed with the aid of fans (position 10). The last steps in production process include fleece cutting to the required dimensions (position 11), material compressing and packaging. [13]

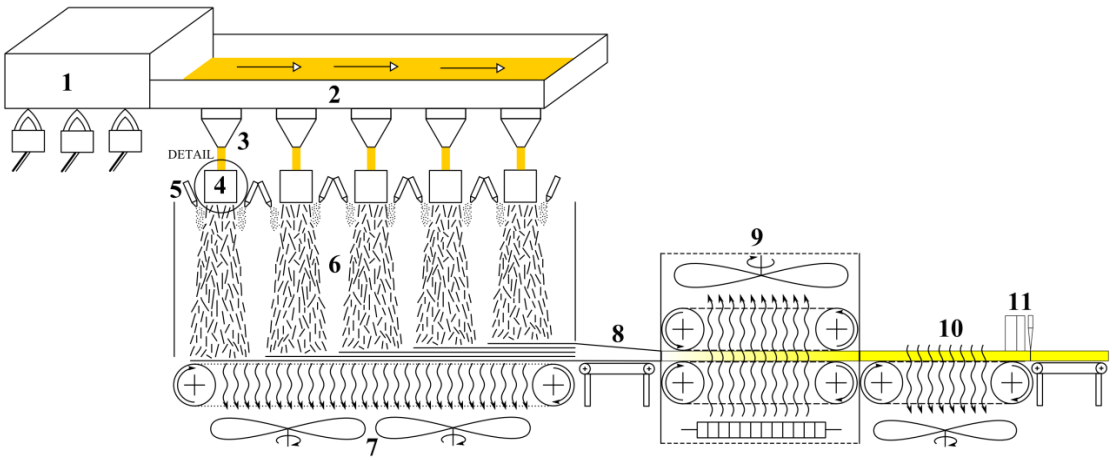


Figure 1. Glass wool production process

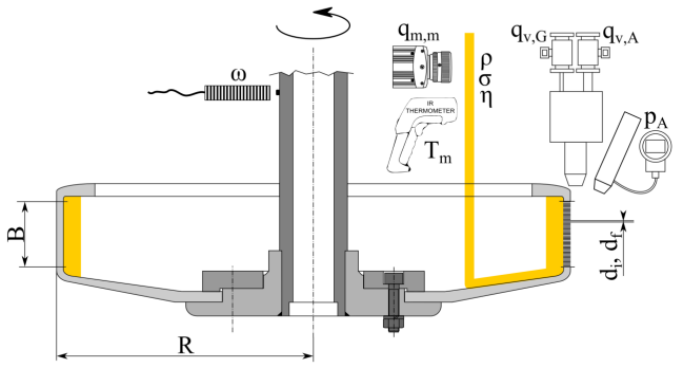


Figure 2. Fiberization process on a spinning machine

This paper focuses on fibre formation. During the production process, the operator's main goal is to produce fibres of constant and optimal properties. As described by Bauckhage[11] and Walzel,[9] viscosity and surface tension are very important glass properties for fibre formation. Viscosity is highly dependent on the composition of the melt, i.e. the optimal fiberization conditions are attained at different temperatures depending on the type of melt.[5] For calculation of viscosity, the Vogel-Fulcher-Tammann equation (Equation (1)) was used.[12]

$$\log\eta = A + \frac{B}{T + T_0} \quad (1)$$

where A and B are constants and T and T_0 are temperatures in °C. [12] The surface tension also depends on chemical composition of the melt. Based on experimental results and a review of the literature, Kucuk[6] obtained a parametric equation for the estimation of the surface tension of silicate melts:

$$\sigma = b_0 + b_1 v[Li_2O] + b_2 v[K_2O] + b_3 v[Rb_2O] + b_4 v[Mg_2O] + b_5 v[CaO] + b_6 v[BaO] + b_7 v[SrO] + b_8 v[FeO] + b_9 v[MnO] + b_{10} v[PbO] + b_{11} v[B_2O_3] + b_{12} v[Al_2O_3] + b_{13} v[MoO_3] \quad (2)$$

where b_i are constants, and $v[X_iO_i]$ are the molar concentrations of the oxides. The surface tension is practically independent of the melt temperature[6] and therefore the temperature was not considered in the calculation. A similar formula for calculation of the surface tension of borosilicate glasses was developed by Goleus.[7] The experimental modelling of chemical composition, fiberization parameters and fibre diameter is presented in Blagojević.[1,2] Experimental modelling has also been used for calculation of the strength of a glass wool composite, thermal insulation properties of the fibres and the distribution of fibre diameters.[14-16]

Glass wool products exhibit a wide range of mechanical properties, depending mostly on the glass wool fibre diameter. Products with thinner fibres have better thermal insulation properties while the larger diameter fibres mean higher end product strength as required by some of the glass wool products. Due to the complexity of glass fibre formation, in this paper a multiple regression model is developed for estimation of fibre thickness. The model was formed using dimensional analysis such as in Zlokarnik[8] with the final goal being to obtain a finite set of characteristic numbers which describe the physical process. The presented model enables online prediction of fibre thickness in a real glass wool production process. Such prediction is much faster than traditional offline fibre diameter measurements using computer based microscopy.

2. The experimental set-up

The experiments were performed on a spinning machine in a real production process (Figure 1) (pos. 4). A total of 100 experiments were performed. Production process parameters were set

in such manner that the product quality was adequate for packaging and sale, hence all measured variables correspond to a set of real production parameters.

The fiberization process on a spinning machine (also known as the spinner) was the main focus of our study, and this is shown in Figure 2. The spinner is constructed from a hollow rotating cylinder radius R, height B and rotational speed ω. A glass melt with melt temperature T_m, density ρ, surface tension σ, dynamic viscosity η and mass flow rate $q_{m,m}$ is poured into the rotating spinner. The gas burner with volume flow rate of gas $q_{v,G}$ and volume flow rate of air $q_{v,A}$ heats the spinner outer wall, facilitating the flow of liquid through the pores in the spinner wall. An important parameter of the heating is the ratio between the volume flow rate of air and the volume flow rate of gas $q_{v,A}/q_{v,G}$. In the fibre formation area the fibres, with fibre diameter d_f, are formed. Actual fibre formation is shown in the Figure 3. With the aid of air pressure p_A, the volume air flow rate orients the fibres down towards the collecting chamber. The final spinner hole diameter d_f, is larger than the initial spinner hole diameter, d_i.

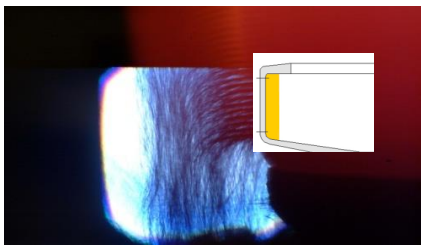


Figure 3. Fibre formation

In the present experiment the glass melt temperature was varied between 1080 and 1120°C, glass viscosity between 280 and 560 dPas, the glass mass flow rate of the melt between 600 and 700 kg/h, air pressure for fibre orientation between 1.4 and 3.6 bar, spinner rotational speed between 1600 and 2000 min^{-1}, spinner life time between 1 and 300 h, volume flow rate of air for spinner holes heating between 440 and 680 Nm^3/h (Nm^3 stands for normal cubic metre), volume flow rate of gas for heating the spinner holes between 37 and 64 Nm^3/h and ratio between the volume flow rate of air and volume flow rate of gas in the range of 9.8 to 12. Among the variables that did not change are the radius and the height of spinner which were 260 and 60 mm, respectively. The average surface tension based on the chemical composition considered in the model was 0.298 N/m and was considered constant.

For each experiment, samples of glass wool were taken and the thickness of glass wool fibres was measured. The fibre diameters of mineral wool samples were determined by computer based microscopy; the fibre diameter varied between 6.1 and 7.9 µm.

Fibre samples were taken directly after fiberization and before impregnation with the binder. Fibre diameter measurements were done in the laboratory on the computer microscopy device as shown in Figure 4. Fibres were cut in small pieces and put under microscope. Then, fibre images were recorded using a CCD camera. The images were analysed with the image analysis software which counted the fibres and sorted them by fibre diameter with resolution of 0.01 µm with an estimated measurement uncertainty of ±0.15 µm. Fibre samples are shown in Figure 5.

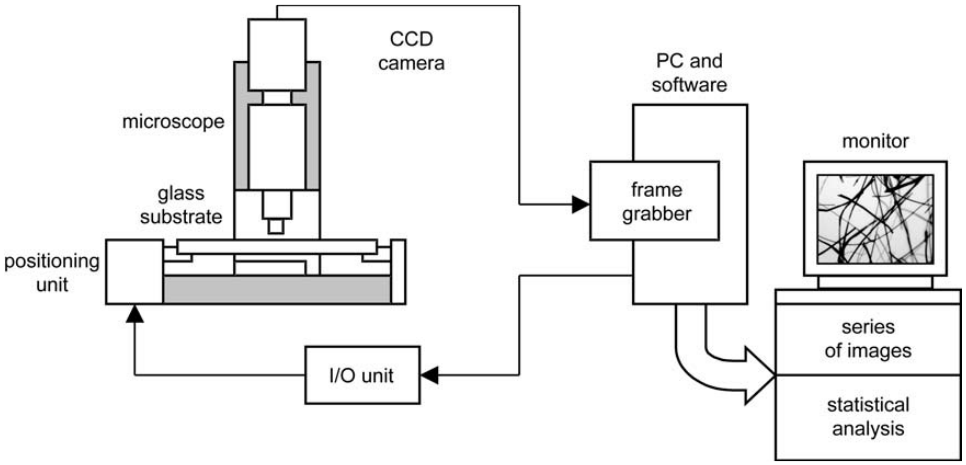


Figure 4. Computer based microscopy of glass wool fibres

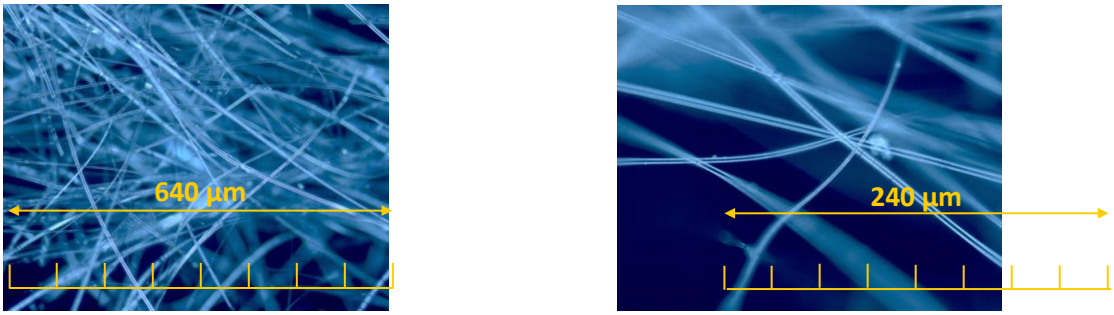


Figure 5. Micrographs of glass wool fibres

The rotational speed of the spinner was measured with built-in inductive incremental sensor connected to a counter unit, which was fixed on the top of spinner axis. The measurement uncertainty was estimated to be ±5 rad/min. Air pressure was measured with a manometer attached just above the blow air nozzle. The measurement uncertainty was estimated to be ±0.03 bar.

Volume flow rates of gas and air were measured with the volume flow counters, which were installed before the combustion chamber. Gas volume counter features compensating variation of measured pressure and temperature, the measurement uncertainty was estimated to ±0.2 Nm^3/h. The same system was used on the air line, where the estimated measurement uncertainty was ±2 Nm^3/h.

The mass flow rate of the molten glass was measured using a flow visualization method. Measurements were performed at constant height h between the outlet throat of the weir and the measurement position of the cross section area of the molten glass jet. The local melt velocity w in the observation plane was estimated with the aid of the relation $w=\sqrt{(2gh)}$; the cross sectional area, A, was determined assuming a circular shaped jet cross section and the measured jet diameter d which was determined with the aid of a computer vision method.[3] The presence of air bubbles and variations in glass viscosity have the greatest influence on the measurement uncertainty which is estimated to ±5 kg/h.

The temperature of the molten glass in the jet was measured with a handheld optical pyrometer. The instrument was directed to the jet axis with the selected measuring point 30 mm below the exit of the molten glass jet. By the pyrometer measurements, the emissivity was estimated to be ε=0.96. The measurements were performed by different operators, which in our opinion, presents the largest influence on the measurement uncertainty, which we estimate to ±10°C. The measured glass melt temperatures were later used for calculation of viscosity using the Vogel- Fulcher-Tammann equation. Based on the chemical composition, the surface tension value was indirectly determined in accordance to the Kucuk equation[6] for the calculation of the surface tension of silicate glass melts at 1000°C.

3. Parametric model of glass wool fibre thickness

The parametric model of glass wool fibre thickness is based on dimensionless analysis of the most important variables which affect the glass wool fiberization process. We want to assess the agreement between the parametric model derived and measured fibre diameter of the glass wool fibres. The agreement between both data sets will be evaluated using the correlation coefficient.

3.1 Dimensionless analysis of fiberization process on a spinning machine

Most of the parameters and characteristic numbers of molten glass which influence the fiberization process were presented by Walzel.[9] In the present model we focus on process parameters that affect the glass wool fibre diameter d_v. A similar fibre diameter regression model was developed by Blagojević et al, [9] but for a different type of a spinning machine. In our research, characteristic numbers were selected from measured, constant and calculated process parameters.

Measured process parameters are:
- volume flow rate of air: $q_{v,A}$ (Nm^3/s);
- volume flow rate of gas: $q_{v,G}$ (Nm^3/s);
- spinner rotational speed: ω (rad/s);
- mass flow rate of melt: $q_{m,m}$ (kg/s);
- air pressure: p_A (bar);
- melt temperature: T_m (°C)

The list of constant and calculated process parameters includes:
- radius of the spinner: R (m);
- spinner height: B (m);
- melt density: ρ (kg/m^3);
- dynamic viscosity of melt: η_m (kg/(ms));
- dynamic viscosity of air: η_A (kg/(ms));
- surface tension: σ (kg/s^2);
- volume flow rate of melt: $q_{v,m}$ (m^3/s);
- mass flow rate of air: $q_{m,A}$ (kg/s);
- reference mass flow rate of air: $q_{m,A,0}$ (kg/s);
- reference volume flow rate of air: $q_{v,A,0}$ (m^3/s);
- mass flow rate of gas: $q_{m,G}$ (kg/s);
- compressor pressure: p_0 (bar);
- initial spinner hole diameter: d_i (m);
- final spinner hole diameter: d_f (m);
- air temperature: T_A (°C);
- caloric value of gas: CV_G (J/Sm^3);
- specific heat of melt: $c_{p,m}$ (J/kgK);
- specific heat of air: $c_{p,A}$ (J/kgK).

Based on the principles of dimensionless analysis,[8] the following characteristic numbers were selected:
- Characteristic rotational speed number ω*, which relates the rotational speed ω, spinner radius R, melt density ρ and surface tension σ:

$$\omega^* = \omega R^{3/2} \sqrt{\frac{\rho}{\sigma}} \tag{3}$$

- Characteristic volume melt flow rate number $q_{v,m}$*, where the ratio between volume melt flow rate $q_{v,m}$ and spinner height B is multiplied by the square root ratio of melt density ρ and the product of surface tension σ and spinner radius R:

$$q_{v,m}* = \frac{q_{v,m}}{B}\sqrt{\frac{\rho}{R\sigma}} \tag{4}$$

- Characteristic viscosity number Z, where the square of dynamic viscosity η is divided by surface tension σ, melt density ρ and spinner radius R:

$$Z = \frac{\eta^2}{\sigma\rho R} \tag{5}$$

The dimensionless numbers, ω*, $q_{v,m}$* and Z, characterize the process of molten glass on the spinner. The important influence of temperature was considered using T* given by:

$$T* = \frac{\Delta T}{T_m} = \frac{T_m - T_A}{T_m} \tag{6}$$

where T_m is the melt temperature and T_A the air temperature. The ratio between mass flow rate and the dynamic viscosities of the melt and air is also of significant importance.[11] This was also shown by Lubanska,[10] who investigated the disintegration of melts in the air flow. On the basis of related empirical correlation for the determination of mean radius of droplets, as reported by Bauckhage,[11] a new characteristic number was defined and chosen by Blagojevič & Širok:[2]

$$Lu = \left(1 + \frac{q_{m,m}}{q_{m,A}}\right)\frac{\eta_m}{\eta_A} \tag{7}$$

where $q_{m,m}$ is the mass flow rate of melt, $q_{m,A}$ the mass flow rate of air, η_m and η_A are the dynamic viscosities of the melt and air, respectively.
The product of the reference mass flow rate $q_{m,A,0}$ and the square root ratio of pressures is equal to the instantaneous mass flow rate of air $q_{m,A}$. With aid of air pressure p_A the volume air flow rate orients the fibres down to the collecting chamber. The reference pressure p_R represents the compressor pressure:

$$q_{m,A} = q_{m,A,0}\sqrt{\frac{p_A}{p_R}} \tag{8}$$

During the spinner life time, t, the fiberization hole diameters increase. The spinner life time can be written as:

$$t = \frac{d - d_i}{d_f - d_i} \tag{9}$$

where d is the instantaneous, d_i the initial and d_f the final spinner hole diameter, respectively.
The gas flow rate measurement position is shown in Figure 2. We have selected Q_G* as a ratio between gas and melt energy, where $q_{m,G}$ denotes mass flow rate of gas, CV_G is the gas calorific value, $q_{m,m}$ mass flow rate of melt, $c_{p,m}$ specific heat of melt, T_m melt temperature and T_A air temperature:

$$Q_G^* = \frac{Q_G}{Q_m} = \frac{q_{m,G} CV_G}{q_{m,m} c_{p,m} (T_m - T_A)} \quad (10)$$

In the similar way as for the gas flow rate, the air flow rate measurement position is shown in the Figure 2. We selected Q_A* as the ratio between air and melt energy, where $q_{m,A}$ presents mass flow rate of air, $c_{p,A}$ specific heat of air and $T_{B,A}$ blowing air temperature (Equation (11)).

$$Q_A^* = \frac{Q_A}{Q_m} = \frac{q_{m,A} c_{p,A} (T_{B,A} - T_A)}{q_{m,m} c_{p,m} (T_m - T_A)} \quad (11)$$

The ratio r is defined by Equation (12), where $q_{v,A}$ is the volume flow rate of air and $q_{v,G}$ the volume flow rate of gas.

$$r = \frac{q_{v,A}}{q_{v,G}} \quad (12)$$

The dimensionless numbers presented above were used to construct characteristic numbers Π as shown in Equation (13). We considered nine characteristic numbers, which predict the thickness of glass wool fibres with the following nonlinear regression model (Equation (13)):

$$\frac{d_v}{R} = a_0 \Pi_1^{a_1} \Pi_2^{a_2} \Pi_3^{a_3} \Pi_4^{a_4} \Pi_5^{a_5} \Pi_6^{a_6} \Pi_7^{a_7} \Pi_8^{a_8} \Pi_9^{a_9} \quad (13)$$

Table 1. Characteristic and dimensionless numbers of the parametric model from Equation (13)

n	Characteristic number	Dimensionless number	Representation
1	Π_1	$\omega R^{3/2} \sqrt{\frac{\rho}{\sigma}}$	ω *
2	Π_2	$\frac{q_{v,m}}{B} \sqrt{\frac{\rho}{R\sigma}}$	$q_{v,m}$ *
3	Π_3	$\frac{\eta^2}{\sigma \rho R}$	Z
4	Π_4	$\frac{\Delta T}{T_m} = \frac{T_m - T_A}{T_m}$	T *
5	Π_5	$\left(1 + \frac{q_{m,m}}{q_{m,A}}\right) \frac{\eta_m}{\eta_A}$	Lu
6	Π_6	$t = \frac{d - d_i}{d_f - d_i}$	t
7	Π_7	$\frac{q_{m,G} CV_G}{q_{m,m} c_{p,m} (T_m - T_A)}$	Q_G *
8	Π_8	$\frac{q_{m,A} c_{p,A} (T_{B,A} - T_A)}{q_{m,m} c_{p,m} (T_m - T_A)}$	Q_A *

9	Π_9	$\frac{q_{v,A}}{q_{v,G}}$	r

In Equation (13), a_i (i=0-9) are the constants of the regression model and Π_i are the corresponding characteristic numbers. The regression model in Equation (13) is of the power law-type and yields an overdetermined set of nonlinear equations which can be solved using the following procedure (the number of equations is equal to the number of data points used for fitting, i.e. 100 in our case). First, logarithms of the non-linear set of equations are taken to obtain a set of linear equations. Then, the constants a_0-a_9 are obtained by solving the overdetermined system of linear equations using the least-squares method. A summary of the selected characteristic numbers and dimensionless numbers is given in Table 1.

4. Results

The results of a comparison between the measured fibre parameters and the ones calculated on the basis of 9-parametric model in accordance to Equation (13) are shown in Figure 6. Good agreement between the modelled and measured values of fibre parameters was confirmed by a high value of the correlation coefficient, r^2=0.852, indicating a good regression model.

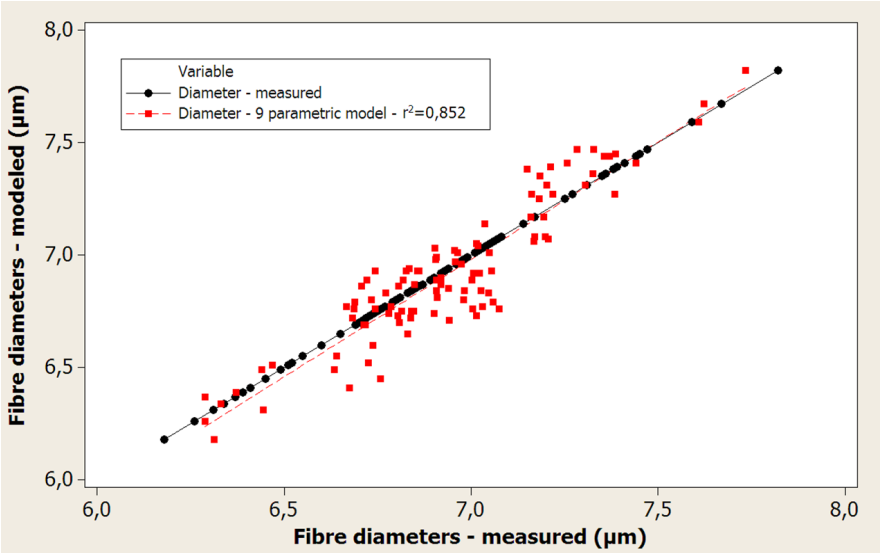


Figure 6. Comparison of the experimentally measured and statistically predicted fibre diameters

Using experimental data with multiple regression analysis, the parameters of the regression model (Equation (13)) were determined. The agreement between measured and calculated fibre parameter values were examined using the F-test. The test results are presented in Table 2. The F-test is an estimate of the hypothesis that the regression is not significant. The probability (P value) that this hypothesis is valid was 10^{-4}, thus the regression is very significant.

Table 2. F-test results of the agreement between the modelled and measured values. DF represents Degrees of Freedom, SS is Sum of squares and MS is Mean Square and P is probability.

Source	DF	SS	MS	F	P
Regression	8	9.7628	1.2203	233.34	0.0001
Residual	91	0.4759	0.0052		
Total	99	10.2387			

Values of regression model constants are presented in Table 3. Parameters with negative values inversely influence the fibre diameter when their characteristic numbers are increased. Their significance was checked with a *t*-test (Table 3).

Table 3. Regression model constant values according to Equation (13) along with the results of the t-test

	a_0	a_1	a_2	a_3	a_4	a_5	a_6	a_7	a_8	a_9
Values	1	-0.002	-0.0067	0.0343	0.0343	-0.4926	0.0012	-0.3111	0.0297	-2.1201
Prob >|t|		4.2	0.2	0.48	0.48	0.0155	12.7	0.28	2.6	0.0169

The results, presented in Table 3 show that parameters a_5 and a_9, i.e. the characteristic numbers Π_5 (effect of air pressure for fibre orientation) and Π_9 (ratio between air and gas volume flow rate) have a significant effect. Constants a_2, a_3, a_4 and a_7 which relate to the mass flow rate of glass, glass melt temperature and volume flow rate of gas (characteristic numbers Π_2, Π_3, Π_4 and Π_7, respectively) are also important. To a lesser extent, parameters a_1, a_6 and a_8, i.e. characteristic number of spinner rotational speed (characteristic number Π_1), spinner life time (characteristic number Π_6) and volume flow rate of air (characteristic number Π_8), are also significant. Statistically, the spinner life time effect was the least significant because it was compensated by adjustment of the other process parameters to maintain the desired fibre diameters.

Figure 7 shows measured fibre diameters for all 100 measurement sets. Measured fibre diameters are shown in black, while modelled fibre diameters are shown in red (grey in printed journal). Each of the intervals has a upper specification limit (USL) and lower specification limit (LSL), which are defined by 95% confidence levels or ±2σ, which is ±0.64 μm in terms of the fibre diameter. There is a reasonable agreement between the measured and predicted fibre diameter values and both lie within the mentioned tolerance interval.

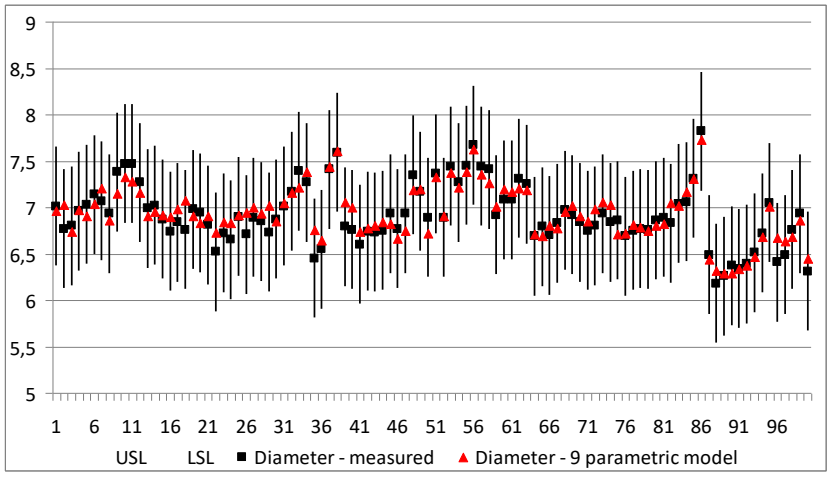


Figure 7. Comparison of the experimentally measured fibre diameters (in μm) and predicted values from the regression model with 95% confidence fitting levels

Two typical histograms of measured fibre diameters are presented in Figure 8, each containing measured diameter values of approximately 15000 individual fibres. The difference between the examined fibre samples included in the upper and lower histograms was in the settings of three process parameters. Characteristic number Π_5 in the upper histogram was 4.8% higher, Π_7 11.9% higher and Π_9 5.6% lower than in the bottom histogram. In the upper histogram, the mean fibre diameter is 8.384 μm with a standard deviation of 2.690 μm. In the bottom histogram, the mean fibre diameter is 5.706 μm with a standard deviation of 2.521 μm.

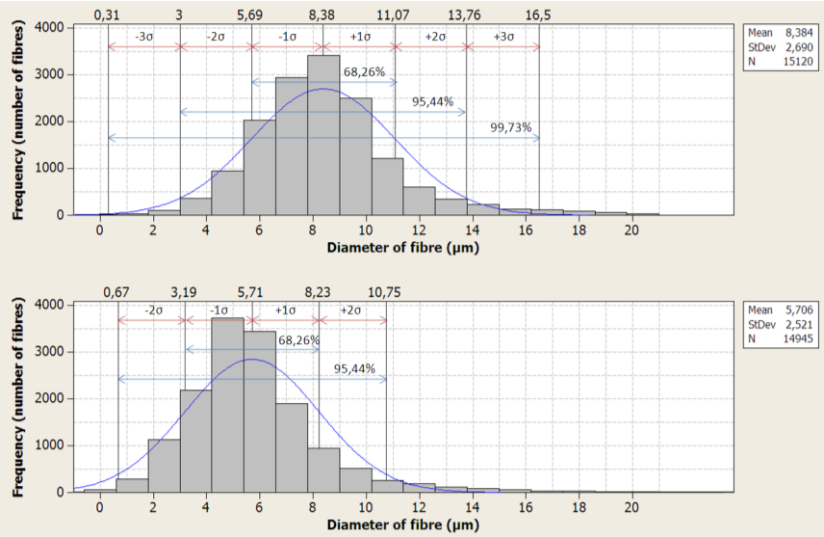


Figure 8. Typical histograms of measured fibre diameters

In Figure 9, the influence of temperature on glass melt viscosity is presented for the temperature range of 800-1400°C. Glass melt viscosity was calculated using the Vogel-Fulcher-Tammann equation (Equation (1)). The chemical composition of the glass melt from the present experiment was used. Unlike the melt viscosity, glass melt temperature has almost no influence on the surface tension.[6]

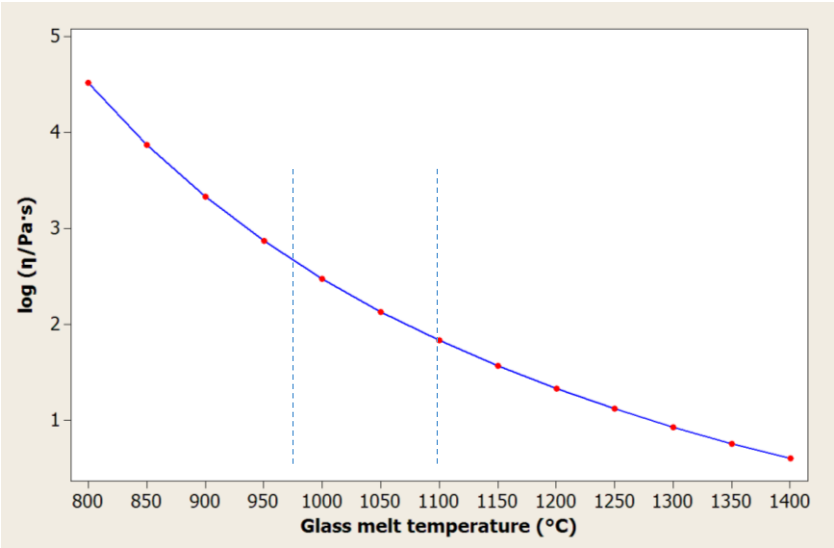


Figure 9. Glass melt viscosity for the chemical composition of glass melt from our experiments calculated using the Vogel–Fulcher–Tammann equation. Two vertical dashed lines show the glass melt temperature range in our experiments

5. Conclusion

The regression model presented here enables prediction of glass wool fibre thickness on a spinning machine. The model provides a good agreement between calculated and measured values and based on the set of measured variables of the production process, we were able to predict fibre diameters reasonably well. The modelling procedure can be further applied to other spinning machines.

Parameters in the model are well correlated and can be used to form some other parametric relations. Special attention should be given to the air flow pressure in relation to the consequent fibre orientation and the ratio between air and gas volume flow rate, which have

the largest impact on the fibre diameter. Also the glass melt temperature, viscosity and surface tension have quite a significant effect on fibre diameter.
A question however remains as to what extent the results of the model can be implemented in the production process. Several steps are required for this purpose, and so far we have only been able to address the fibre diameter modelling performance based on the set of measured variables. Further research should also include an investigation of fibre diameter effect on the quality of the final product, a necessary step for industrial implementation.

References:

1. Blagojević, B., Širok, B. & Štremfelj, B. Simulation of the effect of melt composition on mineral wool fibre thickness. *Ceram. Silikáty,* 2004, 48 (3), 128-34.
2. Blagojević, B. & Širok, B. Multiple regression model of mineral wool fibre thickness on a double-disc spinning machine. *Glass Technol.,* 2002, 43 (3), 120-4.
3. Trdič, F., Širok, B., Bullen, P. R. & Philpott, D. R. Monitoring mineral wool production using real-time machine vision. *Real Time Imaging,* 1999, 5 (2), 125-40.
4. Vaisburd, S. & Brandon, D. G. A combined unit for viscosity, surface tension and density measurements in oxide melts. *Meas. Sci. Technol.,* 1997, 8, 822-6.
5. Lakatos, T., Johansson, L. G. & Simmingsköld, B. Viscosity and liquidus temperature relations in the mineral wool part of the system SiO_2-Al_2O_3-CaO-MgO-Alkalies-FeO-Fe_2O_3. *Glastek.Tidskr*., 1981, 36, 51-5.
6. Kucuk, A., Clare, A. G. & Jones L. E. Estimation of surface tension for silicate glass melts at 1400°C using statistical analysis. *Glass Technol.,* 1999, 40 (5), 149-53.
7. Goleus, V. I., Belyi, A. Y., Sardak, E. M. & Belyi, Y. I. Calculation of the surface tension of molten borosilicate glasses. *Steklo Keram.,* 1996, 53 (8), 6-8.
8. Zlokarnik, M. *Dimensional Analysis and Scale-up in Chemical Engineering*. Springer-Verlag, Heidelberg, Germany, 1991.
9. Walzel, P. Zerstäuben von Flüssigkeiten. Chem.-Ing.-Tech., 1990, 62 (12), 983-94.
10. Lubanska, H. Correlation of spray ring data for gas atomisation of liquid. *J. Metals,* 1970, 22 (2), 45-9.
11. Bauckhage, K. Das zerstäuben metallischer schmelzen, *Chem.-Ing.- Tech*., 1992, 64 (4), 322-32.
12. Kaplan-Diedrich, H., Eckebracht, A. & Frischat, G. H. Viscosity and surface tension of oxynitride glass melts. *J. Am. Ceram. Soc*., 1995, 78 (4), 1123-4.
13. http://www.ursa.si/slsi/izdelki/Documents/EPD_poro%C4%8Dilo_URSA_slo_ 28_ 08_2013.pdf, 22.09.2013.
14. Järvelä, P., Pohjonen, T. & Törmälä, P. An empirical model of the strength of a porous glass wool composite. *Compos. Sci. Technol*., 1985, 23 (2), 113-30.
15. Pincemin, F., Boulet, P. & Jeandel, G. Modelling and Experimental Evaluation of the Thermal Insulation Properties of Mineral Wool Products at High Temperature. *American Society for Testing and Materials Publications*, Philadelphia, 1997, 243-58.
16. Christensen, V. R., Eastes, W., Hamilton, R. D. & Struss, A. W. Fibre diameter distributions in typical MMVF wool insulation products. *Am. Ind. Hygiene Assoc. J*., 1993, 54 (5), 232-8.
17. Širok, B., Blagojević, P. & Bullen, P. Mineral wool: production and properties. *Woodhead Publishing*, Cambridge, UK, 2008.

Chapter 3

Glass Wool Layer Formation in the Collecting Chamber

In this chapter, the article entitled “Glass wool layer formation in the collecting chamber” by Boris Kraševec, Benjamin Bizjan and Branko Širok ([45]) is presented. The paper is published in an English journal Glass Technology. The author’s contribution to this article is the prediction of normalized standard deviation of the optical intensity (σ_{Gn}) and dimensionless distance between the fibre layer centre gravity and the centre of accumulation grid (δ).
This chapter addresses the second hypothesis as the model for prediction of the glass wool layer distribution in the collecting chamber is presented. The blow-away, suction and tangential airflows are the main parameters which were analysed in correlation with σ_{Gn} and δ. The experiments were performed on a model spinning machine with sucrose as a working medium. The purpose of this article was to use a different setting of parameters and determined correlations and show the effect of coaxial and tangential blow away flows on positioning and spatial uniformity of the fibre layer.

Glass wool layer formation in the collecting chamber

Boris Kraševec*[1,4], Benjamin Bizjan[2], Branko Širok[3]

* Corresponding author. Email boris.krasevec@ursa.com

[1]*Ursa Slovenija d.o.o., Production of Glass Wool, Povhova 2, 8000 Novo mesto, Slovenia*
[2]*Abelium d.o.o., Research and Development, Kajuhova 90, 1000 Ljubljana, Slovenia*
[3]*University of Ljubljana, Faculty of Mechanical Engineering, Aškerčeva 6, 1000 Ljubljana, Slovenia*
[4]*Jožef Stefan International Postgraduate School, Jamova 39, 1000 Ljubljana, Slovenia*

Keywords: Glass wool, Fibre, Collecting chamber, Regression model, Spinning machine

Manuscript received: 18 January 2016
Revision received: 15 September 2016
Manuscript accepted: 10 October 2016

Abstract

Glass wool layer formation was investigated experimentally on a model spinning machine with sucrose as a working medium. The fibres were pneumatically transported from the spinner to the accumulation grid with the aid of the blow-away (Q_p), suction (Q_s) and tangential (Q_t) airflows. The fibre layer formed on the accumulation grid was visualized by a camera for several different operating regimes. The optical intensity (gray level) of acquired visualization images was then used to calculate the normalized standard deviation of the optical intensity (σ_{Gn}), local fibre accumulation rates (ψ), and dimensionless distance between the fibre layer centre of gravity and centre of accumulation grid (δ). Based on the measured process quantities, we were able to form multiple regression models with a good correlation to the experimental data. The models as well as the qualitative image analysis results show an important effect of coaxial and tangential blow away flows on positioning and spatial uniformity of the layer of fibres.

Introduction

Glass wool is one of the most commonly used insulation materials and is particularly known for its excellent thermal conductivity properties. Glass wool production process is highly complex and consisting of several different production phases. Sufficient understanding and control of each phase is required in order to optimize the properties (e.g. thermal conductivity, homogeneity and mechanical properties) and production costs of end products.

Production phases which most significantly affect the glass wool quality are the chemical composition of glass melt, fiberization on the spinning machine, fibre pneumatic transport and glass wool layer formation in the collecting chamber [1]. There are several operating and process parameters which can be varied to control the glass wool properties. The chemical composition and temperature of the melt is known to affect both glass melt properties (Kucuk [2], Lakatos [3]) as well as the thickness of fibres forming from the spinner rotor (Blagojevič et al. [4]). There are many other parameters which significantly affect the mineral wool properties, especially the spinning machine rotational frequency and airflows (blow-away flow, suction flow, etc.). The combined effect of these was studied in several experimental and numerical studies (Marheineke [5], Qin et al. [6][7], Kraševec et al. [8] [9], Bizjan et al. [10]).

Fibre formation phase is followed by pneumatic transport of fibres in the blow-away flow to the collecting chamber where a layer of glass wool is formed [1]. A good quality of layer is characterized by a low degree of spatial fluctuations of the fibre deposit, and is very important for achieving optimal insulation and mechanical properties of the end products. Due to the high complexity and multiphase nature of the flow, experimental investigation of the layer formation is difficult and mostly limited to the measurement of aerodynamic characteristics and flow visualization.

The transport of fibres in an axial airflow was modelled numerically by Lin et al. [11] and experimentally by Capone et al. [12], Qi et al. [13] and Bizjan et al. [14]. In studies conducted in [11-13], fibres had a relatively low aspect ratio (i.e. length to diameter ratio) and were treated

as rigid bodies. The aspect ratios of actual glass wool fibres typically exceed 10000, leading to complex 3D flows with mutual intertwining and breakage of fibres. Consequently, the spatial structure of the fibre layer deposited on the accumulation grid may show significant inhomogeneities. To model the fibre transport more accurately, Bizjan et al. [14], performed an experiment on a model spinning machine with sucrose as a working medium, which basically resembled the industrial glass wool spinners. The bulk and surface density of the fibre layer were measured, and were determined to depend significantly on the spinner rotational rate, and the flow rate of the blow-away and suction flow.
Unlike the study by Bizjan et al. [14], the present study also includes the effect of the tangential airflow, and analyzes the temporal evolution of the glass wool layer formation. For this purpose, the forming fibre layer was analysed by a dynamic visualization method, and its quality was characterized by multiple regression models. By introduction of the tangential airflow component, the mechanism of fibre layer positioning on the conveyor belt will more closely resemble the one in the real industrial process, resulting in a greater applicability of experimental results to industrial environment.
This paper is organized as follows. The Methods section presents the theoretical background of the glass wool layer formation and the layer visualization method used in our experiments. In the Experimental section, the model spinning machine and the corresponding measurement setup will be introduced whereas the Discussion section will present qualitative and quantitative results of visualization image analysis.

1 Theoretical background

The glass wool manufacturing process begins with the preparation of raw materials. The basic component of the glass mixture is waste glass. Other components in the mixture are borax pentahydrate (etibor), feldspar, dolomite, soda, quartz sand and calcite. The glass mixture is dosed into the furnace (Figure 1.1) (position 1), where the glass melts at about 1300°C. The molten glass mixture is first supplied into stabilisation channel (position 2) and then poured through the funnel (position 3) into the rotating spinners (position 4). Present in the area of position 4 are the air and gas flows used for the combustion process, pressure arising from the air curtain, air flows from the left and right glass wool side cutting, and the air flow of the recycled material. Fibres are formed by extrusion of the melt through the spinner holes and are then sprayed with the binder (position 5). The air flow with adjustable pressure orients the fibres down to the collecting chamber (position 7). The transversal density distribution can be adjusted by air blowing nozzles (position 6). With the aid of suction fans (position 8), the fibres are collected on the perforated plates to form the raw glass wool (position 9) which is then transported with a conveyor belt through the polymerisation chamber (position 10), where the binder polymerisation process occurs at approximately 250 °C. The glass wool is then cooled with the aid of suction fans (position 11). With the X-Ray device the fibre density distribution (layer bulk density) is measured (position 12). The final steps in production process include fleece cutting to the required dimensions (position 13), material compression and packaging.[11]

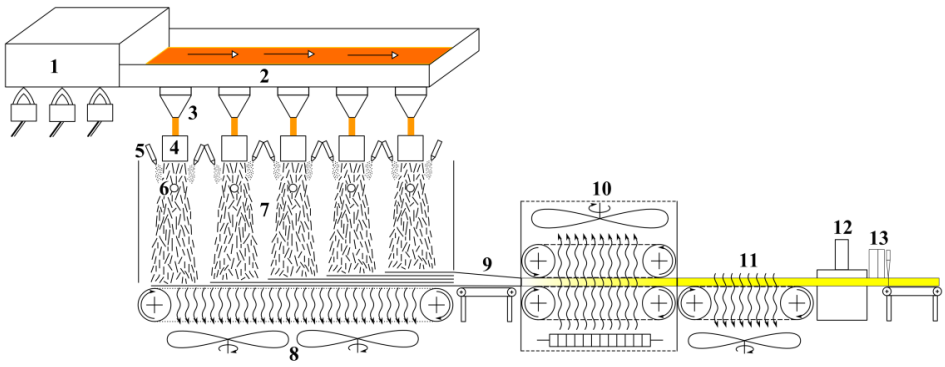


Figure 1. Glass wool production process

The fibre layer formation process is an important part of the glass wool production line (Fig. 1) (position 7). Fibres detached from the spinning machine enter the coaxial blow-away airflow and form complex multiphase flow structures. The blow-away flow with fibres enters the collecting chamber while its velocity is reduced from an initial magnitude in excess of 100 m/s to below 10 m/s. Apart from the blow-away flow, the suction flow (Fig. 1) (position 8) is also present in the collecting chamber to allow the fibres to settle on the accumulation grid and thus form the glass wool layer.

The glass wool layer quality on industrial production lines is usually controlled with an X-Ray scanning device [9][15] which is used to measure the fibre density distribution (i.e. the bulk density of the layer). The X-Ray method is based on detection of radiation intensity [15] and allows for the measurement of local layer densities. Radiation intensity which is passing through the material depends of intensity of the radiation before entering into the material, raw density and thickness of the material and mass attenuation coefficient, which depends on the chemical composition of the glass wool material. Usually, the X-Ray device is located far away from the collecting chamber, resulting in a relatively slow and difficult control of the glass wool layer quality. This results in formation of significant quantities of lower quality glass wool layer with highly inhomogeneous fibre density distribution.

The layer homogeneity depends on homogeneity of different layer properties such as the fibre density distribution (bulk density of the layer), fibre orientation (angle), fibre length distribution etc. While all of these properties have an important effect on the quality of the end product, only the density distribution of fibres can be reliably measured by visualization methods in real time (e.g. on the conveyor belt). Therefore we only refer to the uniform density distribution when discussing the layer homogeneity. Due to the highly complex layer structure and low fibre diameters, all the other layer properties can only be determined in laboratory testing of samples after production.

To reduce the amount of the poor quality material, the time lag involved in adjustment of the operating parameters must be reduced, meaning that the information about the fibre distribution is required at an earlier point. One possible measurement method is the camera visualization of the glass wool layer on the conveyor belt. A sample of layer image is shown in Fig. 2. A good layer quality is characterized by a homogeneous structure of the fibre deposit (Fig. 2a) whereas an inhomogeneous structure (Fig. 2b) indicates a poor quality of the layer.

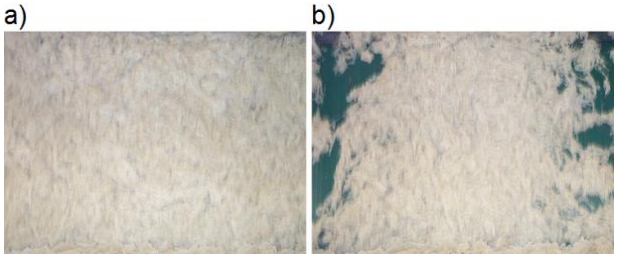


Figure 2. Glass wool layer on the accumulation grid; a) homogeneous structure; b) inhomogeneous structure [1]

Apart from the qualitative analysis, quantitative formulations based on the image gray level can be used to analyze the homogeneity and texture of visualization images. Blagojević et al. [16] and Dimovski et al. [17] used a multiple regression model to predict the layer homogeneity whereas Hočevar et al. [18] employed an approach by neural networks. The same kind of visualization setup was also used by Bajcar et al. [19] and was followed by a computational fluid dynamics (CFD) analysis of the problem, confirming a significant effect of the local aerodynamic characteristics on the layer formation.

2 The experimental set-up

Experiments were conducted on a model spinning machine with a hollow perforated rotor and a vertical collecting chamber (Fig. 3). The spinning machine used was a modified version of the

cotton candy machine "The Breeze 3030EX" [20]. The rotor (Fig. 3) had an integrated heater and was supplied with crystalline sucrose prior to each experiment. During the spinner operation, sucrose was melted by the heater at a rate of approximately 0.65 g/s while the rotor rotational speed was fixed in a value of 50 Hz. Coaxial blow-away airflow was supplied through 45 circular nozzles with 1 mm diameter, evenly distributed around the supply ring. The rate of this flow component was regulated by a valve so that the overpressure in the supply ring Δp was between 20 and 50 kPa. Apart from the coaxial blow-away flow, the tangential blow-away flow was introduced into the colleting chamber through two tangentially oriented pipes. Consequently, a swirl flow component was generated in the direction of the spinner disc rotation. The tangential blow-away flow was regulated with the variable frequency drive (VFD) where the voltage (U_t) was varied between 0 and 7 V.
The spinning machine was placed inside a vertical collecting chamber with a circular cross section (0.63 m in diameter) and a transparent wall. Secondary (i.e. suction) airflow was generated by a 7-blade axial fan powered by a three-phase VFD. The fan was placed on top of the collecting chamber immediately after the horizontal accumulation grid. VFD power supply frequency (f_s) was varied between 15 and 25 Hz. About 40 seconds after the start of the spinner and air supply operation, fibres started to appear on the spinner rotor and were blown to the collecting chamber. After additional 20-30 seconds, the heater was turned off, and after the end of fibre formation, rotor and airflows were stopped.

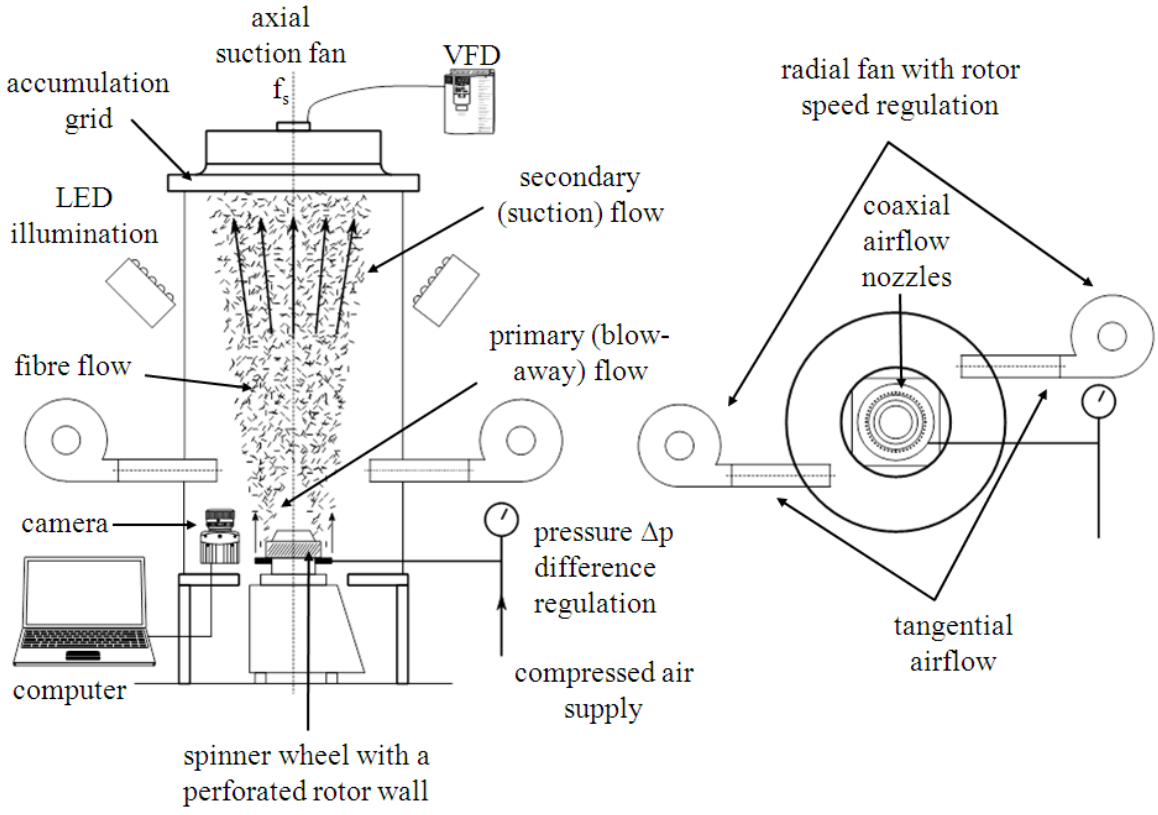


Figure 3. Experimental setup; spinner operation

Table 1. Operating points for fibre layer visualization

Op. point No.	Δp [kPa]	f_s [Hz]	U_t [V]	Q_p [m³/h]	Q_s [m³/h]	Q_t [m³/h]
1	20	15	0	17.8	2700	0
2	20	25	0	17.8	4500	0

3	50	15	0	27	2700	0
4	50	15	0	27	2700	0
5	50	25	0	27	4500	0
6	20	15	3.5	17.8	2700	88.7
7	20	25	3.5	17.8	4500	88.7
8	50	15	3.5	27	2700	88.7
9	50	15	3.5	27	2700	88.7
10	50	25	3.5	27	4500	88.7
11	50	25	5	27	4500	130.2
12	20	15	5	17.8	2700	130.2
13	50	20	3.5	27	3600	88.7
14	50	25	7	27	4500	242.5

The volume flow rates in Table 1 are given for the mean atmospheric conditions during our measurements: 26 °C temperature, 101.8 kPa absolute pressure and 59 % relative humidity.
In each of the operating points listed in Table 1, the fibre layer was visualized so that it was illuminated from below with two 500 W reflectors positioned 180° apart, and recorded with a camera (Basler acA 1300gc), also placed below the accumulation grid. Layer images were recorded using manual frame rate, shutter time and aperture settings (31.85 frames/s, 0.02 s and f/6, respectively). The images (sized 800x800 pixels, with 0.75 mm pixel size) were recorded in an 8-bit grayscale format, beginning at t = 0 when fibres started to accumulate on the accumulation grid. The image gray level G, also known as the optical intensity, can range from G = 0 (black colour) to G = 1 (white colour), with 2n possible discrete gray levels, where n is the image bit depth. In our case (n = 8), there were 256 possible gray levels.
After acquisition, images were processed using a low pass filter to remove the effect of fan blade rotation and moving (airborne) fibres on the layer visualization. Sample processed images are shown in Fig. 4.

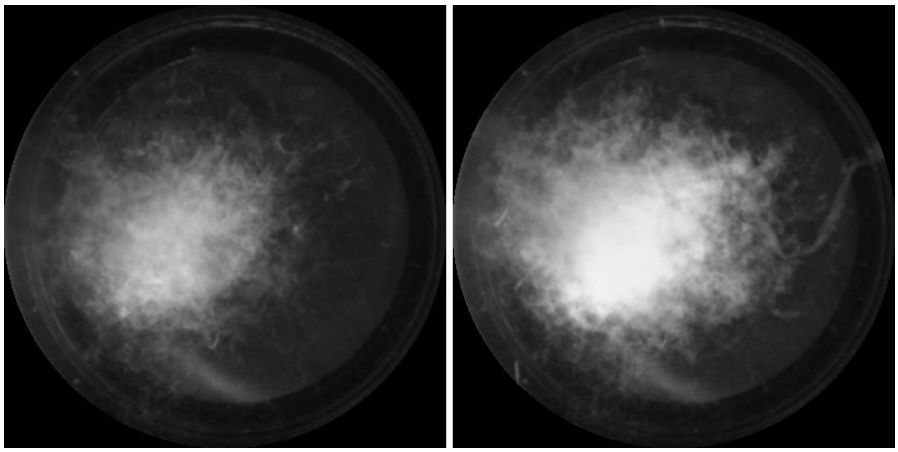


Figure 4. Sample fibre visualization images, experiment no. 10; left: t = 5 s; right: t = 10 s

In locations with continuous fibre accumulation, image optical intensity G (also known as the gray level) increased almost linearly with time to G ≈ 0.75. Since the fibre production rate was constant, this suggests a linear relationship between fibre deposit thickness and the corresponding image gray level. After this threshold, saturation state (G ≈ 0.94) was gradually approached, resulting in inability to detect further fibre deposition, or the layer texture in saturated regions. Note that the camera sensor itself did not become saturated as local G values remained below 1 at all times. Regarding the measurement uncertainty, its main sources are the measurement of air flow rates and rotational frequencies. The measurement

uncertainty can be estimated to about ±2 % for each of the flow rates, and to ±0.5 % for rotational frequencies of the suction fan and the spinner. The measurement uncertainty for the blow-away pressure measurement was estimated to ±0.5 %. The total measurement uncertainty confidence level can be estimated to 5 %.

3 Results and discussion

3.1 Qualitative and quantitative properties of the glass wool layer

Spinning machine operating parameters were varied in a wide range (Table 1) and produced distinct forms of sucrose fibre layer. Temporal dependence of the gray level normalized standard deviation σ_{Gn}=std(G)/G is shown in Fig. (5). Until about t = 10 s, σ_{Gn} increased at a nearly constant rate, then stabilized between 40 % and 55 %.

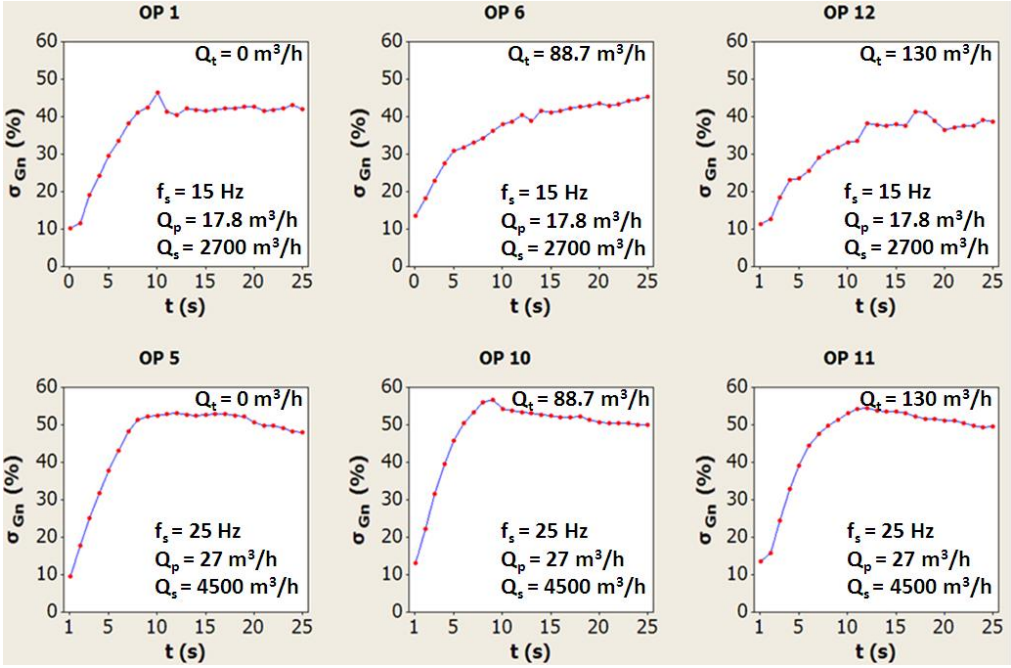


Figure 5. Normalized standard deviation of optical layer intensity for different operating points (OP)

From Fig. 5 it can be seen that σ_{Gn} increases with Q_p and Q_s, which we will also prove with a regression model (Eq. (5)). Q_t seems to have a larger impact when Q_p and Q_s are low (OP 1, OP 6 and OP 12). While the differences in integral σ_{Gn} values (Fig. 5) caused by the tangential blow-away flow are relatively low, the effect of Q_t can be more readily appreciated from the fields of fibre accumulation rate (ψ), which is defined by Eq. (1):

$$\psi = \frac{\mu(t_1) - \mu(t_0)}{t_1 - t_0} = \dot{m}\frac{G(A(t_1))}{\bar{G}(A(t_1))A(t_1)} \tag{1}$$

In Eq. (1), μ is the mean fibre layer area density in [kg/m^2], G is the scalar field of the image gray level ($0 \leq G \leq 1$, each image pixel assumes one value within this interval, corresponding to the pixel's brightness) and $\bar{G}$ its spatial average. All of the scalar fields and their corresponding averages were computed over the area A(t), which denotes the total area covered by fibres at time t (note that A(t = 0) = 0). To avoid problems with image saturation, we selected t_0 = 0 s and t_1 = 15 s.

In Fig. 6, the fields of ψ are shown for the same operating points as those analyzed in Fig. 5. We can see that, in comparison with operating points with Q_t = 0 (i.e. OP 1 and OP 5), the operating points with nonzero tangential blow-away flow feature a fibre layer with a more circular (i.e. less distorted) shape with slightly lower spatial gradients of ψ.

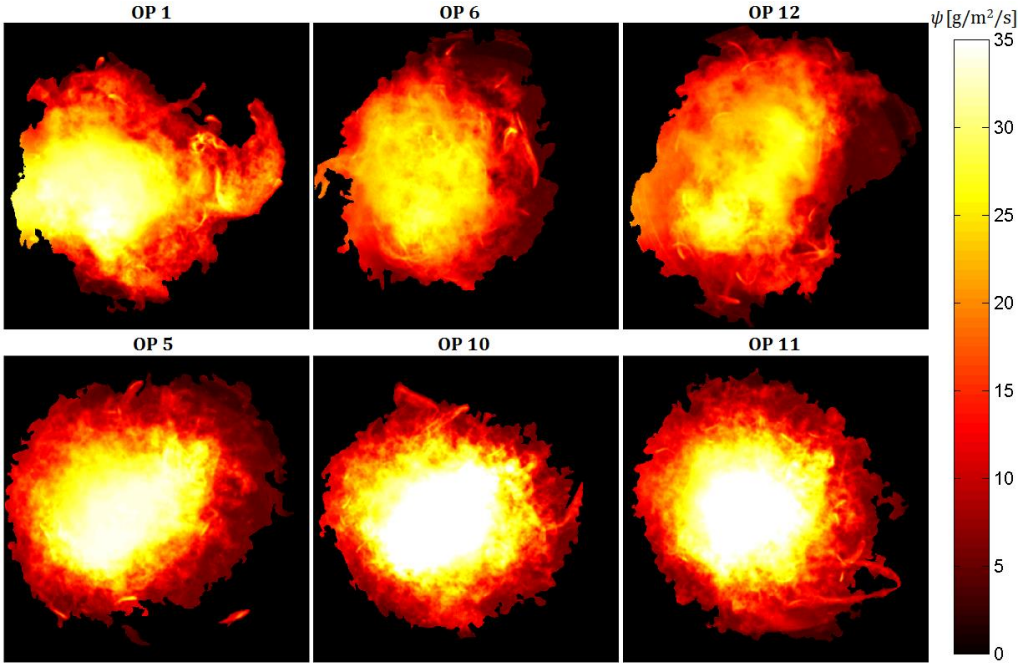


Figure 6. Average fibre accumulation rate ψ on the accumulation grid, for comparison with Fig. 5. The physical dimensions of each subpanel shown are 0.6x0.6 m

Another observation that can be made from Fig. 6 is that the larger Q_p and Q_s values (i.e. OP 5, OP 10 and OP 11) cause higher peaks of σ_{Gn} at the centre of the fibre layer, indicating a less uniform fibre thickness as the fibres concentrate at the centre of the layer.

Apart from the fibre accumulation rate, the position of the fibre layer relative to the accumulation grid is also important. Layer position will be defined by a dimensionless position of its centre of gravity, δ (Eq. (2)). δ is given as a weighted average of layer local radial positions $r_{t,A}$ across the layer surface A, so that $r_{t,A}$ = 0 and δ = 0 define the centre of the accumulation grid.

$$\delta = \frac{r_t}{R} = \frac{1}{R \cdot \overline{G} \cdot A} \int_A r_t \cdot G(r_{t,A}) \cdot dA \qquad (2)$$

In Fig. 7, the diagrams of δ are shown for 6 different operating points. In all operating points, the centre of gravity gradually approaches the centre of the accumulation grid as the mass of deposited fibres increases with time. The upper 3 panels of Fig. 7 compares operating points 7, 11 and 14, where the suction flow was kept constant at Q_s = 4500 m³/h, but Q_p and Q_t were varied. In OP 7, where both Q_p and Q_t were relatively low and Q_t/Q_p = 4.98, the highest δ value occurred both at the beginning and the end of the 23 s time interval, meaning that the fibre layer was well off the accumulation grid centre. Transition from OP 7 to OP 11 is marked by an increase in Q_p and Q_t, while the ratio Q_t/Q_p remains nearly unchanged at 4.82. We can see that δ is reduced across the whole time interval, meaning a more central fibre layer position. In OP 14, the tangential blow-away flow was further increased, resulting in Q_t/Q_p = 8.98. While the initial δ value (i.e. at t = 0 s) was the lowest of the three operating points with Q_s = 4500 m³/h, the fibre layer position remained nearly constant until t = 15 s, and even then did not drop as much as in the case of the OP 11.

The lower 3 panels of Fig. 7 compares operating points 7, 11 and 14, where the suction flow was kept constant at Q_s = 4500 m³/h, but Q_p and Q_t were varied. In OP 3, where only the suction and the coaxial blow-away were present (Q_s = 2700 m³/h and Q_p = 27 m³/h), initial δ value was relatively high, but then dropped almost to zero at t = 22 s. In OP 9, where Q_t = 88.7 m³/h was introduced at unchanged Q_p and Q_s, the final δ value was significantly higher despite a lower initial value. Finally, in OP 13, the suction flow rate was increased to Q_s = 3600 m³/h, and δ value was significantly increased over the complete time interval.

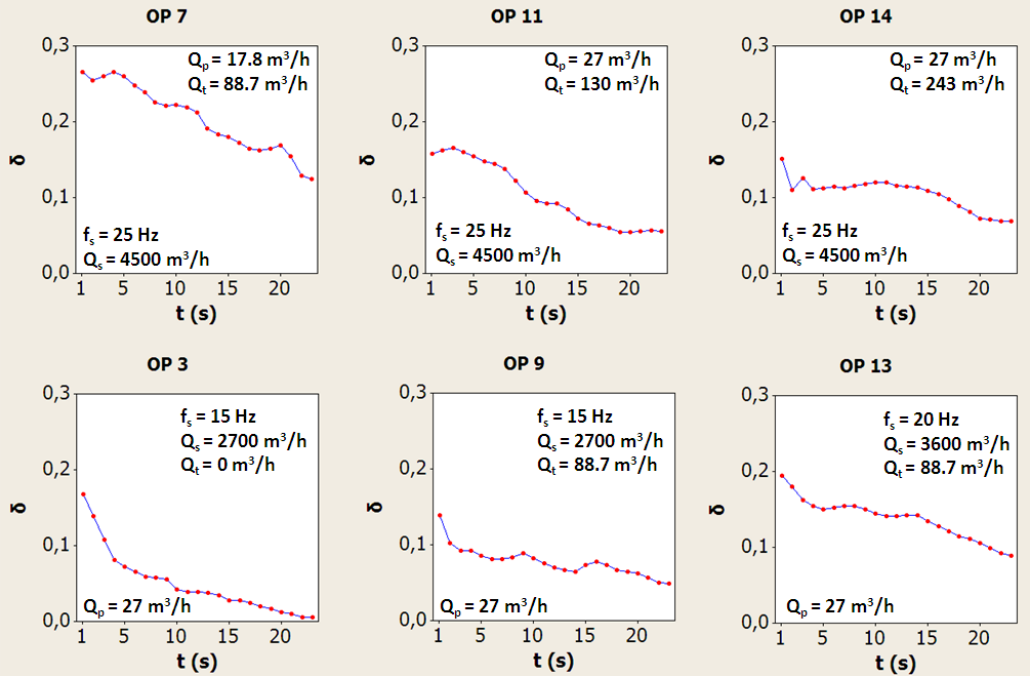


Figure 7. Distance between the fibre layer centre of gravity and the centre of the accumulation grid as a function of time

Considering the results presented in Fig. 7, we can conclude that the position of the fibre layer on the accumulation grid becomes increasingly non-centric with rising suction flow rate, provided that there is even a small flow asymmetry (e.g. due to the placement of suction fan in close proximity to the grid, as in our case). However, the non-centric fibre layer positions marked by higher δ values do not necessary imply lower fibre layer quality, but simply a need to properly adjust the positioning of the coaxial and tangential blow-away nozzles. The position of fibre layer formation is of particular importance in industrial glass wool production lines, where up to 5 spinning machines deposit fibres on a moving accumulation grid. Position of each spinner's fibre layer formation zone must be adjusted so that the final layer entering the polymerization chamber is of uniform thickness and density across its complete width.
Another important finding regarding the blow-away flows is that, for sufficiently high Q_p and Q_t, the time required for stabilization of the fibre layer position is relatively low compared to the case when one or both blow-away flow components are low or zero. When applied to the real industrial process with moving accumulation grid, it can be expected that higher Q_p and Q_t settings should allow achieving a stable fibre layer formation at larger grid velocities.
To adequately assess the fibre layer quality, the δ diagrams from Fig. 7 should be compared to the corresponding scalar fields of the fibre accumulation rate (ψ, Fig. 8). The fibre accumulation rate was most uniformly distributed in OP 11 and OP 14, where δ was also relatively low. A combination of low δ and ψ is certainly desired for attaining optimal fibre layer homogeneity, especially on a production line with multiple spinning machines. In OP 3 and OP 9, the fibre layer was even more centric as in OP 11 and OP 14, but the layer thickness in the centre was much larger, indicating a less uniform spatial distribution of fibres. Without doubt, operating points 7 and 13 yielded fibre layers with the least desirable properties as fibre distribution was both non-centric and highly non-uniform. Similar can also be said for OP 1, which was already analyzed in Figs 5 and 6.

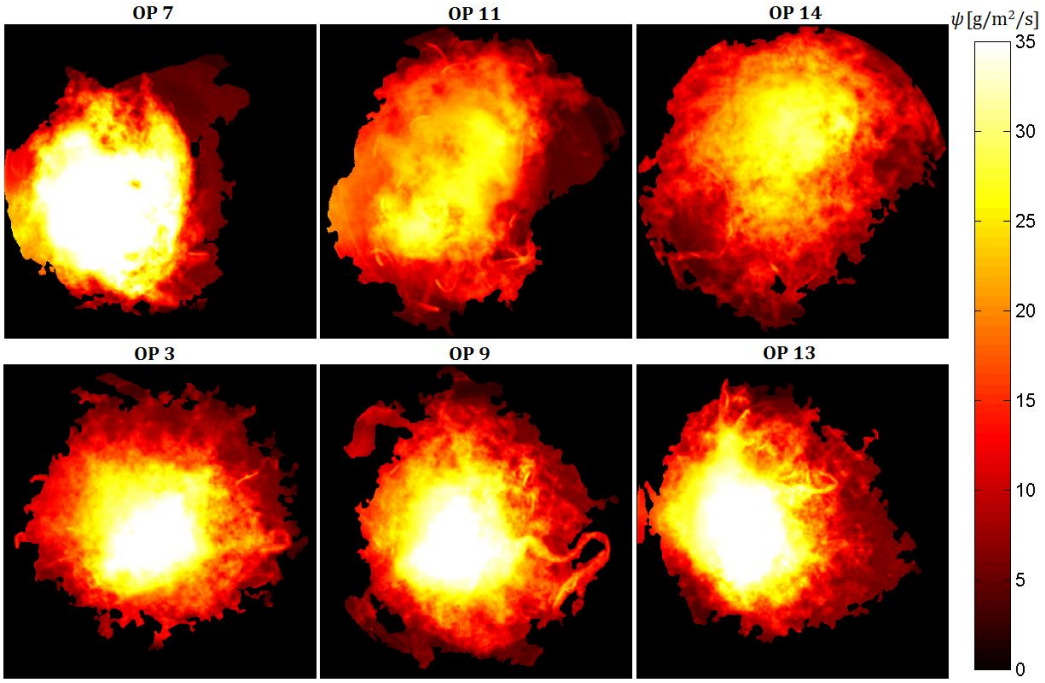


Figure 8. Average fibre accumulation rate ψ on the accumulation grid, for comparison with Fig. 7. The physical dimensions of each subpanel shown are 0.6x0.6 m

3.2 Multiple regression models

Based on the results presented in the previous subsection, a good correlation is expected between the characteristic properties of the fibre layer (σ_{Gn} and δ, Table 1) and the process input parameters (Q_p, Q_s, Q_t, t). This hypothesis will be confirmed by the following power law regression models:

$$\sigma_{Gn} = a_0 \cdot Q_p^{a1} \cdot Q_s^{a2} \cdot Q_t^{a3} \cdot t^{a4}, \quad (3)$$

$$\delta = b_0 \cdot Q_p^{b1} \cdot Q_s^{b2} \cdot Q_t^{b3} \cdot t^{b4}. \quad (4)$$

The exponents a_0-a_4 and b_0-b_4 were determined by fitting of the power law models in Eqs. (3) and (4) to data in Table 1, and corresponding measurement results.

For Eq. (3), we obtained a_0 = 1.3282, a_1 = 0.478, a_2 = 0.278, a_3 = -0.241, a_4 = 0.195 and a high coefficient of determination (R^2 = 0.90). This indicates a good correlation between modelled and input parameters.

For Eq. (4), the following values were calculated: $b_0 = 1.0089 \cdot 10^{-4}$, b_1 = -1.540, b_2 = 0.578, b_3 = -0.092, b_4 = -0.425 and a R^2 = 0.91. Again, a high R^2 value leads to a conclusion that the δ statistical parameter is representative of the process quality and can be modelled from selected input parameters.

Regression models can now be rewritten in a final form:

$$\sigma_{Gn} = 1.3282\, Q_p^{0.478} \cdot Q_s^{0.278} \cdot Q_t^{-0.241} \cdot t^{0.195}, \quad (5)$$

$$\delta = 1.0089\, 10^{-4} \cdot Q_p^{-1.540} \cdot Q_s^{0.578} \cdot Q_t^{-0.092} \cdot t^{-0.425}. \quad (6)$$

The model in Eq. (5) suggests that σ_{Gn} increases with the blow-away flow rate, suction flow rate and time since the start of fibre accumulation on the grid, but seems to decrease with tangential flow rate.

On the other hand, the fibre layer position, defined by parameter δ Eq. (6), more non-centric (i.e. δ increases), if blow-away flows (Q_p and Q_t) and fibre deposition time are decreased, or if the suction flow rate is increased. This is in good agreement with the findings of qualitative analysis presented in the previous sub section.
Exponent values of all independent model variables (Q_p, Q_s, Q_t and t) in Eqs. (5) and (6) are sufficiently high (absolute values between 0.1 and 1.5) to say that all of these variables significantly affect the fibre layer properties.

In Figs. 9 and 10, models given by Eqs. (5) and (6) are also graphically represented. It is evident that most of the measurements are in a good agreement with the model.

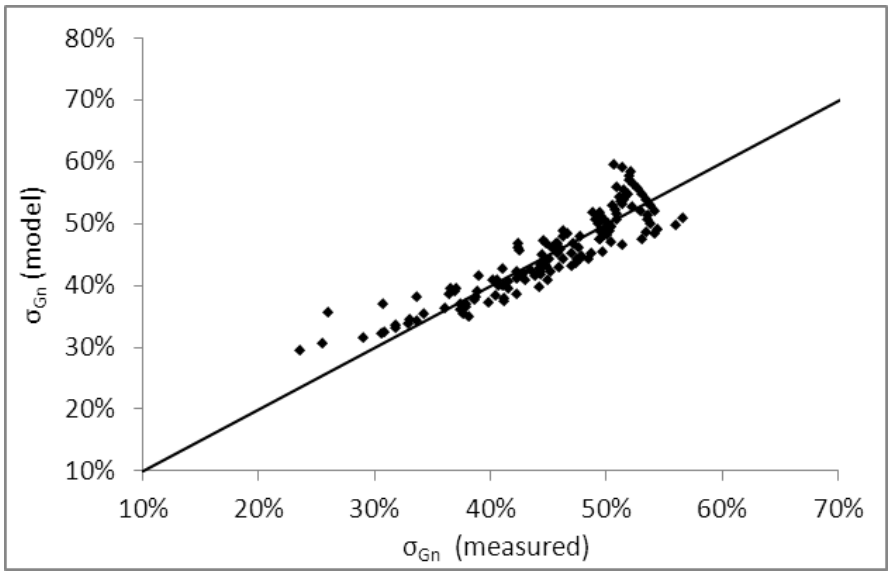


Figure 9. Correlation between measured and modelled values of σ_{Gn} (R^2 = 0.90)

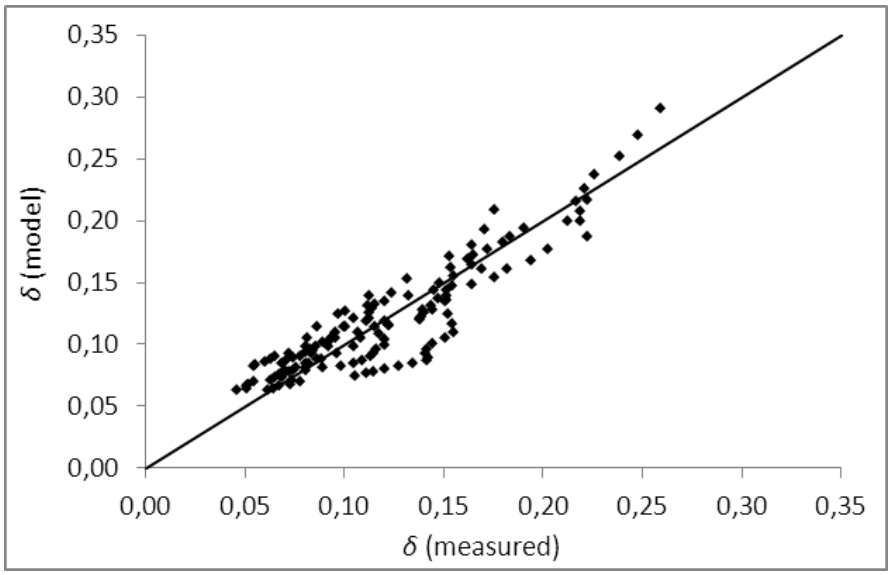


Figure 10. Correlation between measured and modelled values of δ (R^2 = 0.91)

4 Conclusions

The process of the glass wool layer formation was studied experimentally on a model spinning machine with sucrose as a working medium. The main focus was on the fibre layer formation

on the accumulation grid, which was visualized dynamically by a camera. Despite the relatively simple visualization approach which used direct fibre layer illumination rather than light absorption approach, we were able to obtain three distinct layer properties only from the optical intensity data: fibre accumulation rate (ψ), normalized standard deviation of the optical intensity (σ_{Gn}) and dimensionless distance between the mass centre of the fibre layer and the centre of accumulation grid.

Multiple regression models for δ and σ_{Gn} have shown an important effect of the suction flow, coaxial and tangential blow-away flows as well as fibre deposition time on the fibre layer properties. Also, these models are in a good agreement with measured values of δ and σ_{Gn}, and also with estimated fields of fibre accumulation rate (ψ). Presented regression models and qualitative analysis results will improve the understanding of the fibre transport and fibre layer formation process, leading to new possibilities for process monitoring and automation. Further research in this area should include the modelling of an actual glass wool manufacturing process with a moving accumulation grid where fibre layer formation is continuous.

References

1. Širok, B., Blagojević, B., P. & Bullen, P. Mineral wool: Production and properties. Cambridge, UK: Woodhead Publishing, 2008.
2. Kucuk, A., Clare, A. G. & Jones L. E. (1999). Estimation of Surface Tension for Silicate Glass Melts at 1400°C Using Statistical Analysis. *Glass Technology*, 40 (5), 149-153.
3. Lakatos, T., Johansson, L. G. & Simmingsköld, B. (1981). Viscosity and Liquidus Temperature Relations in the Mineral Wool Part of the System SiO_2-Al_2 O_3-CaO-MgO-Alkalies-FeO-Fe_2 O_3. *Glastek. Tidskr.*, 36, 51-55.
4. Blagojević, B., Širok, B. & Štremfelj, B. (2004) Simulation of the Effect of Melt Composition on Mineral Wool Fibre Thickness. *Ceramics - Silikáty*, 48(3), 128-134.
5. Marheineke, N., Liljo, J., Mohring, J., Schnebele, J. & Wegener, R. (2012). Multiphysics and multimethods problem of rotational glass fiber melt-spinning. *International Journal of Numerical Analysis and modelling, Series B*, 3(3), 330-344.
6. Qin, Y., Lv, X., Bai, C., Chen, P. & Qiu, G. (2013). Dry granulation of molten slag using a rotating multinozzle cup atomizer and characterization of slag particles. *Steel Research International*, 84(9), 852-862.
7. Qin, Y., Lv, X., Bai, C., Chen, P., Qiu, G. & Jie, Z. (2014). Mechanism of dry molten slag granulation using a rotating multi-nozzle cup atomizer. *Steel Research International*, 85(1), 44-52.
8. Kraševec B., Širok B., Hočevar M. & Bizjan B. (2014). Multiple regression model of glass wool fibre thickness on a spinning machine. *Glass Technology*, 55 (4), 119–125.
9. Kraševec, B., Širok, B., Bizjan, B. & Hočevar, M. (2015). Fibre density distribution in a layer of glass wool. *Glass Technology*, June 2015, 56 (3), 145–152.
10. Bizjan, B., Peternelj, M. & Širok, B. (2015). Experimental investigation of melt fiberization from a perforated rotor spinning machine. *Chemical Engineering Research and Design*, 104, 626-637.
11. Lin, J.Z., Liang, X.I., Zhang, S.L. (2012). Numerical simulation of fiber orientation distribution in round turbulent jet of fiber suspension. *Chemical Engineering Research and Design,* 90(6) 766-775.
12. Capone, A., Romano, G.P. & Soldati, A. (2015). Experimental investigation on interactions among fluid and rod-like particles in a turbulent pipe jet by means of particle image velocimetry. *Experiments in Fluids*, 56, paper No. 1, 15 p.
13. Qi, G., Nathan, J.G. & Lau, C.W.T. (2015). Velocity and orientation distributions of fibrous particles in the near-field of a turbulent jet. *Powder Technology*, 276, 10-17.
14. Bizjan B., Peternelj M. & Širok B. (2016). Mineral wool primary layer formation in collecting chamber; *Journal of Mechanical Engineering*, 62(3), 181-188.
15. E Badel, J-M Letang, G Peix & D Babot (2003). Quantitative microtomography: measurement of density distribution in glass wool and local evolution during a one-dimensional compressive load; *Measurement Science & Technology*, 14, 410–420.

16. Blagojević B., Širok B. & Hočevar M. (2003). Monitoring and Control of Quality of the Primary Layer of Mineral Wool on a Disc Spinning Machine, *Instrumentation Science & Technology*, 31(1), 67–80.
17. Dimovski, D., Blagojević, B., Širok, B. & Karič, Z. (2004). Mineral wool primary layer structure influence on the fibre distribution in the final product. *Glass Technology*, 45(4), 188-194.
18. Hočevar, M., Širok, B. & Blagojević, B. (2005). Mineral wool production monitoring using neural networks. *International Journal of Information Technology*, 11(9), 64-72.
19. Bajcar T., Blagojević B., Širok B. & Dular M. (2007). Influence of flow properties on a structure of a mineral wool primary layer; *Experimental Thermal and Fluid Science*, 32, 440–449.
20. The Breeze Instruction Manual: Models 3030, 3030SR, 3030EX, 3040, 3040SR; https://www.gmpopcorn.com/products/manuals/42147.pdfaccessed on 2015-12-29.

Chapter 4

Fibre Density Distribution in a Layer of Glass Wool

In this chapter, the article entitled “Fibre density distribution in a layer of glass wool” by Boris Kraševec, Branko Širok, Benjamin Bizjan and Marko Hočevar ([20]) is presented. The paper is published in an English journal Glass Technology. The author's contribution to this article is the model for prediction of transversal fibre density distribution in a layer of glass wool.
This chapter addresses the second hypothesis where an analysis was carried out based on the key parameters that influence the transversal fibre density distribution in a layer of glass wool and with the aid of measurements carried out with the X-Ray device. The fibre diameter, rotational speed of suction fan motors, spinner rotational speed and positions of air blowing nozzles, are the main fiberization parameters which were analysed in correlation with the measurements of X-Ray device.
The experiments were performed on a spinning machine in an industrial glass wool production process. The purpose of this article was to use a different setting of fiberization parameters to determine the equation for the fibre density distribution in a layer of glass wool.

Fibre density distribution in a layer of glass wool

Boris Kraševec[1,4], Branko Širok[2], Benjamin Bizjan[3], Marko Hočevar[2]

[1]Ursa Slovenija d.o.o., Production of Glass Wool, Povhova 2, 8000 Novo mesto, Slovenia
[2]University of Ljubljana, Faculty of Mechanical Engineering, Aškerčeva 6, 1000 Ljubljana, Slovenia

[3]*Abelium d.o.o., Research and Development, Kajuhova 90, 1000 Ljubljana, Slovenia*
[4]*Jožef Stefan International Postgraduate School, Jamova 39, 1000 Ljubljana, Slovenia*
E-mail: boris.krasevec@ursa.com

Keywords: Glass wool, Fibre density distribution, Collecting chamber, Regression model

Manuscript received: 24 January 2015
Revision received: 17 May 2015
Manuscript accepted: 10 June 2015

Abstract

In this paper, the fibre density distribution in a layer of glass wool was investigated. Our study included an analysis of the air suction flow velocity in the collection chamber and measurements of the glass wool density at the exit from the collection chamber. Glass wool density was measured by two different methods. The first method employed a camera visualization followed by the analysis of image greyness. The second method involved an X-Ray device through which the glass wool layer was passed. A good correlation between air suction flow velocity and glass wool density was determined (r^2=0.81). Based on the key parameters that influence the transversal fibre density distribution in a layer of glass wool and with the aid of measurements made with the X-Ray device, a regression model was formed. Model constants were determined from experimental results obtained in a glass wool collecting chamber. Results show a good correlation between measured and modelled transversal fibre density distribution (r^2=0.84). By using the proposed regression model, the optimal transversal fibre density distribution can be achieved more rapidly, leading to an improvement of end product properties.

1. Introduction

Glass wool is one of the most commonly used insulation materials and is particularly known for its excellent thermal insulation properties. Glass fibre distribution in the end product must be as homogeneous as possible to obtain optimal thermal insulation properties.
The collecting chamber [2] was the focus of our study. Firstly, the velocity of the air suction flow in the collection chamber was studied. In order to investigate the dependence of primary layer structure on the air flow velocity field inside the collection chamber, a study of the distribution of primary layer structure at selected longitudinal regions on the perforated mesh was necessary. [6] Velocity of the air suction flow in the collecting chamber has already been measured on stone wool, where the velocities were two times smaller than in case of glass wool. [1] Ablitzer [14] reported an analysis of the blow away velocity field in the coaxial flow of a centrifuge, as well as its interaction with the suction flow in the collection chamber and the influence of both flows on the formation of mineral wool primary layer on the perforated mesh in the collection chamber. Additional work about the influence of the blow away velocity field on the primary layer fibre structure in the mineral wool production process was studied by Širok. [8]
Analysis of glass wool transversal density distribution was performed with the aid of the visualization method developed by Blagojević. [1] A computer-aided visualization method was used for quantitative description of the homogeneity of glass wool layer. This method is based on the acquisition of subsequent images of the layer immediately after its exit from the collection chamber. [3] The density of the glass wool material produced by individual fiberization machines was measured with an X-Ray device [5] and compared with the velocity of the air suction flow in the collecting chamber.
The final part of the paper presents the regression model for relation between fiberization parameters and X-Ray measurements. The model can be applied for prediction of the transversal density distribution. [2]

2. The experimental set-up

The glass wool manufacturing process begins with the preparation of raw materials. The basic component of the glass mixture is waste glass. Other components in the mixture are borax pentahydrate (etibor), feldspar, dolomite, soda, quartz sand and calcite. The glass mixture is dosed into the furnace (Figure 1) (position 1), where the glass melts at about 1300°C. The molten glass mixture is first supplied into stabilisation channel (position 2) and then poured through the funnel (position 3) into the rotating spinners (position 4). Present in the area of position 4 are air and gas flows used for the combustion process, pressure arising from the air curtain, air flows from the left and right glass wool side cutting and from the recycled material. Fibres are formed by extrusion of the melt through the spinner holes and are then sprayed with the binder (position 5). The air flow with adjustable pressure orients the fibres down to the collecting chamber (position 7). The transversal density distribution can be adjusted by air blowing nozzles (position 6). With the aid of suction fans (position 8), the fibres are collected on the perforated plates to form the raw glass wool (position 9) which is then transported with a conveyor belt through the polymerisation chamber (position 10), where the binder polymerisation process occurs. The heat from the glass wool is removed by the fans (position 11). The fibre density distribution is measured with the X-Ray device (position 12). The final steps in production process include fleece cutting to the required dimensions (position 13), material compression and packaging. [2]

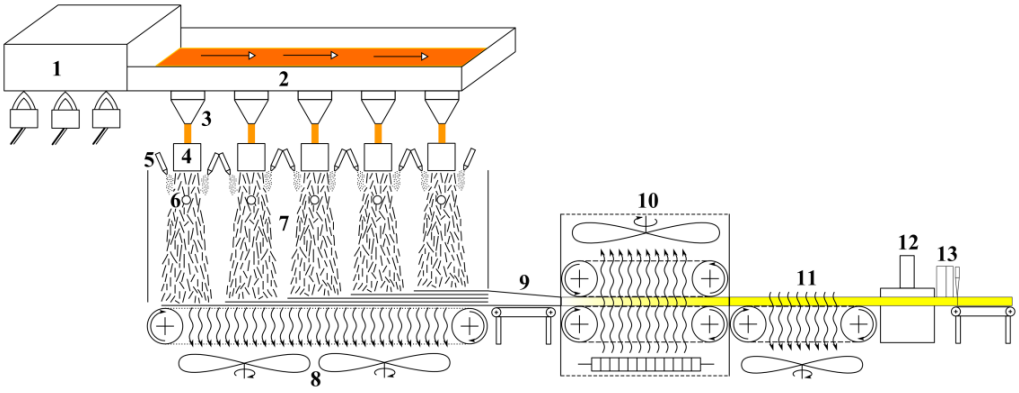


Figure 1. Glass wool production process

Experiments were performed in the collection chamber (position 7). To measure the air flow velocity field in the chamber an anemometer was placed on the perforated plates. Velocity was measured by transversal and longitudinal movement of the anemometer across the chamber giving a two-dimensional measurement grid. Process visualization was performed by a camera which was installed above the conveyor belt (position 4), orientated towards the glass wool layer (Figure 3) and which captured successive layer images. During the glass wool production on an individual machine (i.e. a single machine operation), camera visualization was performed simultaneously with the glass wool sample density measurements using the X-Ray device (position 12).
Suction fan setting (position 8), position of the air blowing nozzle (position 6) and the resulting diameter of fibres produced on the fiberization machine (position 4) were used in the regression model to predict the transversal density distribution. The actual density distribution was measured by the X-Ray device (position 12).

3. Velocity of the air suction flow in the collecting chamber

The first characteristic process property to be analysed was the vertical air flow velocity component at the bottom of the collection chamber. [1] The air flow was produced by a combination of the blow away and suction flows. Its vertical velocity component was

measured using a vane anemometer (Schiltknecht Messtechnik MiniAir 20) with a velocity range of 0-40 m/s. The uncertainty for the measured velocity is a combination of the measurement uncertainty of the anemometer position in longitudinal and transversal directions of the collection chamber, velocity measurement and separability of the measured velocities. The measurement uncertainty was estimated to be ±2%. Data from the anemometer was acquired with the National Instruments 16 bit A/D measurement board with a sampling frequency of 100 Hz. Locally measured velocities were analysed using Excel.
The anemometer was attached to the transporter belt of the collection chamber so that its fan was placed 20 cm above the belt. Eight different transversal positions of the anemometer with respect to the collecting chamber were used, i.e. 0.17, 0.37, 0.58, 0.8, 0.97, 1.19, 1.38 and 1.55 m from the right edge of the transporting belt (with respect to the transport direction, Figure 2) which was 1.74 m wide. The anemometer was then moved together with the transporting belt over a distance of 8 m and with a velocity of 5 m/min. During velocity measurements, the local air flows on all machines were set to their normal values. The natural gas flow for all fiberization machines was between 40 and 70 Nm^3/h, the air flow between 300 and 800 Nm^3/h and the pressure of the air curtain was between 1.5-4 bars (Figure 1) (position 4). Four suction fans were rotated at a frequency between 300 and 900 min^{-1} (Figure 1) (position 8). Also present were the air flow of the left and right glass wool side cutting (Figure 1) (position 4), air flow of the recycled material (Figure 1) (position 4), air flow of the binder rings (Figure 1) (position 5) and the air flow of the nozzles used for fibre distribution (Figure 1) (position 6).
At each of the eight transversal measurement positions, a one-dimensional profile of the vertical air flow velocity was obtained. Assuming steady, time-independent velocities, the velocity profiles were formed into a two-dimensional velocity field which is shown in Figure 2. The velocity field shows the local flow characteristics as a consequence of the cumulative effects of individual air flow generators and depending on the local aerodynamic characteristics of the flow tract of the observed system. During the measurements shown in Figure 2, glass wool was not produced.

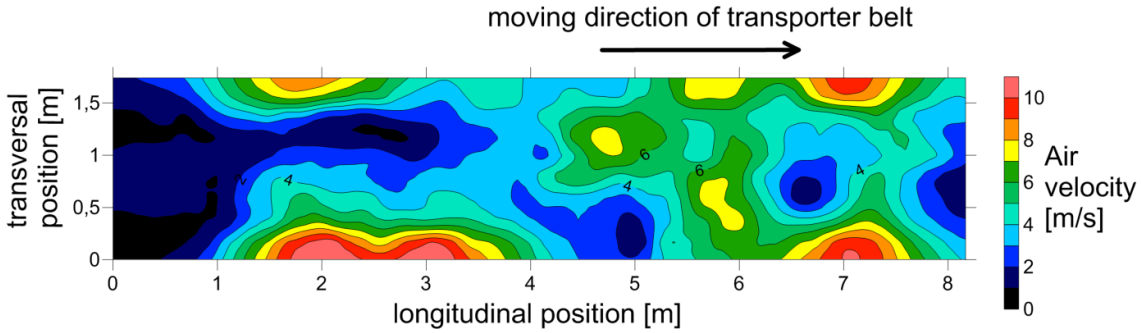


Figure 2. Velocity distribution above the transporter belt in the collection chamber

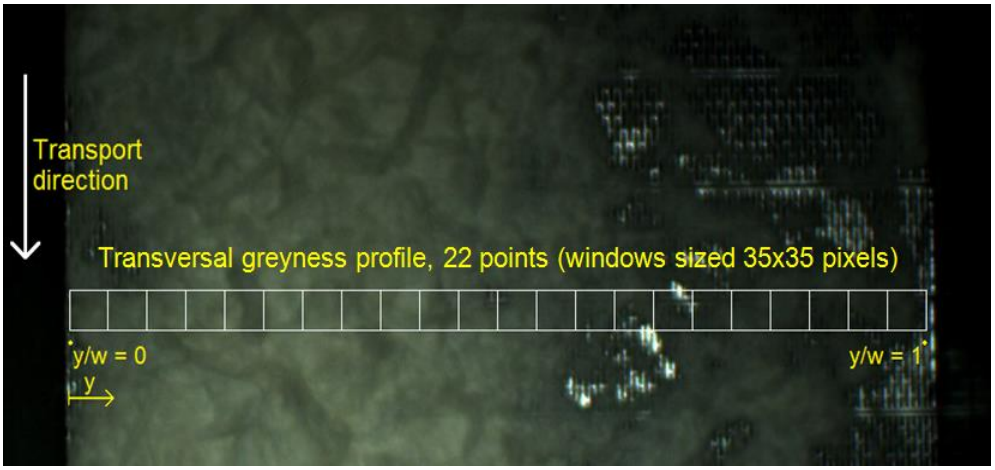


Figure 3. Visualization of the glass wool layer at the exit of the collecting chamber. Greyness profile acquisition area is shown by a white rectangle

From Figure 2 we can determine that the velocity field above transporter belt is relatively heterogeneous. Clearly visible are the asymmetrical velocity extremes which can be related to the setting of the distribution nozzle air flow (Figure 1) (position 6) intended to distribute the fibres in the collection chamber. Also, the areas with markedly low velocities can be observed, indicating a possible effect of lifting of already settled glass wool fibres during production. These areas are present in the initial part of the chamber at the longitudinal position between 0 and 1 m (Figure 2). This is the starting point of the glass wool layer formation. In this area a local horizontal transport of larger fibrous structures in the longitudinal and transversal directions can occur due to the relatively large lateral velocity (and consequently, pressure) gradients. Very high velocity peaks are present near the right edge (with respect to the transport direction) of the chamber (an area with a width of 0-0.5 m) which is certainly unfavourable for glass wool layer formation. A similar situation occurs near the exit from the chamber. Here, the local velocity maxima occur on both walls about 1 m from the exit. Also, two notable areas of low velocity are located 1.5 and 0.2 m from the exit of collection chamber, respectively. Again, the sharp velocity gradients and resulting pressure gradients may cause significant changes in the magnitude and direction of local fibre velocity. The described phenomena are generators of local anomalies in the layer of glass wool and, consequently, the transversal fibre density distribution of glass wool. The present anomalies can be reduced by setting the nozzle air flow (Figure 1) (position 6) more optimally and by modifications to the geometry of suction channels and fans.

4. Measurements of the glass wool luminous intensity (greyness) at the exit of collecting chamber

In this step, the glass wool layer leaving the collection chamber was analysed by a camera visualization method.[3] The camera, which captured successive glass wool layer images, was installed above the conveyor belt. The structure of the layers was evaluated on the basis of the measured greyness transversal to the collection chamber conveyor (Figure 3). The level of greyness was assumed to be proportional to the local thickness of the glass wool deposit on the conveyor. In each of the 22 windows, a greyness time series was acquired from successive images (a sample image is shown in Figure 3). Then, the time series were temporally averaged and the averages for individual acquisition windows were joined together into a mean (temporally averaged) transversal greyness profile to assess the spatial uniformity of the glass wool deposit. Analogously, a transversal profile of greyness standard deviation was obtained as a measure of the layer thickness temporal fluctuations. To ensure the optimal quality of the end product, the transversal glass wool layer density should be as uniform as possible while its temporal fluctuations should be kept to a minimum.

Visualization was performed using a Basler Ace acA1300-30gc colour camera with a resolution of 1294×964 pixels. The camera acquired images at a frequency of 30 Hz during the experiment. The glass wool layer was illuminated from above using 35 Cree XLamp XM-L LEDs, arranged in groups of seven at convenient locations to achieve homogenous illumination and to prevent reflections from conveyor belt. The images were saved to a personal computer for further analysis.

The experiment was performed such that spinning machines were operated individually, while other spinning machines were operated with equivalent parameters except for the glass melt flow. From the image shown in Figure 3 and the other visualization images we determine the glass wool distribution from individual spinning machines to be relatively non-uniform as we can clearly see the areas with a thick glass wool deposit as well as the areas with little or no deposit (areas where the perforated conveyor surface is partly visible). In this way it is possible to assess the quality of fibre transport and deposition process on each individual machine.

In order to quantify the uniformity of the transversal fibre layer thickness and structure, greyness profiles are shown in Figure 4. On the abscissa the value of y/w=0 belongs to the leftmost point on the belt and the value of y/w=1 to the rightmost point on the conveyor belt (viewed in the direction opposite to belt movement) where w=1.74 m. On the ordinate axis the

temporally averaged greyness level A is shown. The value 0 means completely black and 255 completely white colour. Time averaging was performed on the interval length of 100 s, which corresponds to 3000 successive images recorded at 30 frames per second. Here we assume the greyness level to be proportional to the thickness of the glass wool layer deposited on the belt as the wool-covered areas are typically lighter than the uncovered ones. In Figure 4, the mean greyness profiles are shown for five different cases where only one fiberization machine was operated at a time.

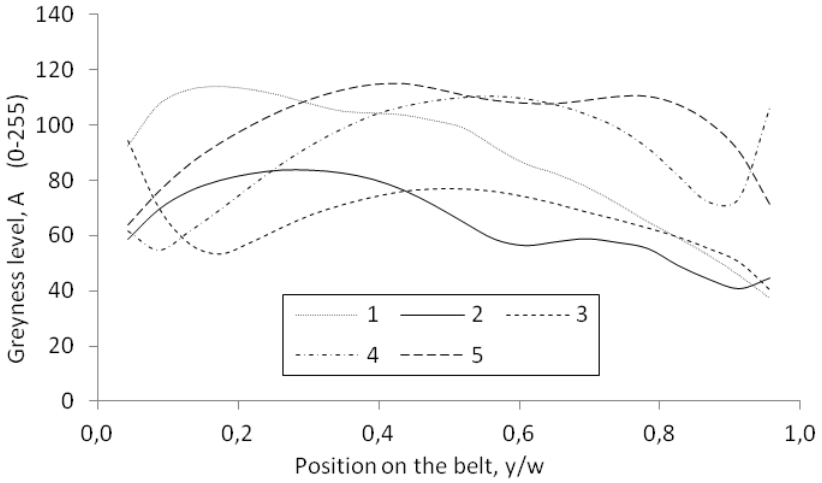


Figure 4. The mean greyness level profile transversal to the conveyor for a single machine operation of fiberization machines 1-5

From Figure 4 we can see that the operation of fiberization machines 1 and 2 results in accumulation of glass wool material on the left side of the belt, while the fiberization machines 3, 4 and 5 produce the maximum layer thickness near the middle of belt. At the edges, the thickness of the layer is lower. The observed asymmetry of glass wool layer distribution may be explained by velocity extremes between the 2 and 3 m longitudinal positions (Figure 2).
Apart from the greyness level which was introduced as a measure of spatial uniformity of the glasswool layer thickness in the direction transversal to the belt (y coordinate), the thickness uniformity in the longitudinal direction (x coordinate) is also important. The variability of material thickness in the longitudinal direction is characterised by the standard deviation of greyness level, std(A) (Equation (1)). In Equation 1, n=3000 is the number of images included in the time series. The variable $\bar{A}_i$ in Equation (1) is the greyness average of the i-th window (i=1 ... 22) on the profile transversal to the belt in all of the recorded images (Figure 3) and $A_{i,j}$ is the local greyness average in the same window on the j-th consecutive image.

$$\mathrm{std}(A_i) = \sqrt{\frac{1}{n-1}\sum_{i=1}^{n}\left(A_{i,j} - \overline{A_i}\right)^2} \tag{1}$$

In the next step, the standard deviation of greyness was normalised to the mean greyness value $\bar{A}_i$ to compensate for non-uniform illumination of the belt. Therefore, the normalised standard deviation of greyness, nstd(A), is introduced in Equation (2).

$$\mathrm{nstd}(A_i) = \frac{\mathrm{std}(A_i)}{\overline{A_i}} = \sqrt{\frac{1}{n-1}\sum_{i=1}^{n}\left(\frac{A_{i,j}}{\overline{A_i}} - 1\right)^2} \tag{2}$$

Standard deviation of greyness for all operating points is shown in Figure 5 and the normalised standard deviation is shown in Figure 6.

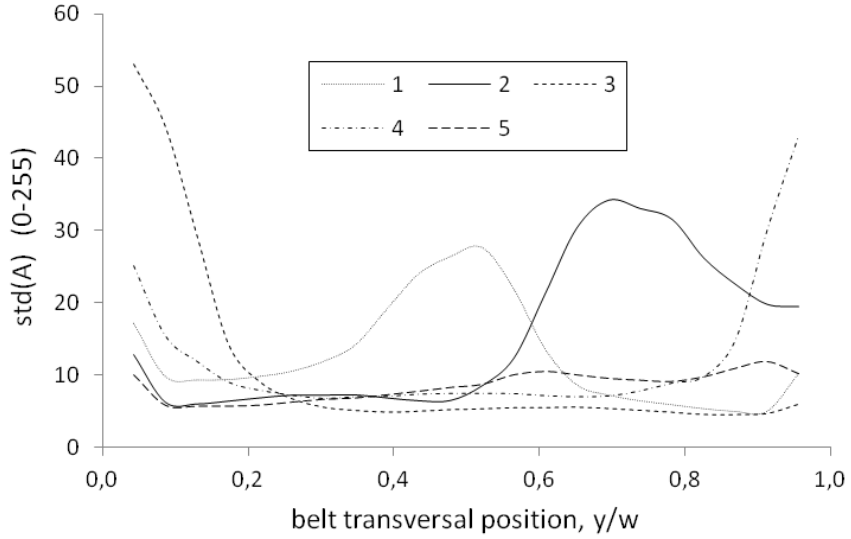


Figure 5. The profile of the greyness level standard deviation in the direction transversal to the conveyor for a single machine operation of fiberization machines 1-5

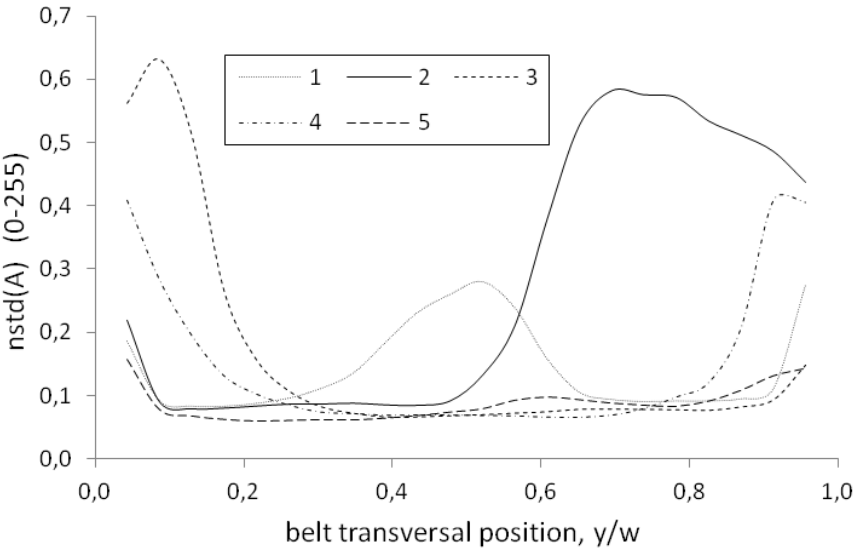


Figure 6. The profile of the greyness level normalised standard deviation in the direction transversal to the conveyor for a single machine operation of fiberization machines 1-5

From Figures 5 and 6 we can see that the maxima of the standard deviation of greyness (and consequently, of the glass wool layer thickness) are present at the edges of the belt and are significantly reduced towards its centre. An exception is the fiberization machine 1, where the largest temporal fluctuations of the thickness occur near the belt centre and in case of fiberization machine 2 where a large positive bias of the standard deviation can be observed on the right side of the belt.

5. X-Ray measurements

Measurements of glass wool density were performed also using an X-Ray method. The X-Ray device works on a non-contact principle. A radiation source is located above the device main structure while the radiation detector is placed below the line belt. The X-Ray radiation from the source penetrates the measured material and is partly absorbed in it, depending on the

quantity and specific weight of the analyzed material. The unabsorbed radiation component is picked up by the detectors and converted into electrical signals for further evaluation.

The absorption is given by Equation 3:

$$I = I_0 \exp(-\mu_m \rho x) \tag{3}$$

In Equation 3, I is the remaining radiation intensity after passing through the material of thickness, I_0 is the intensity of the radiation before entering into the material, μ_m [m^2/kg] is the mass attenuation coefficient of the material and ρ [kg/m^3] is the raw density of the material. The mass attenuation coefficient is a material attribute which depends on the chemical composition of the material. The area weight f [kg/m^2] can be calculated directly from the corrected intensity values (Equation (4))

$$f = \frac{\log\left(\frac{I_0}{I}\right)}{\mu_m} \tag{4}$$

From the area weight and the material thickness, the raw density (Equation (5)) is calculated[5]

$$\rho = \frac{f}{x} \tag{5}$$

During the X-Ray measurements the scan width was 1.3 m while the length of the glass wool layer passed through the device was 7.3 m. Results with a spatial resolution of 10×10 mm were obtained. In Figure 7, surface plots of the local glass wool layer density are shown for different operating regimes. In single machine operation mode, the distribution of the glass wool density is spatially non-uniform. A significant difference in the glass wool layer density can be observed between the belt centre and edges, which can be attributed to the air flow interaction with the collecting chamber walls and consequently, non-uniform fibre deposit thickness.

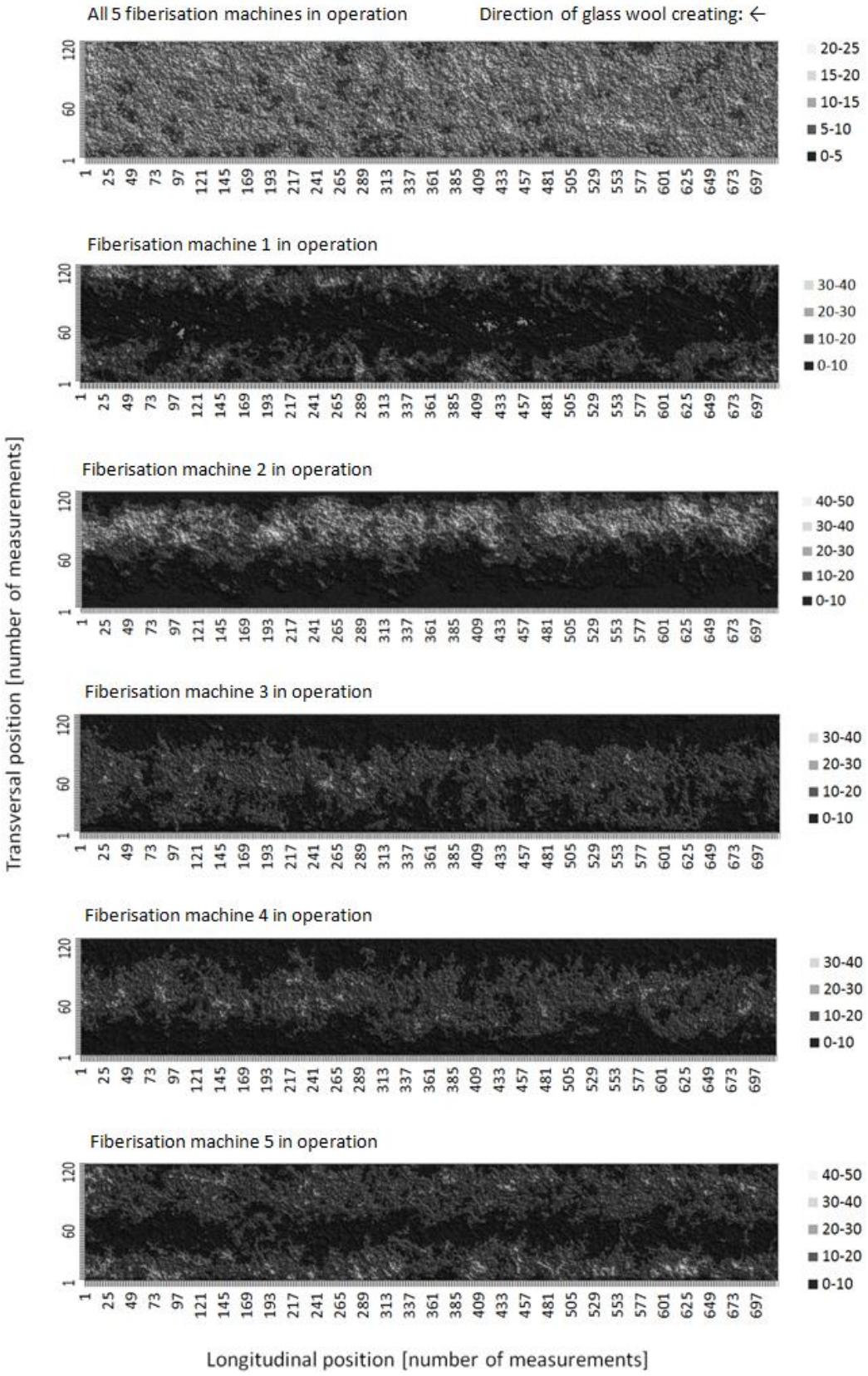


Figure 7. Fibre density distribution in a layer of glass wool [kg/m^3]

When all five machines are in operation (uppermost plot on Figure 7), the sum of glass wool flows from individual machines results in a spatially much more uniform wool layer (especially in the transversal direction) which completely covers the belt. However, there are still some

random anomalies, i.e. local maxima and minima of glass wool thickness, with the thickness magnitude at the firmer about twice the magnitude of the latter.
Considering the image greyness analysis results and the fact that the glass wool layer mass distribution does not change after the last fiberization machine, we can conclude that these anomalies are mainly caused by the layer thickness fluctuations in the collecting chamber. As said, the glass wool layer formation on the conveyor belt is strongly affected by the turbulent flow properties in the blowing area as well as suction through the perforated conveyor belt.
Figure 8 presents the correlation between air flow velocity in the collection chamber and transversal glass wool density distribution measured with the X-Ray device. A good correlation between parameters is confirmed with the coefficient r^2=0.81. The data from the Figure 2 was used to plot the velocity area of individual fiberization machines against the glass wool density from Figure 7. With the layout of the fiberization machines and collecting chamber the common surface area was determined. Eight average air flow velocities and fibre density distributions were compared for five fiberization machines presented as 40 data points in the plot.

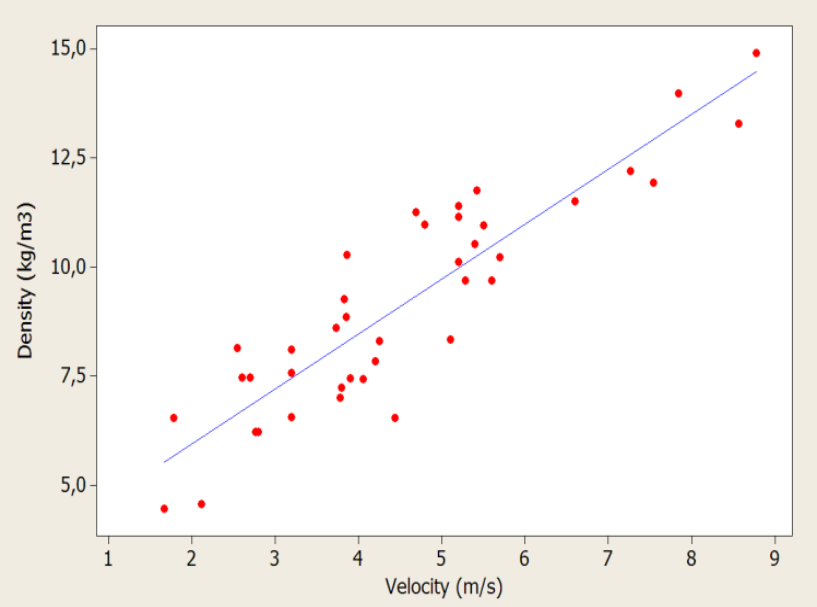


Figure 8. Correlation between air flow velocity in the collecting chamber and glass wool layer density obtained with the X-Ray device (r^2 = 0.81)

6. Prediction of the transversal density distribution by a regression model

In the first subsection of this section, the principle of calculating the transversal density distribution is presented. The second subsection presents a regression model analysis of acquired X-Ray data.

6.1 Calculation of the transversal density distribution

The output result of the X-Ray device is the transversal density distribution over four sections of the product width. Measurements are conducted on the production line where the glass wool product is passed through the X-Ray head and detection area of the device. The density of the left part (L), left middle part (LM), right middle (RM) and right part (R) of the glass wool are obtained. Yearly data of fibre density distribution was used for the study. Dividing the product width into four strips is sufficient to notice the impact of varied parameters related to the X-Ray results. Each minute four moving average values of the X-Ray measurements were sent to the process computer.

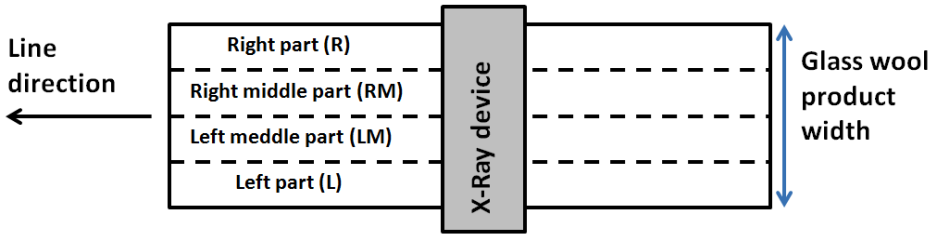


Figure 9. Product width divided into four sections

The average density is calculated from the density of the four strips shown in Figure 9. Delta density of a particular strip is calculated as the difference between the strip density and the average density:

$$\Delta\rho_{(L-R)} = \rho_{(L-R)} - \bar{\rho} \tag{6}$$

The range value (Equation (7)) describes the quality of transversal density distribution and is calculated as the difference between $\Delta\rho_{MIN}$ and $\Delta\rho_{MAX}$.

$$\text{Range} = \Delta\rho_{(L-R)_{MIN}} - \Delta\rho_{(L-R)_{MAX}} \tag{7}$$

6.2 Regression model

The experiments were performed in a collection chamber of a real production process (Figure 1) (position 7). A total of 93 experiments were performed. Production process parameters were set in such manner that the product quality was adequate for packaging and sale and all measured variables corresponded to a set of real production parameters.
The fibre density distribution in the collection chamber was the main focus of our study. The fibre diameter (Figure 1) (position 4), rotational speed of suction fan motors (Figure 1) (position 8) and positions of air blowing nozzles (Figure 1) (position 6) were used as variable parameters, while the X-Ray device was used to measure the fibre density distribution. In the present experiment the fibre diameter ranged between 5 and 8 μm, the angle positions on the air blowing nozzles which were used to control the fibre density distribution were varied in the range between -60° to 16°. Suction fan motor rotational speed was varied between 500 min^{-1} and 1300 min^{-1}.
The comparison between the measured densities and the ones calculated on the basis of the regression model is shown in Figure 10. A good agreement between modelled and measured values of density is confirmed by a high value of correlation coefficient, r^2=0.84, indicating good quality of regression modelling.

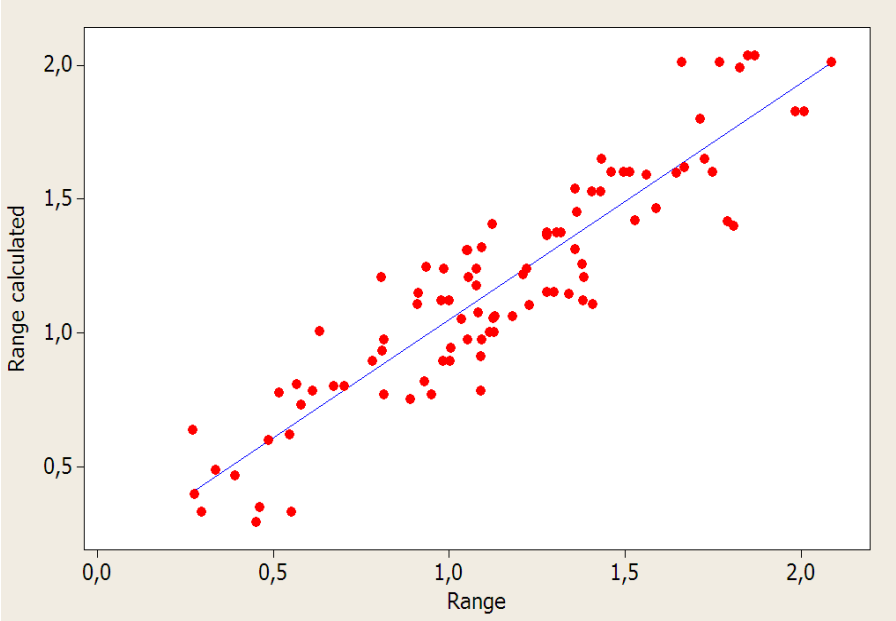


Figure 10. Comparison of experimentally measured (Range) and statistically predicted fibre density distribution (Range calculated)

Using experimental data with multiple regression analysis, the regression model parameters were determined. The agreement between measured and calculated fibre density distribution values was examined with an F-test. The test results are presented in Table 1. F-test is an estimate of the hypothesis that the regression is not significant. The probability (P value) that this hypothesis is valid was 10^{-4}, thus the regression is very significant.

Table 1. F-test results of agreement between the modelled and measured values. DF represents Degrees of Freedom, SS is the Sum of squares, MS is Mean Square and P is probability

Source	DF	SS	MS	F	P
Regression	29	18.75043	0.64657	44.28	0.0001
Residual	63	0.91996	0.01460		
Total	92	19.67040			

Values of regression model constants are presented in Table 2. Parameters with negative values inversely influence the fibre density distribution. Their significance was checked with a t-test (Table 2).

Table 2. Regression model constant values along with the results of the t-test

	a_0	a_1	a_2	a_3	a_4	a_5	a_6	a_7	a_8	a_9
Values	-1.34	0.00092	-0.00359	-0.00315	0.00628	0.240	-0.0125	0.385	0.0386	-0.0840
Prob >|t|		12.5	15	17.6	19.8	0.0374	0.0538	0.0423	0.0333	0.0487

	a_{10}	a_{11}	a_{12}	a_{13}	a_{14}	a_{15}	a_{16}	a_{17}	a_{18}	a_{19}
Values	0.0798	0.066	-0.00040	-0.12	-0.0103	-0.0659	-0.0590	-0.0688	0.0056	0.0024
Prob >|t|	0.350	0.379	0.307	0.235	1.34	0.293	0.36	0.256	0.299	0.346

	a_{20}	a_{21}	a_{22}	a_{23}	a_{24}	a_{24}	a_{25}	a_{26}	a_{27}	a_{28}
Values	0.0606	0.0281	0.0260	0.0677	0.0066	0.0070	-0.0909	-0.0200	0.0388	-0.0125
Prob >|t|	0.466	0.455	0.332	0.151	0.489	0.361	0.323	0.209	0.691	0.277

The results presented in the Table 2 show the parameter impact on the fibre density distribution range. Parameters a_5–a_9 present the fibre diameter for each fiberization machine and have the biggest impact on the fibre density distribution range. Also important are the parameters a_{10}-a_{28} which presents the horizontal and vertical positions of air blowing nozzles of individual fiberization machines. The smallest impact results from the suction fans (parameters a_1-a_4) used for gas suction from the collection chamber.
In Figure 11, the measured density range is presented for all 93 measurements and is shown in black, while modelled density range is shown in red (grey in the printed journal). Each of the intervals have an upper specification limit (USL) and lower specification limit (LSL), which are defined by 95% confidence levels or ±2σ, which is ±0.92 in terms of the density range. There is a fairly good agreement between the measured and predicted density range values as both lie within the selected interval.

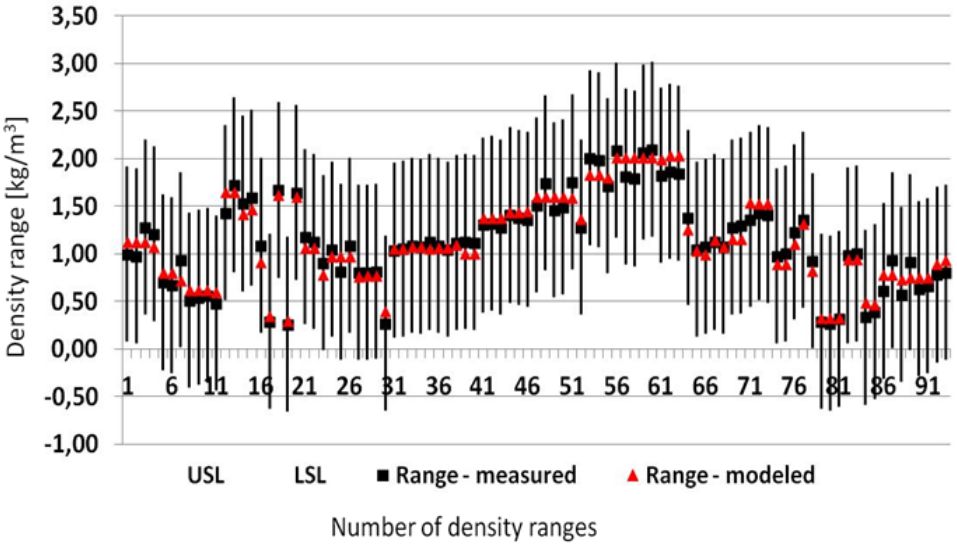


Figure 11. Comparison of experimentally measured density range and predicted values of regression model with 95% confidence fitting levels

7. Conclusions

Performance of the glass wool collection chamber was assessed by an analysis of the air suction flow velocity in the collection chamber and measurements of density with an X-Ray device and with a visualization method. A good correlation between air suction flow velocities and fibre density distribution in the layer of glass wool was determined, indicating the significance of the former for the quality of the final product. We estimate that glass wool quality can be improved by improving the uniformity of the air flow velocity distribution.
A regression model for the transversal fibre density distribution was formed and a good agreement between calculated and measured values was determined. Based on the set of measured variables of the production process, we were able to predict transversal density distribution reasonably well. The modelling procedure can be applied in production process where the main expected benefit is the improvement of the end product properties and a reduction of waste and second-class product quantity.

References

1. Širok, B., Blagojević, P. & Bullen, *P. Mineral wool: production and properties*. Woodhead Publishing, Cambridge, 2008.
2. Kraševec, B., Širok, B., Hočevar, M. & Bizjan, B. Multiple regression model of glass wool fibre thickness on a spinning machine. *Glass Technol.*, 2014, 55 (4), 119-25.

3. Blagojević, B., Širok, B. & Hočevar, M. Monitoring and control of quality of the primary layer of mineral wool on a disc spinning machine. *Instrum. Sci. Technol*., 2003, 31 (1), 67-80.
4. Cendre, E., Duvauchelle, P., Peix, G., Buffière, J.-Y. & Babot, D. Conception of a high resolution X-Ray computed tomography device; application to damage initiation imaging inside materials. *Proc. First World Congr. on Industrial Process Tomography*, Buxton, Derbyshire,14-17 Apr. 1999.
5. Badel, E., Letang, J.-M., Peix, G. & Babot, D. Quantitative microtomography: measurement of density distribution in glass wool and local evolution during a one-dimensional compressive load. *Meas. Sci. Technol*., 2003, 14, 410-20.
6. Bajcar, T., Blagojević, B., Širok, B. & Dular, M. Influence of flow properties on a structure of a mineral wool primary layer. *Exper. Therm. Fluid Sci*., 2007, 32, 440-9.
7. Bhouri, N., Badel, E., Ben Nasrallah, S. & Perre, P. Shrinkage/swelling behavior of knitted fabrics during relative humidity cycles determined by X-Ray imaging. *J. Porous Media*, 2009, 12 (5), 403-15.
8. Širok, B., Blagojević, B. & Novak, M. Influence of blow away velocity field on the primary layer fibre structure in the mineral wool production process. *Glass Technol*., 2002, 43 (5), 188-94.
9. Dimovski, D., Blagojević, B., Širok B. & Kariž, Z. Mineral wool primary layer structure influence on the fibre distribution in the final product. *Glass Technol*., 2004, 45 (4), 188-94.
10. Badel, E & Perré, P. Using a digital X-Ray imaging device to measure the swelling coefficients of a group of wood cells *NDT&E Int*., 2001, 34, 345-53.
11. Hočevar, M., Širok, B. & Blagojević, B. Mineral wool production monitoring using neural networks. *Int. J. Inf. Technol*., 2005, 11 (9), 64-72.
12. Rothe, P. H. & Block, J. A. Aerodynamic behaviour of liquid sprays. *Int. J. Multiphase Flow*,1976, 3, 263–72.
13. Trdič, F., Širok, B., Bullen, P. R. & Philpott, D. R. Monitoring mineral wool production using real-time machine vision. *Real Time Imaging*, 1999, 5 (2), 125-40.
14. Ablitzer, C., Gruy, F. & Perrais, *C. Chem. Eng. Sci*., 2001, 56, 2409-20.

Chapter 5

Summary of Results

In this chapter, the most important results of the research work performed during this doctoral study are presented. In Section 5.1 a multiple regression model of glass wool fibre thickness on a spinning machine is summarized. Results of glass wool layer formation in the collecting chamber are presented in the second section (5.2), while fibre density distribution in a layer of glass wool can be found in the last subsection (5.3).

5.1 Multiple Regression Model of Glass Wool Fibre Thickness on a Spinning Machine

Nine characteristic numbers were considered to form a nonlinear regression model for predicting the thickness of glass wool fibres. Dimensionless numbers presented in Table 5.1 were used as characteristic numbers Π in Equation 5.1.

$$\frac{d_v}{R} = a_0 \Pi_1^{a_1} \Pi_2^{a_2} \Pi_3^{a_3} \Pi_4^{a_4} \Pi_5^{a_5} \Pi_6^{a_6} \Pi_7^{a_7} \Pi_8^{a_8} \Pi_9^{a_9} \qquad (5.1)$$

Table 5.1. Characteristic and dimensionless numbers of the parametric model from Equation 5.1

n	Characteristic number	Dimensionless number	Representation
1	Π_1	$\omega R^{3/2}\sqrt{\frac{\rho}{\sigma}}$	ω^*
2	Π_2	$\frac{q_{v,m}}{B}\sqrt{\frac{\rho}{R\sigma}}$	$q_{v,m}^*$
3	Π_3	$\frac{\eta^2}{\sigma\rho R}$	Z
4	Π_4	$\frac{\Delta T}{T_m} = \frac{T_m - T_A}{T_m}$	T *
5	Π_5	$\left(1 + \frac{q_{m,m}}{q_{m,A}}\right)\frac{\eta_m}{\eta_A}$	Lu

6	Π_6	$t = \frac{d - d_i}{d_f - d_i}$	t
7	Π_7	$\frac{q_{m,G} CV_G}{q_{m,m} c_{p,m} (T_m - T_A)}$	Q_G *
8	Π_8	$\frac{q_{m,A} c_{p,A} (T_{B,A} - T_A)}{q_{m,m} c_{p,m} (T_m - T_A)}$	Q_A *
9	Π_9	$\frac{q_{v,A}}{q_{v,G}}$	R

The results of a comparison between measured fibre parameters and those calculated on the basis of nine parameter model in accordance to Equation (5.1) are shown in Figure 5.1. A good agreement between the modelled and measured values of fibre parameters was confirmed by a high value of the correlation coefficient, r^2=0.852, indicating a good regression model.

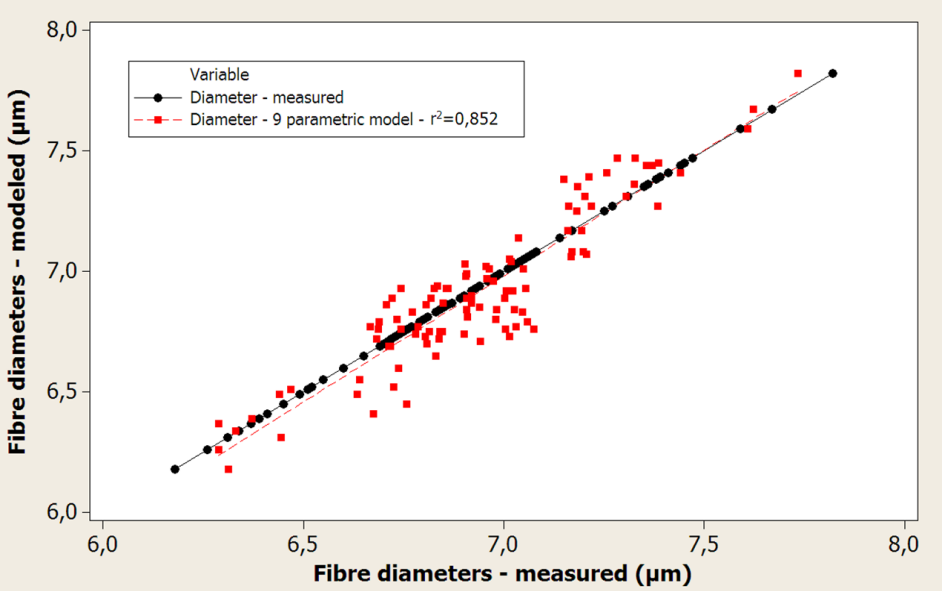


Figure 5.1. Comparison of the experimentally measured and statistically predicted fibre diameters

Results presented in Table 5.2 show that parameters a_5 and a_9, i.e. the characteristic numbers Π_5 (effect of air pressure for fibre orientation) and Π_9 (ratio between air and gas volume flow rate) have a significant effect. Constants a_2, a_3, a_4 and a_7 which relate to the mass flow rate of glass, glass melt temperature and volume flow rate of gas (characteristic numbers Π_2, Π_3, Π_4 and Π_7, respectively) are also important. To a lesser extent, parameters a_1, a_6 and a_8, i.e. characteristic number of spinner rotational speed (characteristic number Π_1), spinner life time (characteristic number Π_6) and volume flow rate of air (characteristic number Π_8), are also significant. Statistically, the spinner life time effect was the least significant because it was compensated by adjustment of the other process parameters to maintain the desired fibre diameters.

Table 5.2. Regression model constant values according to Equation 5.1 along with the results of the t-test

	a_0	a_1	a_2	a_3	a_4	a_5	a_6	a_7	a_8	a_9
Values	1	-0.002	-0.0067	0.0343	0.0343	-0.4926	0.0012	-0.3111	0.0297	-2.1201
Prob >|t|		4.2	0.2	0.48	0.48	0.0155	12.7	0.28	2.6	0.0169

5.2 Glass Wool Layer Formation in the Collecting Chamber

Glass wool layer formation was investigated experimentally on a model spinning machine with sucrose as a working medium. The fibres were pneumatically transported from the spinner to the accumulation grid with the aid of the blow-away (Q_p), suction (Q_s) and tangential (Q_t) airflows. Spinning machine operating parameters were varied in a wide range (Table 5.3) and produced distinct forms of sucrose fibre layer.

Table 5.3. Operating points for fibre layer visualization

Op. point No.	Δp [kPa]	f_s [Hz]	U_t [V]	Q_p [m³/h]	Q_s [m³/h]	Q_t [m³/h]
1	20	15	0	17.8	2700	0
2	20	25	0	17.8	4500	0
3	50	15	0	27	2700	0
4	50	15	0	27	2700	0
5	50	25	0	27	4500	0
6	20	15	3.5	17.8	2700	88.7
7	20	25	3.5	17.8	4500	88.7
8	50	15	3.5	27	2700	88.7
9	50	15	3.5	27	2700	88.7
10	50	25	3.5	27	4500	88.7
11	50	25	5	27	4500	130.2
12	20	15	5	17.8	2700	130.2
13	50	20	3.5	27	3600	88.7
14	50	25	7	27	4500	242.5

The fibre layer formed on the accumulation grid was visualized by a camera for several different operating regimes. The optical intensity (gray level, G) of acquired visualization images was then used to calculate its normalized standard deviation (σ_{Gn}, Fig. 5.2), local fibre accumulation rates (ψ, Fig. 5.3) and dimensionless distance between the fibre layer centre of gravity and centre of accumulation grid (δ, Fig. 5.4).

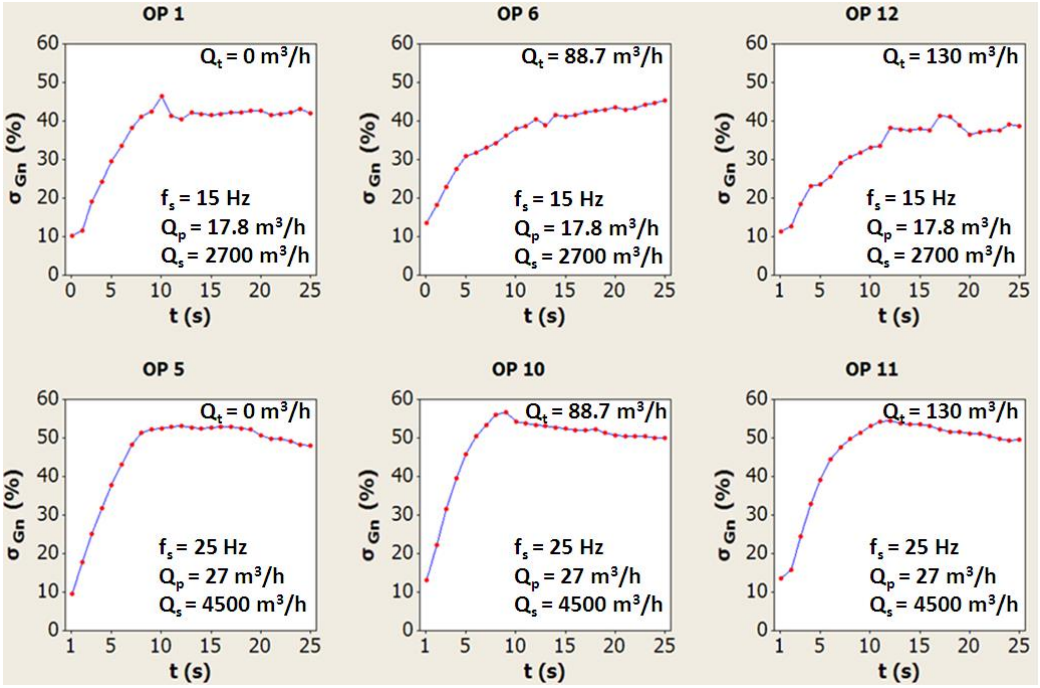


Figure 5.2. Normalized standard deviation of optical layer intensity for different operating points (OP)

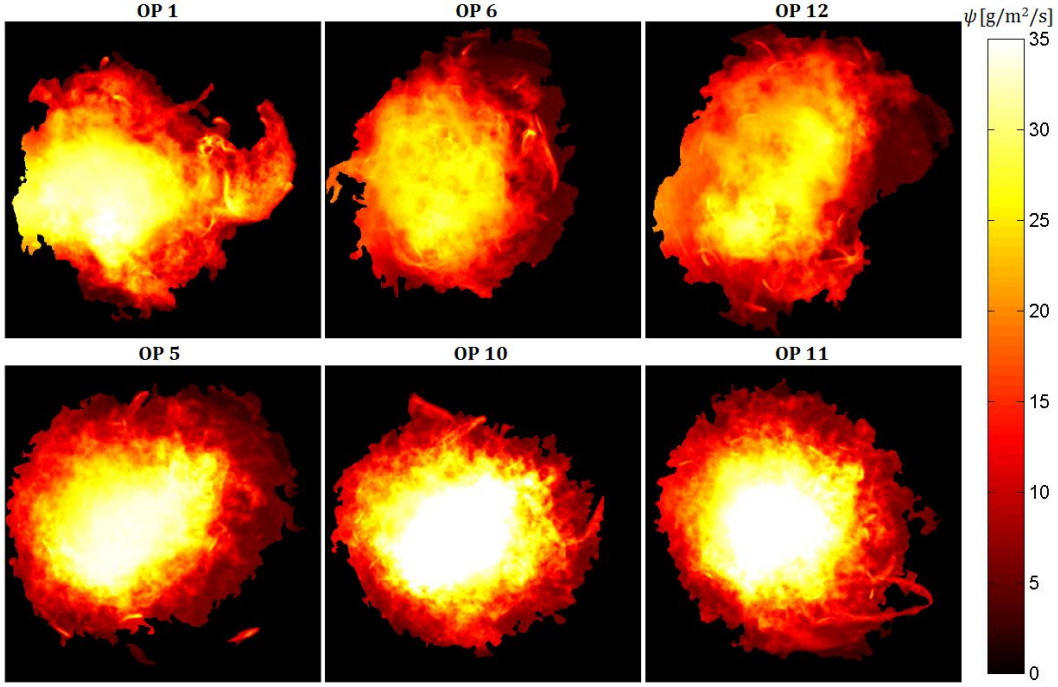


Figure 5.3. Average fibre accumulation rate ψ on the accumulation grid, for comparison with Fig. 5.2. The physical dimensions of each subpanel shown are 0.6x0.6 m

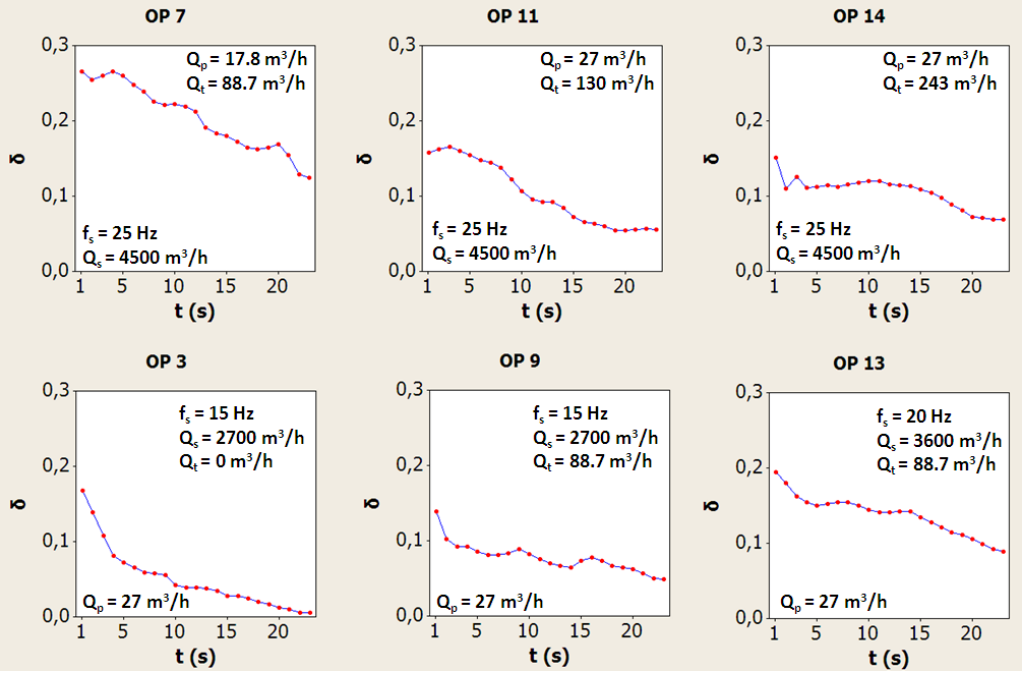


Figure 5.4. Distance between the fibre layer centre of gravity and the centre of the accumulation grid as a function of time

A good correlation was achieved between the characteristic properties of the fibre layer (σ_{Gn} and δ) and the process input parameters (Q_p, Q_s, Q_t, t,) (Table 5.3). This hypothesis is confirmed by the following power law regression models:

$$\sigma_{Gn} = a_0 \cdot Q_p^{a1} \cdot Q_s^{a2} \cdot Q_t^{a3} \cdot t^{a4}, \quad (5.2)$$

$$\delta = b_0 \cdot Q_p^{b1} \cdot Q_s^{b2} \cdot Q_t^{b3} \cdot t^{b4}. \quad (5.3)$$

The exponents a_0-a_4 and b_0-b_4 were determined by fitting of the power law models in Eqs. (5.2) and (5.3) to data in Table 5.3, and the corresponding measurement results.

For Equation (5.2), we obtained a_0 = 1.3282, a_1 = 0.478, a_2 = 0.278, a_3 = -0.241, a_4 = 0.195 and a high coefficient of determination (R^2 = 0.90). This indicates a good correlation between modelled and input parameters.

For Equation (5.3), the following values were calculated: b_0 =1.0089 · 10^{-4}, b_1 = -1.540, b_2 = 0.578, b_3 = -0.092, b_4 = -0.425 and a R^2 = 0.91. Again, a high R^2 value leads to a conclusion that the δ statistical parameter is representative of the process quality and can be modelled from selected input parameters.

The model in Equation (5.2) suggests that σ_{Gn} increases with the blow-away flow rate, suction flow rate and time since the start of fibre accumulation on the grid, but seems to decrease with tangential flow rate.
On the other hand, the fibre layer position, defined by parameter δ (Equation (5.3)), more non-centric (i.e. δ increases), if blow-away flows (Q_p and Q_t) and fibre deposition time are decreased, or if the suction flow rate is increased.
Exponent values of all independent model variables (Q_p, Q_s, Q_t and t) in Equations (5.2) and (5.3) are sufficiently high (absolute values between 0.1 and 1.5) to say that all of these variables significantly affect the fibre layer properties.

5.3 Fibre Density Distribution in a Layer of Glass Wool

In this section, the fibre density distribution in a layer of glass wool was investigated. Our study included an analysis of the air suction flow velocity in the collecting chamber (Fig. 5.5) and measurements of the glass wool density at the exit from the collecting chamber (Fig. 5.6).

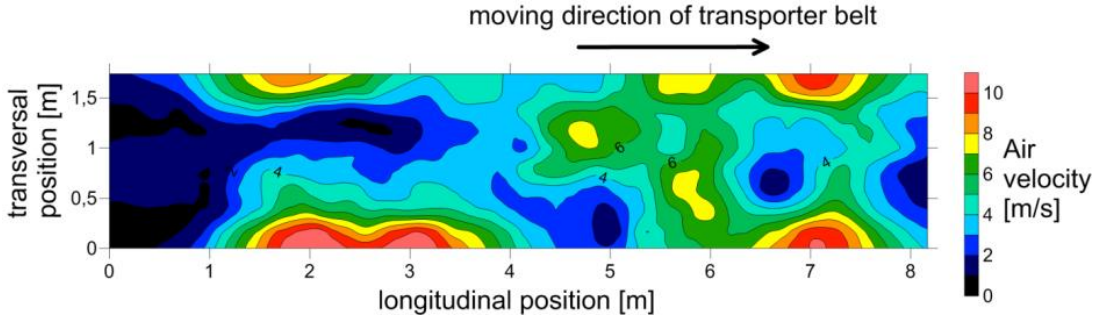


Figure 5.5. Velocity distribution above the transporter belt in the collection chamber

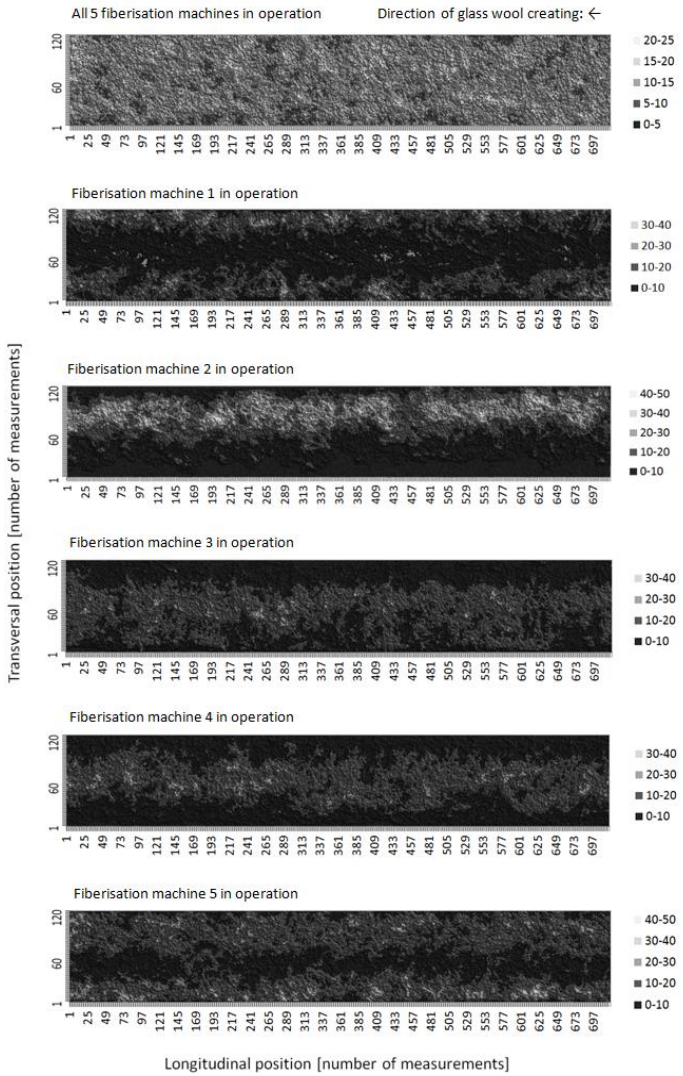


Figure 5.6. Fibre density distribution in a layer of glass wool [kg/m^3]

Glass wool density was measured by two different methods. The first method employed a camera visualization followed by an analysis of image greyness. The second method involved

an X-Ray device through which the glass wool layer was passed. Figure 5.7 presents the correlation between air flow velocity in the collecting chamber and transversal glass wool density distribution measured with the X-Ray device. A good correlation between parameters is confirmed with the coefficient $r^2 = 0.81$. The data from the Figure 5.5 was used to plot the velocity area of individual fiberization machines against the glass wool density from Figure 5.6. With the layout of the fiberization machines and collecting chamber the common surface area was determined. Eight average air flow velocities and fibre density distributions were compared for five fiberization machines presented as 40 data points in the plot.

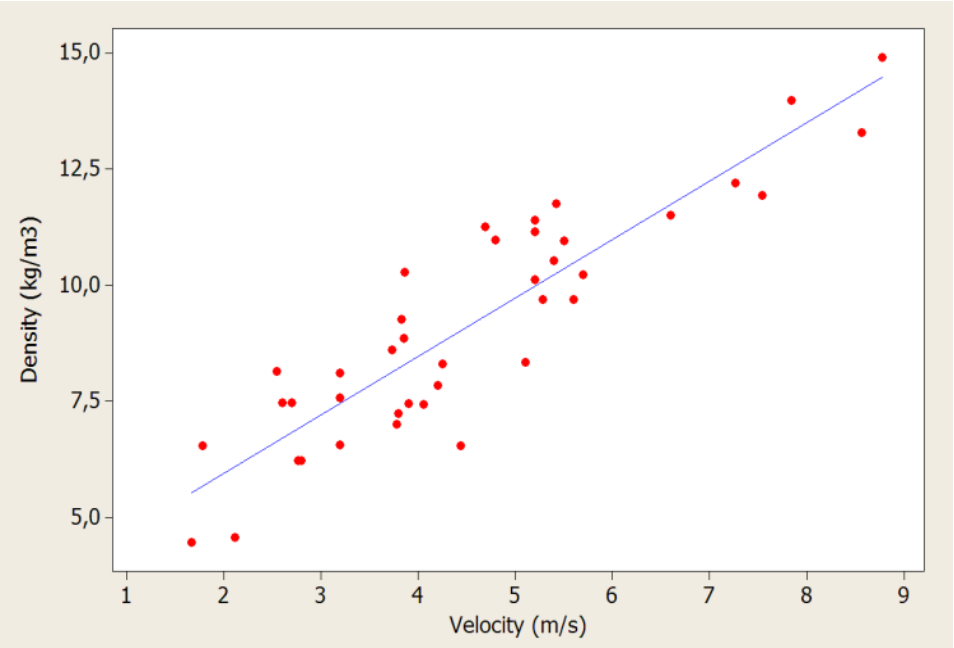


Figure 5.7. Correlation between air flow velocity in the collecting chamber and glass wool layer density obtained with the X-Ray device ($r^2 = 0.81$)

Based on the key parameters that influence the transversal fibre density distribution in a layer of glass wool and with the aid of measurements done with the X-Ray device, a main regression model was formed. Model constants were determined from experimental results obtained on a glass wool collecting chamber. Results show a good correlation between measured and modelled transversal fibre density distribution ($r^2 = 0.84$) (Fig. 5.8). By using the proposed regression model, the optimal transversal fibre density distribution can be achieved more rapidly, leading to an improvement of end product properties.

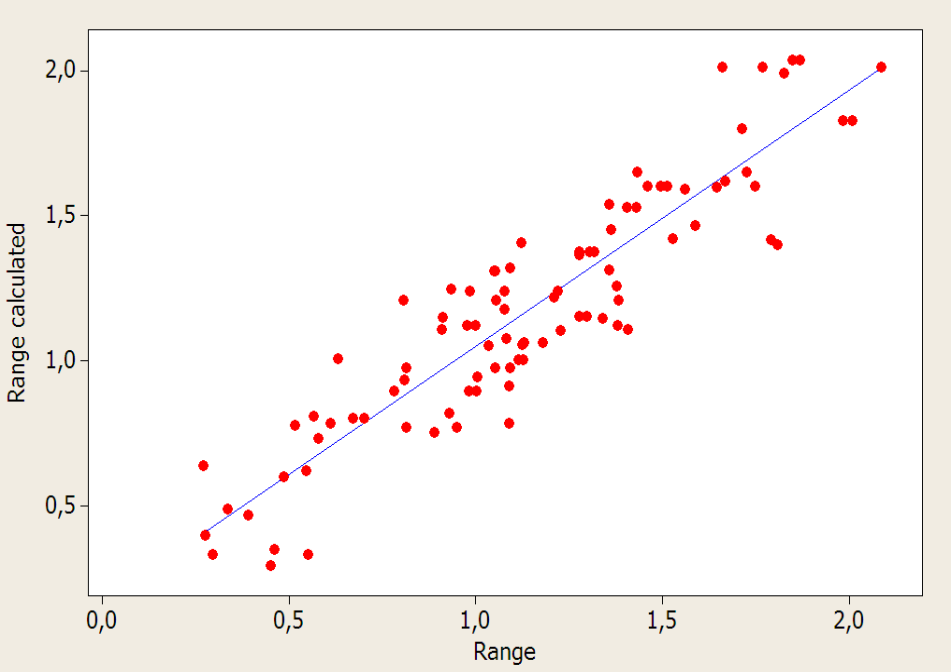


Figure 5.8. Comparison of experimentally measured (Range) and statistically predicted fibre density distribution (Range calculated)

Using experimental data with multiple regression analysis, the regression model parameters were determined. The test results are presented in Table 5.4. Parameters with negative values inversely influence the fibre density distribution. Their significance was checked with a t-test (Table 5.4).

Table 5.4. Regression model constant values along with the results of the t-test

	a_0	a_1	a_2	a_3	a_4	a_5	a_6	a_7	a_8	a_9
Values	-1.34	0.00092	-0.00359	-0.00315	0.00628	0.240	-0.0125	0.385	0.0386	-0.0840
Prob >|t|		12.5	15	17.6	19.8	0.0374	0.0538	0.0423	0.0333	0.0487
	a_{10}	a_{11}	a_{12}	a_{13}	a_{14}	a_{15}	a_{16}	a_{17}	a_{18}	a_{19}
Values	0.0798	0.066	-0.00040	-0.12	-0.0103	-0.0659	-0.0590	-0.0688	0.0056	0.0024
Prob >|t|	0.350	0.379	0.307	0.235	1.34	0.293	0.36	0.256	0.299	0.346
	a_{20}	a_{21}	a_{22}	a_{23}	a_{24}	a_{24}	a_{25}	a_{26}	a_{27}	a_{28}
Values	0.0606	0.0281	0.0260	0.0677	0.0066	0.0070	-0.0909	-0.0200	0.0388	-0.0125
Prob >|t|	0.466	0.455	0.332	0.151	0.489	0.361	0.323	0.209	0.691	0.277

The results presented in Table 5.4 show the parameter impact on the fibre density distribution range. Parameters a_5 - a_9 present the fibre diameter for each fiberization machine and have the largest impact on the fibre density distribution range. Also important are the parameters a_{10} - a_{28} which presents the horizontal and vertical positions of air blowing nozzles of individual fiberization machines. The smallest impact results from the suction fans (parameters a_1 - a_4) used for gas suction from the collecting chamber.

Chapter 6

Conclusions

In the last three years we have published three scientific articles regarding fibre diameter and density distribution in a layer of glass wool. We studied the prediction of glass wool fibre thickness on a spinning machine, and determined the pressure for fibre orientation and ratio between air and gas volume flow rate to have a significant influence on the fibre diameter. Also important are mass flow rate of glass, glass melt temperature and volume flow rate of gas. To a lesser extent, the spinner rotational speed, spinner life time and volume flow rate of air also affect the spinner diameter. Statistically, the spinner life time has the lowest influence on the fibre diameter. During manual setting of process parameters, spinner life time results in the need to change other parameters.

The process of the glass wool layer formation was also studied on a model spinning machine with sucrose as a working medium. The main focus was on the fibre layer formation on the accumulation grid, which was visualized by a camera. Despite the relatively simple and straightforward visualization approach we are able to obtain three distinct layer properties only from the optical intensity data: fibre accumulation rate (ψ), normalized standard deviation of the optical intensity (σ_{Gn}) and dimensionless distance between the mass centre of the fibre layer and the centre of accumulation grid (δ). Multiple regression models for δ and σ_{Gn} have shown an important effect of the suction flow, coaxial and tangential blow-away flows as well as fibre deposition time on the fibre layer properties. Also, these models are in good agreement with the measured values of δ and σ_{Gn} and also with the estimated fields of fibre accumulation rate. The presented regression models and qualitative analysis results can improve the understanding of the fibre transport and fibre layer formation process, leading to new possibilities for process monitoring and automation. Further research in this area should include the modelling of an actual glass wool manufacturing process with a moving accumulation grid where fibre layer formation is continuous.

In the last part of the study we carried out an analysis of the air suction flow velocity in the collecting chamber and measurements of density with the X-Ray device and visualization method. We estimated that glass wool quality can be increased by improving the uniformity of the air flow velocity distribution which was confirmed with a high correlation coefficient (r^2) of the regression model.

Based on the set of measured variables of the glass wool fiberization process, we are able to predict transversal density distribution reasonably well. The fibre diameter of each fiberization machine has the largest impact on the fibre density distribution. Also important are the parameters which present the horizontal and vertical positions of air blowing nozzles of individual fiberization machines. The smallest impact results from the suction fans used for gas suction from the collecting chamber. The modelling procedure can be applied in the production process where the main expected benefit is the improvement of the end product properties and a reduction in quantity of waste and poor quality products.

References

[1] D. Bozsaky, "The historical development of thermal insulation materials," *Architecture 41/2 49–56;* Periodica Polytechnica 2010; Department of Architecture and Building Construction, Széchenyi István University, H-9026 Gyor, Egyetem tér 1., Hungary, 2010.

[2] B. Kraševec, B. Širok, M. Hočevar & B. Bizjan, "Multiple regression model of glass wool fibre thickness on a spinning machine," *Glass Technology*, 55 (4), 119–125, August 2014.

[3] K. Bauckhage, "Das Zerstäuben metallischer Schmelzen," *Chem.Ing.-Tech.,* 64 (4), 322–332, 1992.

[4] P. Walzel, "Zerstäuben von Flüssigkeiten," *Chem.-Ing.-Tech.,* 62 (12), 983–994, 1990.

[5] T. Lakatos, L.G. Johansson, B. Simmingsköld, "Viscosity and liquidus temperature relations in the mineral wool part of the system SiO2-Al2 O3-CaO-MgO-Alkalies-FeO-Fe2 O3," Glastek. Tidskr. 36, 51-55, 1981.

[6] H. Kapplan-Dietrich, A. Eckerbracht & G. H Frischat, "J. Am. Ceram. Soc.," 78 (4), 1123–1124, 1995.

[7] A. Kucuk, A. G. Clare & L.E Jones, "Estimation of Surface Tension for Silicate Glass Melts at 1400°C Using Statistical Analysis," Glass Technology 40 (5) 149-153, 1999.

[8] V. I. Goleus, A. Y. Belyi, E. M. Sardak & Y. I. Belyi, "Calculation of the Surface Tension of Molten Borosilicate Glasses," Steklo Keram., 53 (8), 6–8, 1996.

[9] B. Blagojević, B. Širok & B. Štremfelj, "Simulation of the Effect of Melt Composition on Mineral Wool Fibre Thickness," Ceramics – Silikáty, 48 (3), 128-134, 2004.

[10] B. Blagojević, B. Širok, "Multiple Regression Model of Mineral Wool Fibre Thickness on a Double-Disc Spinning Machine," *Glass Technol.* 43, 120, 2002.

[11] P. Järvelä, T. Pohjonen, P. Törmälä, "An empirical model of the strength of a porous glass wool composite," Tempere University of Technology, Department of Mechanical Engineering, Laboratory of Polymer and Fibre Technology, Finland.

[12] F. Pincemin, P. Boulet, G. Jeandel, "Modelling and experimental evaluation of the thermal insulation properties of mineral wool products at high temperature," *American Society for Testing and Materials*, Philadelphia, pp. 243-258, 1997.

[13] V. R. Christensen, W. Eastes, R. D. Hamilton, A. W. Struss, "Fibre diameter distributions in typical MMVF wool insulation products," *American Industrial Hygiene Association*, Journal Volume 54, Issue 5, 1993.

[14] T. Bajcar, B. Širok, B. Bizjan, A. Orbanić, "Mineral Wool Melt Fibreization on a Spinner Wheel," *Chemical Engineering Research and Design*, vol. 92 no. 1, p. 80-90, 2014, DOI: 10.1016/j.cherd.2013.06.014.

[15] T. Bajcar, B. Blagojević, B. Širok, M. Dular, "Influence of flow properties on a structure of a mineral wool primary layer," *Experimental Thermal and Fluid Science* 32 440–449, 2007.

[16] B. Širok, B. Blagojević & P. Bullen, "Mineral wool: Production and properties. Cambridge," UK: Woodhead Publishing, 2008.

[17] C. Ablitzer, F. Gruy & C. Perrais, *"Chem. Engng Sci.,"* vol 56, pp. 2409-2420, 2001.

[18] B. Širok, B. Blagojević, M. Novak, "Influence of blow away velocity field on the primary layer fibre structure in the mineral wool production process," *Glass Technology* 43 (5) 188–194, 2002.

[19] B. Blagojević, B. Širok, and M. Hočevar, "Monitoring and Control of Quality of the Primary Layer of Mineral Wool on a Disc Spinning Machine," *INSTRUMENTATION SCIENCE & TECHNOLOGY,* Vol. 31, No. 1, pp. 67–80, 2003.

[20] B. Kraševec, B. Širok, B. Bizjan, M. Hočevar, "Fibre density distribution in a layer of glass wool," *Glass Technology,* 56 (3), 145–152, June 2015.

[21] E. Badel, J-M. Letang, G. Peix and D. Babot, "Quantitative microtomography: measurement of density distribution in glass wool and local evolution during a one-dimensional compressive load," *Meas. Sci. Technology,* 14 410–420, 2003.

[22] B. Blagojević, B. Širok & B. Štremfelj, "Simulation of the Effect of Melt Composition on Mineral Wool Fibre Thickness, " *Ceramics – Silikáty,* 48 (3), 128-134, 2004.

[23] S. Vaisburd & D. G. Brandon, "A Combined Unit for Viscosity, Surface Tension and Density Measurements in Oxide Melts," *Meas. Sci. Technol.,* 8, 822-826, 1997.

[24] S. Panda, "The Dynamics of Viscous Fibres," *PhD Thesis*, TU Kaiserslautern, Germany, 2006.

[25] Y. Qin, X. Lv, C. Bai, P. Chen, G. Qiu, "Dry granulation of molten slag using a rotating multi-nozzle cup atomizer and characterization of slag particles," *Steel Research International*, vol. 84, no. 9, p. 852-862, 2013. DOI: 10.1002/srin.201200325.

[26] Y. Qin, X. Lv, C. Bai, P. Chen, G. Qiu, Z. Jie, "Mechanism of dry molten slag granulation using a rotating multi-nozzle cup atomizer," *Steel Research International*, vol. 85, no. 1, p. 44-52, 2014. DOI: 10.1002/srin.201300007.

[27] B. Bizjan, B. Širok, M. Hočevar, A. Orbanić, "Ligament-type Liquid Disintegration on a Spinning Wheel," *Chemical Engineering Science*, vol. 116, p. 172-782, 2014. DOI: 10.1016/j.ces.2014.04.043.

[28] B. Bizjan, B. Širok, M. Hočevar, A. Orbanić, "Liquid Ligament Formation Dynamics on a Spinning Wheel," *Chemical Engineering Science*, vol. 119, p. 187-198, 2014. DOI: 10.1016/j.ces.2014.08.031.

[29] J.Z. Lin, X.I. Liang, S.L. Zhang, "Numerical simulation of fibre orientation distribution in round turbulent jet of fibre suspension," *Chemical Engineering Research and Design*, Vol. 90, No. 6, p. 766-775, 2012. DOI:10.1016/j.cherd.2011.09.016.

[30] A. Capone, G.P. Romano, A. Soldati, "Experimental investigation on interactions among fluid and rod-like particles in a turbulent pipe jet by means of particle image velocimetry," *Experiments in Fluids*, vol. 56, paper No. 1, 15 p., 2015. DOI: 10.1007/s00348-014-1876-4.

[31] G. Qi, J.G. Nathan, C.W.T. Lau, "Velocity and orientation distributions of fibrous particles in the near-field of a turbulent jet," *Powder Technology*, Vol. 276, p. 10-17, 2015. DOI: 10.1016/j.powtec.2015.02.003.

[32] B. Bizjan, M. Peternelj, B. Širok, "Mineral wool primary layer formation in collecting chamber," *Journal of Mechanical Engineering*, in press.

[33] D. Dimovski, B. Blagojević, B. Širok, Z. Kariž, "Mineral wool primary layer structure influence on the fibre distribution in the final product," *Glass Technology*, vol. 45, no. 4, p. 188-194, 2004.

[34] M. Hočevar, B. Širok, B. Blagojević, "Mineral wool production monitoring using neural networks," *International Journal of Information Technology*, vol. 11, no. 9, p. 64-72, 2005.

[35] R. T. Bynum, "Insulation Handbook," *The McGraw-Hill Companies*, New York (USA), 2001.

[36] P. M. Dämmstoffarten, "Detail Praxis – Dämmstoffe Grundlagen, Materialen,

Anwendungen)," *Institut für internationale Architektur Dokumentation GmbH & Co. KG*, München, Deutschland, 2007.

[37] Prof. V. Karpov, "Mathematical modelling in glass wool production," Russia, November 2003, unpublished.

[38] F. Trdič, B. Širok, P. R. Bullen & D. R. Philpott, "Real Time Imaging," 5 (2), 125–140, 1999.

[39] M. Zlokarnik, "Dimensional analysis and scale-up in chemical engineering," *Springer-Verlag,* Heidelberg, 1991.

[40] H. Lubanska, *J.Met.* 22, 45 (1970).

[41] E. Cendre, P. Duvauchelle, G. Peix, J.-Y. Buffière, D. Babot, "Conception of a High Resolution X-Ray Computed Tomography Device; Application To Damage Initiation Imaging Inside Materials," Buxton, Greater Manchester, April 14-17, 1999.

[42] N. Bhouri, E. Badel, S. Ben Nasrallah and P. Perre, "Shrinkage/Swelling Behavior of Knitted Fabrics during Relative Humidity Cycles Determined by X-ray Imaging," *Journal of Porous Media* 12(5), 403-415, 2009.

[43] E. Badel and P. Perr´e, "Using a digital x-ray imaging device to measure the swelling coefficients of a group of wood cells," *NDT&E* Int. 34 345–53, 2001.

[44] P. H. Rothe, J. A. Block, "Aerodynamic behaviour of liquid sprays," *Int. J. Multiphase Flow,* vol. 3., pp 263-272, 1976.

[45] B. Kraševec, B. Bizjan & B. Širok, "Glass wool layer formation in the collecting chamber," *Glass Technology,* in press.

[46] I. Ohberg, "Technological development of the mineral wool industry in Europe," *Ann. Occup. Hyg.,* vol. 31, no. 4B, pp. 529-45, 1987.

[47] A. W. Angwafo, P. R. Bullen & D.R. Philpott, *"Melt flow in the production of mineral wool by centrifugal spinning Proc. FEDSM'98,"* 1998 ASME Fluids Engineering Division Summer Meeting, 21-25, Washington, USA, June 1998.

[48] T. Westerlund & T. Hoikka, "On the modelling of mineral fibre formation. Computers Chem. Engng.," *Computers Chem. Engng.,* vol. 13, no. 10, pp. 1153-1163, 1989.

[49] P. Eisenklam,"On ligament formation from spinning discs and cups," *Chem. Eng. Sci.,* vol. 19, pp. 693-694, 1963.

[50] B. Širok, B. Mihovec, F. Bradeško, P. Možina, "Conveyor scale for controlling rock wool surface," *European Patent Nr. EP 1 194754 B1 Bulletin*, Munich, 2005/35.

[51] M. R. Spiegel, "Theory and problems of Probability and Statistics," *Schaum's Outline Series,* McGraw-Hill, New York, 1975.

[52] W. Vogel, "Chemistry of Glass," *American Ceramic Society*, 1985.

[53] P. Shelby, "Introductionto glass science and technology, ISBN 0854045333, 1997.

[54] B. Blagojević, B. Širok, "Computer programme for calculating density, viscosity, surface tension and mineral wool layer thickness," Ljubljana, 2004.

[55] P. Walzel, "Liquid atomization by film splitting," *Ger. Chem. Eng.,* vol. 5, pp. 121-129, 1982.

[56] L. R. Glicksmann, "The cooling of Glass fibres," *Glass Technol.,* vol. 9, No. 5, pp. 131-138, 1968.

[57] A. Ziabacki, "Fundamentals of fibre formation, "*Wiley*, New York, 1976.

[58] Y. Sano, "Formation of Fibres and Development of Their Structure," *Society of Fibre Science and Technology*, Japan, 1969.

[59] P. H. Rothe, J. A. Block, "Aerodynamic behaviour of liquid sprays.," *Int. J. Multiphase Flow,*

vol. 3, pp 263-272, 1976.

[60] J. Smrekar, J. Oman, B. Širok, M. Mori, M. Hočevar, "A crosscorrelation optical velocimeter,C *Meas. Sci. technol.,* vol. 18, No. 3, pp. 555-560, 2007.

[61] D. R. Philpott, P. Bullen, A. Angwafo, F. Trdič, B. Širok "Monitoring of jet flow fluctuations in the production of mineral wool using realtime computer vision," *Int. J. COMADEM*, vol. 1, no. 2, pp. 14-19, 1998.

[62] R. B. Wicker, J. K. Eaton, *Int. J. Multiphase Flow*, vol. 27, pp. 949-970, 2001.

[63] H. A. Warda, S. Z. Kassab, K. A. Elshorbagy, E. A. Elsaadawy, *Flow Meas. Instrum*., vol. 12, no. 3, pp. 29-35, 2001.

[64] J. M. Caceres, J. E. Garcia Hernandez, J. M. Rincon, "Characterization of fibres as rockwool for insulation obtained from Canary Island basalts," *Materiales de Construccion*, vol. 46, no. 3, pp. 61-78, 1996.

[65] Tonder, Jespersen, "Man-made vitreous fibre products and processing and apparatus for their production," I. P.No: WO96/38391, I. A. No: PCT/EP96/02068, 1996.

[66] R. C. Gonzales, R. E. Woods, "Digital Image Processing," Addison – Wesley, 1992.

[67] D. R. Philpott, P. R. Bullen, A. Angwafo, F. Trdič, B. Širok, "Measures derived from image analysis for use in the monitoring of mineral wool production," *IMECHE'95,* pp. 309-314, London, Proceedings, 1995.

[68] B. Širok, B. Blagojević, P. R. Bullen, "The influence of the spinning disc film temperature on the fibre diameter distribution in mineral wool produced by a double-disc spinning machine," *Glass Technology,* vol. 45, no. 5, 334-340, 2005.

[69] B. Širok, B. Blagojević, P. R. Bullen, D. Dimovski, "Density and viscosity of the silicate melts for the production of the mineral wool fibres," *Int. J. of Microstructure and Materials Properties,* vol. 1, no. 1, 61-73, 2005.

[70] Blagojević, B. Širok, U. Primožič, "An experimental method for measuring the thickness of mineral wool fibres," *Int. J. COMADEM,* vol. 9, no. 4, 23-29, 2006.

Bibliography

List of publication

Journal Articles

Kraševec Boris, Širok Brane, Hočevar Marko, Bizjan Benjamin "Multiple regression model of glass wool fibre thickness on a spinning machine," *European journal of glass science and technology*, Part A, Glass technology ISSN: 1753-3546. Vol. 55, nr. 4 (Aug. 2014), str. 119-125. COBISS.SI-ID: 13639707.

Kraševec Boris, Širok Brane, Bizjan Benjamin, Hočevar Marko, "Fibre density distribution in a layer of glass wool," *European journal of glass science and technology*, Part A, Glass technology ISSN: 1753-3546. Vol. 56, nr. 5 (Oct. 2015), str. 145-152. Doi: 10.13036/17533546.56.5.145. COBISS.SI-ID: 14301723.

Kraševec Boris, Bizjan Benjamin, Širok Brane, "Glass wool layer formation in the collecting chamber," *European journal of glass science and technology*, Part A, Glass technology ISSN: 1753-3546. Accapted: 10.10.2016, in press.

Other Publications

Graduate thesis:
Boris Kraševec, Kopač Janez, Dolinšek Slavko. Zasnova in rekonstrukcija vpenjalne naprave na operaciji vrtanja bata = [Reduction of clamping jaws wear, on operation drilling of piston]: diplomska naloga. Fakulteta za strojništvo, Ljubljana. Univerza v Ljubljani, Fakulteta za strojništvo, 2006. COBISS.SI-ID: 9174043.

Specialist thesis:
Kraševec Boris, Soković Mirko, Starbek Marko. Zagotavljanje kakovosti obdelave bata: specialistično delo. Univerza v Ljubljani, Fakulteta za strojništvo, 2009. COBISS.SI-ID: 11244571.

Seminar:
Kraševec Boris, Soković Mirko. Izboljšanje cilindričnosti kompletiranega bata UFO/NLX. Seminarska naloga pri predmetu Menedžment kakovosti. Univerza v Ljubljani, Fakulteta za strojništvo, 2009. COBISS.SI-ID: 10979611.

Supervision to student:
Štrbenc Leon, Boris Kraševec, Tonkovič-Prijanovič Marica. Vpliv različnega števila lukenj na cilindričnost kompletiranega bata: diplomska naloga višjega strokovnega izobraževanja. Šolski center Novo mesto, Višja strokovna šola, program strojništvo, 2010. COBISS.SI-ID: 81654.

Biography

Boris Kraševec was born on July 7, 1982 in Novo mesto, Slovenia. He graduated in 2006 with the thesis titled "Reduction of clamping jaws wear on operation drilling of piston" at the Faculty of Mechanical Engineering, University of Ljubljana, Slovenia. After finishing the undergraduate programme, he started his specialist study at the Faculty of Mechanical Engineering, University of Ljubljana, Slovenia and graduated in 2009 with the work titled "Quality assurance of piston machning". In 2011 he started his doctoral study at the Jožef Stefan International Postgraduate School at the Ecotechnology programme and cooperation with the Faculty of Mechanical Engineering, University of Ljubljana, Slovenia, and company Ursa Slovenia, d.o.o from Novo mesto. In the last three years he published three scientific articles in the field of glass wool.

His engineer experience began at Danfoss Compressors d.o.o. company in Črnomelj, where from 2004 and 2006 he worked as an assistant to a process engineer, while still attending school. After graduating he worked as a production technologist in rotor production between 2006 and 2008. In 2009 he was promoted to the position of a process engineer for valve plate system and piston production of compressor. Regarding the compressor topic he prepared two graduate papers. At the beginning of year 2010, before the above-mentioned company was closed, he changed employment and started working in a glass wool production factory named Ursa Slovenija d.o.o as a process engineer in the production management department.